EXPLOITING THE ANTIOXIDANT POTENTIAL AND SIRNA DELIVERY FUNCTION OF MESOPOROUS SILICA NANOPARTICLES FOR THE TREATMENT OF SKIN FIBROSIS AND BREAST CANCER METASTASIS

By
Jingga Morry
Master of Science in Biomedical Engineering
University of Michigan, 2007

A DISSERTATION

Presented to the Department of Biomedical Engineering
and the Oregon Health & Science University School of Medicine
in partial fulfillment of the requirements for the degree of

Doctor of Philosophy

October 2016

School of Medicine

Oregon Health & Science University

CERTIFICATE OF APPROVAL

This is to certify that the PhD dissertation of

Jingga Morry

has been approved

Thesis Advisor/ Wassana Yantasee, PhD, MBA

Committee Chair/ Pepper Schedin, PhD

Committee Member/ Shiuh-Wen Luoh, MD, PhD

Committee member/ Xiaolin Nan, PhD

Committee member/ Sara Courtneidge, PhD

ABSTRACT

The increased production of reactive oxygen species (ROS) is a hallmark of fibrosis and cancer. In fibrosis, the release of ROS along with secretion of pro-fibrotic cytokines by the immune cells during the inflammatory phase has been known to promote the activation of fibroblasts and induce collagen deposition. In cancer, ROS also plays a crucial role in various signaling cascades involved in cellular survival, proliferation, resistance to apoptosis, angiogenesis, as well as metastasis. However, the results from clinical studies involving antioxidant therapies in patients have been disappointing, mostly due to the low bioavailability of the conventional antioxidant therapies.

Nanoparticles with intrinsic antioxidant properties have great potential to be used for attenuating oxidative stress in various oxidative-induced diseases including fibrosis and cancer. Our group has recently developed and optimized a polymer-coated mesoporous silica nanoparticle (NP) for siRNA and drug delivery. The platform consists of a 50-nm mesoporous silica nanoparticle (MSNP) core coated layer-by-layer with bioreducible cross-linked 10-kDa polyethyleneimine (PEI) for effective siRNA binding and endosomal escape, and polyethylene glycol (PEG) for preventing nanoparticle aggregation, minimizing enzyme degradation of siRNAs, shielding the toxic effect of PEI, and preventing recognition by the immune system.

In this dissertation, I sought to evaluate the antioxidant activity and siRNA delivery efficiency of our NP platform for the treatment of fibrosis and cancer metastasis. In my first project, I investigated the intrinsic antioxidant property of our NPs and assessed the added benefit of silencing heat shock protein 47 (HSP47) as a gene target in a skin

fibrosis model. HSP47 is a collagen-specific molecular chaperone responsible for proper assembly of collagen molecule and its overexpression has been observed in numerous fibrotic diseases. To this end, I have made the novel discovery on the antioxidant property of our nanoparticle which is attributed by its MSNP core. I also found that the nanoparticle was far superior to n-acetyl cysteine (NAC) at modulating pro-fibrotic markers. Intradermal administration of siHSP47-nanoparticles effectively reduced HSP47 protein expression in skin to normal level. In addition, the antioxidant MSNP also played a prominent role in reducing the pro-fibrotic markers, NOX4, alpha smooth muscle actin (α-SMA), and collagen type I (COL I), as well as skin thickness of the mice.

In my second project, I explored the therapeutic potential of the nanoparticle platform for treating metastatic breast cancer. PLK1 was identified as the top therapeutic target for TNBC cells and tumor initiating cells in a kinome-wide screen. NP inhibited cancer migration and invasion in TNBC cells owing to its ROS and NOX4 modulating properties. *In vivo*, siPLK1-NP knocked down 80% of human PLK1 mRNA expression in metastatic breast cancer cells residing in mice lungs, inhibited distant metastasis from lung to other organs, and reduced overall tumor burden. Long term treatment delayed the onset of death in mice by 36 days and improved the overall survival.

In conclusion, in this dissertation I have shown that our NP platform has great potential for the treatment of fibrosis and cancer. Given the most optimal gene target, our nanoparticles will be able to provide combinatorial treatment not only for fibrosis and cancer, but also for other types of oxidative-induced inflammatory diseases.

ACKNOWLEDGEMENTS

I would first like to thank my advisor, Dr. Wassana Yantasee, for her support during my PhD journey. Thanks for being a supportive, caring, and understanding mentor. Your advice on both research as well as on my career have been invaluable. I am very grateful for your expertise and contributions.

I would like to thank the members of my Dissertation Committee for their insights and direction throughout the course of my studies: Dr. Pepper Schedin, Dr. Shiuh-Wen Luoh, Dr. Xiaolin Nan, and Dr. Sara Courtneidge. They have given me superb scientific guidance, many insightful suggestions and demonstrated sincere interest in my work. I am fortunate to have them on my committee.

I would like to recognize the members of former and current members of Yantasee lab who have all contributed to the progress I have made. I would like to thank Dr. David Castro for assisting in reviewing this dissertation. I also wish to thank Dr. Worapol Ngamcherdtrakul (Boom) and Moataz Reda for their help in material synthesis and characterization of the nanoparticle. I would also like to thank Dr. Xinran Li, Brandon Beckman and Richard Lee for their help in assisting me with the animal studies. Also, I would like to thank Thanapon Sangvanich (Built) for his help in running elemental analysis for the copper-binding study. The Yantasee lab members are a wonderful group of people who I have enjoyed working with and learning from.

I thank Dr. Owen McCarty, Dr. Monica Hinds, and Nermina Radaslic for helping me with all the questions and completing the paperwork required throughout my graduate study.

Also, I would like to thank Virginia Howard for her help in ordering much-needed reagents and in fulfilling my last-minute requests for lab supplies.

Finally, I would like to thank my family and friends for their continued support and encouragement. To my unbelievably supportive husband Cheng Yi Ong, thank you for being my rock when I needed it most and for supporting me through every decision I made. To my parents and my sister, I would not have gotten to where I am today without your wonderful support and confidence in me. To my close good friend, Sara Botto, thank you for all the advice and for being there for me when the challenges of graduate school seemed too great to overcome. To my pup, Simba, thank you for keeping me company while I was writing this thesis and for being the best kind of distraction.

LIST OF ABBREVIATIONS

AP-1	activator protein-1
α-SMA	alpha smooth muscle actin
CAT	catalase
CCl_4	carbon tetrachloride
CeO_2	Cerium oxide
COL I	collagen I
CTGF	connective tissue growth factor
DNA	deoxyribonucleic acid
DPI	diphenyleneiodonium chloride
DUOX	dual oxidase
ECM	extracellular matrix
EMT	epithelial–mesenchymal transition
EPC	endothelial progenitor cell
FDA	Food and Drug Administration
FGF	fibroblast growth factor
GPx	glutathione peroxidases
GRAS	generally regarded as safe
GSH	glutathione
H_2O_2	hydrogen peroxide
HER2	human epidermal growth factor 2
HIF-1α	hypoxia-inducible factor-1 alpha
HOCl	hypochlorous acid
HRE	hypoxia response elements
HSP47	heat shock protein 47
i.d.	intradermal
i.p.	intraperitoneal
i.t.	intrathecal
i.v.	intravenous
ICP-MS	Inductively Coupled Plasma Mass Spectrometry
IL-13	interleukin-13
IL-6	interleukin-6
IPF	idiopathic pulmonary fibrosis
JNK	c-Jun N-terminal kinases
LLC	Lewis lung carcinoma
MPO	myeloperoxidase
mRNA	messenger RNA
MSNP	mesoporous silica nanoparticle
NAC	n-acetyl cysteine
NADPH	nicotinamide adenine dinucleotide phosphate
NFκB	nuclear factor kappa B
NOS	nitric oxide synthase

NOX	nicotinamide adenine dinucleotide phosphate-oxidase
NOX4	NADPH oxidase 4
NP	MSNP-PEI-PEG
NSCLC	non-small cell lung carcinoma
$^1O_2$	singlet oxygen
$O_2^{\bullet-}$	superoxide anion radical
O_3	ozone
OH^-	hydroxyl ion
$OH^\bullet$	hydroxyl radical
p.o.	per os
p38 MAPK	p38 mitogen-activated protein kinases
PDGF	platelet-derived growth factor
PEG	polyehtylene glycol
PEI	polyethyleneimine
PET	positron emission tomography
PHD	prolyl hydroxylase domain
PI3K	phosphatidylinositol-3-kinase
PLK1	polo-like kinase 1
PtNP	platinum nanoparticle
pVHL	von Hippel-Lindau tumor suppressor gene
RCS	reactive chloride species
RNA	ribonucleic acid
RNS	reactive nitrogen species
ROS	reactive oxygen species
RSS	reactive sulfur species
s.c.	subcutaneous
shRNA	short hairpin RNA
siHSP47	siRNA against HSP47
siPLK1	siRNA against PLK1
siRNA	small interfering RNA
siSCR	scrambled (non-targeting) siRNA
SOD	superoxide dismutase
TEPA	tetraethylenepentamine (copper chelator)
TGF-β	transforming growth factor beta
TM	tetrathiomolybdate (copper chelator)
TNBC	triple negative breast cancer
TNF	tumor necrosis factor
UV	ultraviolet
VEGF	vascular endothelial growth factor

Table of Contents

List of Figures

List of Tables

Chapter 1: Introduction and Background

1.1 Introduction

The regulation of redox homeostasis is crucial for the maintenance of normal cellular growth, metabolism, and survival. Oxidative stress is defined as the imbalance between the production of reactive oxygen species (ROS) and the capability of the cell to elicit an effective antioxidant response. At lower concentrations, ROS are important signaling molecules involved in cellular proliferation, migration, and apoptosis [1, 2]. Several sources of ROS in cells and tissue have been identified, including mitochondrial electron transfer chain [3] and NADPH oxidase (NOX) enzymes [4]. At higher concentrations, these molecules could be useful against pathogens, resulting in increased leukocyte and platelet activation, and increased leukocyte recruitment [5]. While this is true in the context of innate immunity and inflammatory signaling in the immune cells, most ROS are harmful to cells due to the accumulation of irreversible damages to proteins, lipids, and most importantly, to DNA leading to mutations and cell death [6, 7].

ROS and oxidative stress have been implicated in a number of diseases, including fibrosis and cancer [8]. In particular, NOX-derived ROS has been found to be the main source of oxidative stress which promotes key events in the development of fibrotic diseases (such as skin fibrosis [9], idiopathic pulmonary fibrosis [10], liver fibrosis [11], and kidney fibrosis [12]) as well as the initiation and progression of the cancer disease [13].

To date, there is no cure for these diseases. Current approaches are limited to attempts on slowing down disease progression in fibrotic diseases (such as pirfenidone for pulmonary fibrosis). For cancer, there are several treatment approaches including, chemotherapy, surgery, radiation, immunotherapy and other novel targeted therapies. Cures can be achieved in some cases (e.g., when tumors are diagnosed early), but resistance and recurrence are common. Chemotherapy and radiation also generate ROS, which, at high levels, are toxic to cancer cells. Nevertheless, sub-lethal ROS generated by these treatments were also reported to promote cancer invasion and metastasis [14]. ROS are thus considered one of the mediators of drug resistance and metastasis in cancer [14-16].

In recent years, antioxidants have drawn much attention as potential therapeutic interventions due to their ability to fight oxidative stress (and thereby negate its role) in fibrosis and cancer development. The main function of antioxidants is to scavenge or neutralize free radical formation and inhibiting the deleterious downstream effects of ROS. However, most antioxidants, taken orally, have limited absorption profiles, which lead to low bioavailability and insufficient concentrations at the target site [17, 18]. To overcome this issue, current research is focused on developing nanoparticles with intrinsic antioxidant properties which can be functionalized to provide localized or targeted therapy [19, 20]. These nanoparticles are mostly made up of inorganic materials such as mesoporous silica, cerium oxide, and fullerene, which exhibit antioxidant activities due to their ability to protect cells against oxidative stress *in vitro* and in animal models [19]. The antioxidant capacities of these nanoparticles are thought to be contributed by their redox and catalytic properties, electronic configuration, oxygen

vacancy defects, and, high-surface-to-volume ratio. Additionally, nanoparticles can be designed to be multi-functional, also serving as delivery platforms for other therapeutics.

Much excitement has also been directed at the development of targeted therapies, a strategy in which drugs are designed to block or interfere with a specific molecule in the disease process. Small molecule drugs or monoclonal antibodies have garnered some initial success, but a commonly encountered drawback is the propensity to develop therapeutic resistance leading to the unfortunate exhaustion of treatment options. An RNA interference strategy has attracted great interest as an alternative solution due to its therapeutic potential in silencing disease-related genes with high specificity, minimizing off-target effects commonly associated with small molecule inhibitors. Although promising, the utility of siRNA as a therapeutic agent has been hindered by its poor cellular uptake and short half-life [21]. To combat this, significant progress has been made in recent years on the development of nanoparticles as gene delivery platforms and silica nanoparticles have emerged as one of the more promising gene delivery agents for treatment of various preclinical cancer disease models upon systemic delivery [22, 23]. In addition, mesoporous silica nanoparticles (MSNP) have also been reported to have reactive oxygen species (ROS) scavenging capability [24, 25], which will be beneficial for reducing oxidative stress-induced processes such as fibrosis, carcinogenesis and metastasis. In addition, MSNP can be surface-modified through covalent bonding or electrostatic interactions with polymers to facilitate gene delivery into the cells [26]. Thus, MSNPs have great potential to be used as a gene delivery agent for fibrosis and cancer treatments.

1.1.1 Overview of Reactive Oxygen Species (ROS)

Reactive species are broadly categorized into 4 groups: ROS, reactive nitrogen species (RNS), reactive sulfur species (RSS), and reactive chloride species (RCS) [27]. Among these groups, ROS is found to be the most abundantly produced [27]. ROS are generally defined as oxygen-containing small species including superoxide anion radical ($O_2^{\bullet -}$), hydroxyl radical ($OH^{\bullet}$), hydroxyl ion (OH^-), hydrogen peroxide (H_2O_2), singlet oxygen ($^1O_2$), and ozone (O_3) [4, 27]. ROS can be generated either by exogenous sources such as UV radiation, toxic chemicals and drugs, physiological changes such as aging or injury/inflammation [28], or by intracellular (endogenous) sources such as NOX enzymes on the plasma membrane [4], myeloperoxidases (MPO) in phagocytes [29], and as by-products of respiratory chain function in mitochondria [3]. As highlighted in **Figure 1.1**, ROS generation is a cascade of reactions initiated by the production of $O_2^{\bullet -}$ inside the cells, contributed by endogenous and exogenous cellular sources. Cellular defenses against these ROS molecules involve endogenous antioxidants such as glutathione peroxidases (GPx), catalases (CAT), and superoxide dismutases (SOD). Under normal physiological conditions, the formation and elimination of ROS is tightly regulated through the help of the ROS-scavengers/endogenous antioxidants to maintain homeostasis and avoid the harmful effects of oxidative stress. However, the elimination process can become saturated and the increased accumulation of ROS leads to permanent changes and/or damages to the DNA, lipids and proteins with detrimental effects such as cell death, mutagenesis, carcinogenesis and fibrosis.

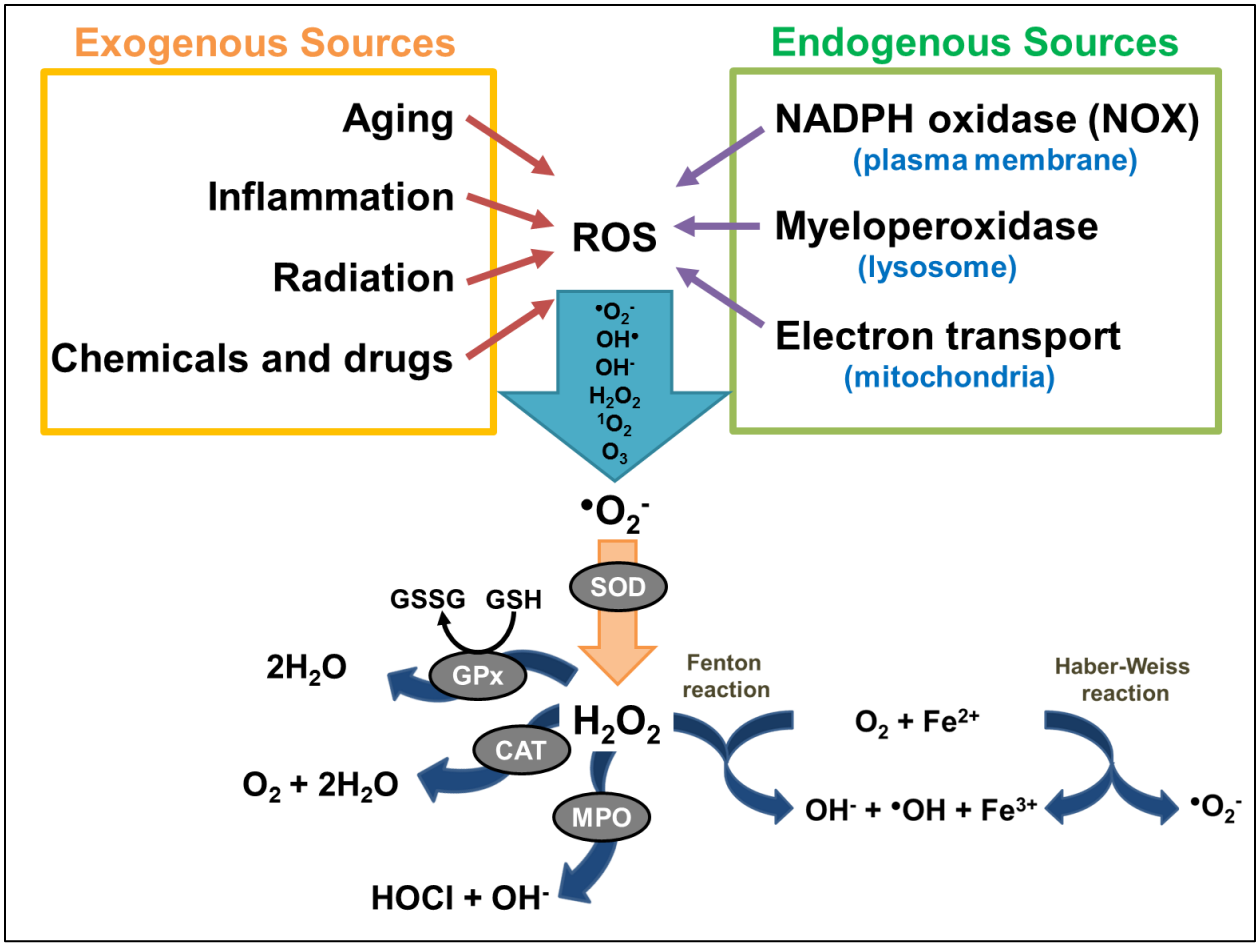

Figure 1.1 Sources of ROS and key ROS molecules in signaling.
ROS generation is a cascade of reaction initiated by the production of $^{\bullet}O_2^-$ inside the cells, contributed by endogenous and exogenous cellular sources. Molecular oxygen is reduced to superoxide anion ($O_2^{\bullet-}$) by enzymes such as NOX and nitric oxide synthases (NOS), or as by-products of redox reactions in mitochondrial respirations. $O_2^{\bullet-}$, being a cell-impermeant molecule, is then rapidly dismutated to H_2O_2 either spontaneously or enzymatically by antioxidant enzyme superoxide dismutases (SODs). The intracellular removal of H_2O_2 can be categorized into three different mechanisms: 1) by the action of catalase (CAT) and glutathione peroxidases (GPx) which reduces H_2O_2 to water, 2) through conversion of H_2O_2 into hypochlorous acid (HOCl) and $^1O_2$ by the heme enzyme myeloperoxidase (MPO) the neuthrophils which results in antimicrobial activity, and 3) by Fenton reaction whereby H_2O_2 is converted to the highly reactive $OH^{\bullet}$ through oxidation of Fe^{2+} to Fe^{3+}. The $OH^{\bullet}$ produced will then react with H_2O_2 to form $O_2^{\bullet-}$, which, again, reacts with H_2O_2 to form $OH^{\bullet}$ and OH^-, as a part of Haber-Weiss reaction.

1.1.2 Roles of ROS in fibrosis

Fibrosis is a complex disease characterized by the excessive synthesis and accumulation of extracellular matrices that occurs as a result of activation and proliferation of fibroblasts and myofibroblasts. Fibrogenesis can be broadly categorized into four different stages: 1) initiation of tissue injury, 2) inflammation and activation of fibroblasts, 3) extracellular matrix (ECM) synthesis, and 4) deposition of ECM which eventually leads to organ failure [30]. The causes of fibrosis vary greatly, but common contributing factors include i) physical or chemical injury, ii) autoimmune disease (e.g., systemic sclerosis) [31], iii) virus-induced (e.g., hepatitis C virus-induced liver fibrosis) [32], iv) alcohol-induced (e.g., liver fibrosis) [33], v) hypertension (e.g., hypertensive myocardial fibrosis), or vi) unknown (e.g., idiopathic pulmonary fibrosis) [31, 34, 35]. Notably, nearly 45% of all naturally-occurring deaths in the western world are attributed to some form of fibrotic disease [36].

The release of ROS along with the secretion of chemokines and growth factors (such as platelet-derived growth factor (PDGF), transforming growth factor beta (TGF-β), connective tissue growth factor (CTGF), interleukin-6 (IL-6), and interleukin-13 (IL-13)) by immune cells during the inflammation phase are known to promote the activation of fibroblast and collagen deposition in fibrosis [37, 38]. Among them, TGF-β is the most potent profibrogenic cytokine which plays a vital role in regulating important biological processes such as cellular proliferation, extracellular matrix (ECM) production, and epithelial–mesenchymal transition (EMT) [28]. TGF-β mRNA and/or protein expression has been found to be elevated in most fibrotic diseases in patients [39-41] as well as

experimental fibrosis models [42-44]. As shown in **Figure 1.2**, the presence of ROS could activate TGF-β signaling pathways, which then signal through either SMAD-dependent or SMAD-independent pathways (e.g. phosphatidylinositol-3-kinase (PI3K), c-Jun N-terminal kinases (JNK)) [45]. Increased TGF-β signaling also induces elevated production of NOX4-generated ROS [46], which further stimulates the transcriptional activities of pro-fibrotic genes such as collagen I (COLI), alpha smooth muscle actin (αSMA), and NOX4. In addition, the presence of NOX4-generated ROS could activate signaling pathways such as JNK and nuclea factor kappa B (NFκB) [47, 48], and trigger DNA oxidation as the initial step in a cascade of events which lead to myofibroblast differentiation and overaccumulation of collagen deposition into ECM, leading to fibrosis.

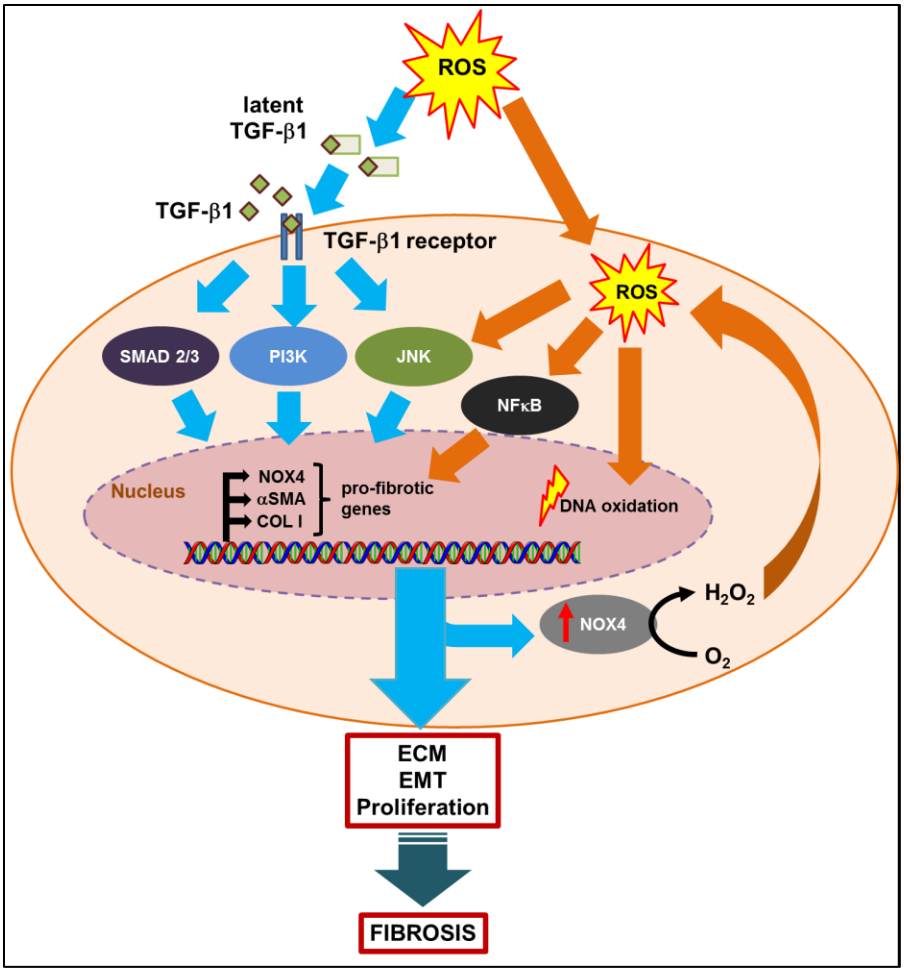

Figure 1.2. ROS contributes to the induction and persistence of TGF-β-mediated fibrosis.

The presence of ROS induces the conversion of latent TGF-β complex to its active form, which binds to its receptor and triggers signalling pathways such as SMAD2/3, PI3K, and JNK. This in turn increases the transcriptional activity of various pro-fibrotic genes such as NOX4, αSMA, and COL I. Increased in NOX4 expression also results in ROS generation, which leads activation of other ROS-dependent signaling transduction pathways such as, NFκB and JNK. Elevated ROS also causes irreversible DNA damage, through oxidization of its bases. Together, enhanced ROS and activated TGF-β signaling contributes to proliferation and transdifferentiation of fibroblast cells into myofibroblast, and excessive ECM deposition leading to fibrosis.

1.1.3 Roles of ROS in cancer

Cancer is the second leading cause of death in the United States and was responsible for 584,872 deaths in 2013 [49]. The number of new cancer cases is estimated to climb to 22 million worldwide within the next two decades [50]. Metastases are the main cause of cancer-related mortality, which accounts for 90% of death in cancer patients [51]. Elevated ROS levels have been detected in most cancer cell lines [52] and have been implicated in malignant progression and resistance to treatment [53]. As highlighted in **Figure 1.3**, ROS plays a critical role in various signaling cascades relating to survival, proliferation, resistance to apoptosis, neovascularization, invasion, and extravasation and growth into a distant metastasis site [54, 55]. The roles of ROS in cancer can be described as follows.

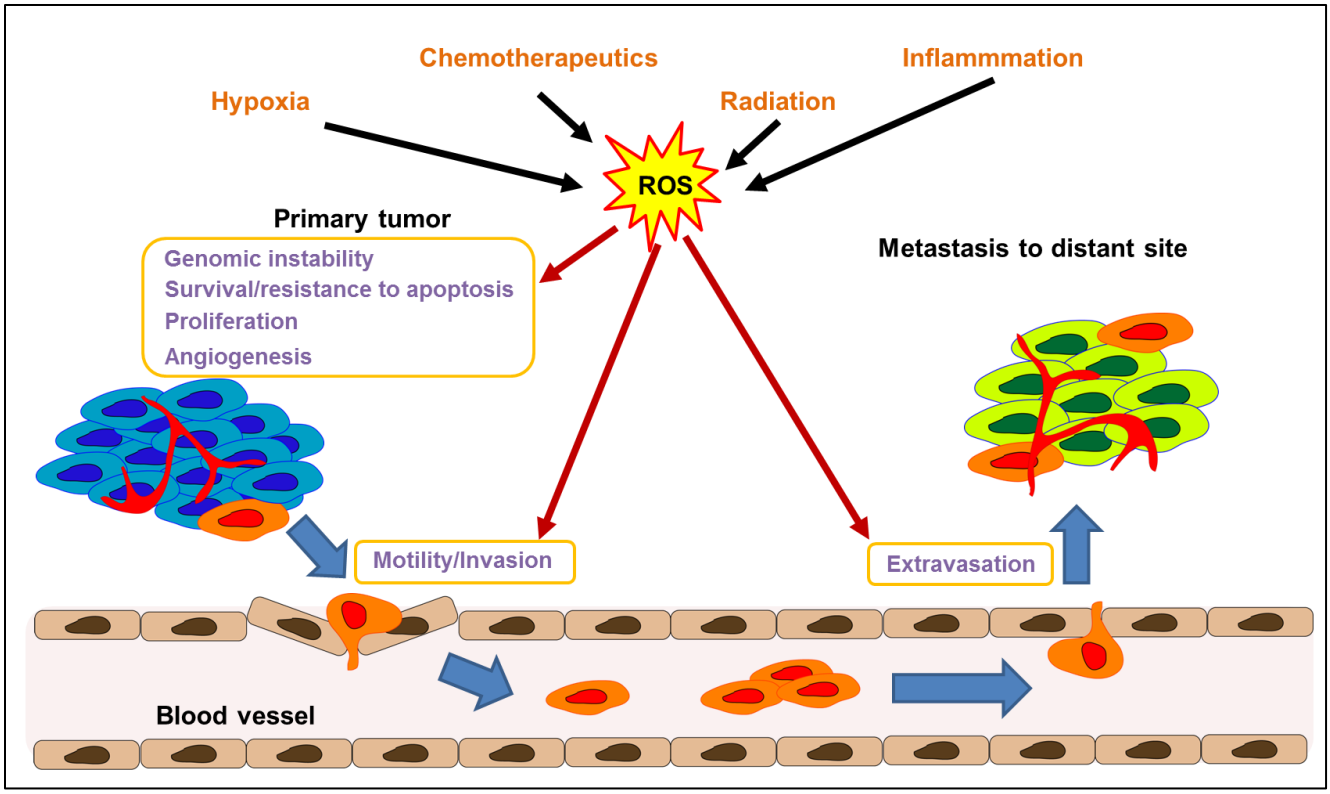

Figure 1.3. ROS plays multiple roles in cancer progression.
ROS generated by multiple sources including chemotherapeutics, radiation, inflammation, and hypoxia conditions contributes to genomic intsability of the cancer cells, survival, resistance to apoptosis, proliferation, angiogenesis, invasion (through invadopodia formation), as well as extravasation into a distant metastasis site.

Effects of ROS on redox-mediated cellular mechanisms. ROS are capable of modifying numerous cellular pathways by altering the DNA binding sites of redox-sensitive transcription factors (such as hypoxia-inducible factor-1 alpha (HIF-1α), NFκB, activator protein-1 (AP-1), and p53), or by oxidizing the cysteine residues on these molecules [48]. At the post-translational level, ROS could also directly oxidize multiple types of amino acids, such as methionine to sulfoxide and cysteine to sulfonic acids [56]. These oxidative modifications on the amino acids will lead to structural and conformational change of the tertiary protein structure, which might cause protein degradation by proteasomes or activation/inhibition of the protein activities. Direct protein carbonylation can also occur through oxidative attack on amino acids involved in catalysis such as lysine, arginine, proline, and threonine, which leads to enzyme inactivation [56].

Role of ROS in genomic instability. ROS generated from either the extracellular/intracellular sources could also lead to DNA damage, which in turns activate a number of stress response genes and DNA repair mechanisms. The redox-sensitive p53 protein is an active transcription factor that is involved in numerous cell processes including cell cycle arrest, senescence, and apoptosis [57]. In the presence of excess ROS, p53 plays a crucial role in preventing the propagation of DNA damage [58]. However, in cancer cells TP53 (gene which encodes p53) is a commonly mutated gene varying from 10% occurrence in diseases such as hematopoeitic malignancies, to close to 100% in high-grade serous carcinoma of the ovary [59]. In these cancers, DNA damage will accumulate more readily due to inadequate DNA repair mechanisms, resulting in gene mutation and/or deletion. The genomic instability will further activate a number of oncogenes resulting in abnormal metabolic activity and decreased

antioxidant production. All these events will eventually lead to an increase in intracellular ROS production in a positive-feedback manner [60].

Role of ROS in tumor hypoxia and angiogenesis. As primary tumors continue to grow, the demand for nutrients and oxygen supply will increase in parallel. However, these demands are not always met in rapidly growing tumors and regions of the tumor will become deprived of oxygen. In order to support tumor growth and proliferation in these hypoxic microenvironments, cancer cells undergo several changes in order to adapt to this oxygen- and nutrient-deprived state, including genotype selections favouring survival (such as TP53 mutation [61]) and activation of hypoxia inducible factor-1 (HIF-1) transcription factor [62]. The HIF family regulates a broad array of genes in response to oxygen deprivation and has been comprehensively reviewed elsewhere [62, 63]. In hypoxic conditions, the hydoxylation of HIF-1α is inhibited which prevents it from being degraded as in normoxic conditions. The HIF-1α then dimerizes with HIF-1β, which later binds to hypoxia response elements (HREs) on the DNA and stimulates the transcription of its target genes, such as vascular endothelial growth factor (VEGF), N-myc downstream-regulated gene (NDRG), and glucose transporter I [64]. These hypoxia-responsive genes are involved in glucose transport, glycolysis, and angiogenesis, allowing cancer cells to survive in such harsh environment. A hypoxic microenvironment also contributes to ROS formation through the release of superoxide, hydrogen peroxide, and hydroxyl radical from the mitochondrial electron transport chain, and ROS, in turn, also stabilizes HIF-1α under both normoxic and hypoxic conditions [65-67].

Interplay between ROS and TGF-β signaling in cancer. Similar to fibrosis, the cross-talk between ROS and TGF-β signaling in cancer has been well-documented and comprehensively reviewed [68-70]. TGF-β1 is one of the most potent cytokines known to contribute to immunosuppression of immune cells and promoting angiogenesis and EMT in cancer cells.

TGF-β1 induces apoptosis in immune cells by directly supressing the production of cytolytic factors in T-cells, inhibiting proliferation and differentiation of numerous immune cells, and decreasing the tumor surface immunogenicity through inhibition of major histocompatibility complex class II antigens [71]. Gorelik et al. showed that T-cell specific blockade of TGF-β signaling could enhance anti-tumor immunity by the generation of CD8+-mediated tumor-specific cytotoxic T-cells response [72].

Tumor angiogenesis is vital for tumor growth and can also facilitate the dissemination of tumor cells. TGF-β plays a critical role in promoting angiogenesis. The TGF-β SMAD-dependent signaling pathway has been shown to induce vascular endothelial growth factor (VEGF) expression. In addition, different levels of TGF-β expression show distinct effects on angiogenesis: at low levels, TGF-β upregulates angiogenic factors including VEGF, CTGF, and fibroblast growth factor (FGF), while at high levels, TGF-β stimulates smooth muscle cells recruitment and cell differentiation, while inhibiting endothelial cell growth [73].

TGF-β is a major inducer of EMT and cell migration through a combination of SMAD-dependent and -independent pathways (e.g., p38 MAPK) [74]. The downstream effects

of the EMT response include transcriptional reprogramming which promotes inactivation of genes (such as E-cadherin) that encodes for epithelial markers and activation of genes for mesenchymal proteins such as N-cadherin and vimentin [75, 76]. Downregulation of E-cadherin is a common feature in many cancers such as metastatic breast cancer [77] and non-small cell lung cancer (NSCLC) [78]. Studies have shown that forced expression of E-cadherin in cancer cells *in vitro* could suppress cellular migration and invasiveness [79], while forced expression of N-cadherin in cancer cells caused the opposite effects [80]. The shift in expression from E- to N-cadherin and their distinctive expression patterns reflects the EMT phenotype, which is associated with cancer malignancy and metastasis [75].

In addition, TGF-β has been identified as a major contributor of intracellular ROS production through NOX4 activation. NOX4-derived ROS has been implicated in the EMT phenotype in pancreatic cancer cells [81], increased cell survival in urothelial carcinoma [82], and increased cellular migration and invasiveness in breast cancer [83] and ovarian cells [84], respectively.

Role of ROS in metastases. Metastasis is the main cause of cancer-related mortality, which accounts for 90% of death in cancer patients [51]. The metastatic cascade, as shown in **Figure 1.3**, is a complex process encompassing multiple steps, which lead to cancer cell dissemination, such as: 1) loss of cellular adhesion, 2) increased motility and invasiveness of cancer cells through ECM, 3) intravasation and entry into the circulation, 4) exit into a distant tissue (extravasation), and 5) colonization of a new foreign environment [51]. ROS can activate several pathways involved in metastasis. For

example, ROS can activate matrix metalloproteinases (MMPs), which can degrade basement membranes and extracellular matrices, facilitating intravasation and extravasation of cancer cells [85]. Furthermore, ROS generated by the NOX family (to be discussed in the next section) was shown to be crucial for the formation of invadopodia, actin-rich membrane protrusions of cancer cells that facilitate pericellular proteolysis and invasive behavior [86]. Reduction of ROS using antioxidant such as N-acetylcysteine (NAC) or NOX inhibitor, DPI, in cancer cells has the ability to decrease cell viability [87], invasion and invadopodia formation [86], suggesting the role of antioxidant in mitigating metastasis.

1.1.4 NOX4: the main source of ROS in fibrosis and cancer

NADPH oxidase (NOX) family and ROS. NOX family is comprised of seven members including NOX1-5 and dual oxidase DUOX1-2, which are among the best-characterized intracellular ROS-generating enzymes (as shown in **Figure 1.4**). All are transmembrane flavoproteins, which generate superoxide by transferring an electron to an oxygen molecule, resulting in superoxide anion ($O_2^{\bullet -}$), which is then either spontaneously (by low pH) or catalytically (by SOD) dismutated to H_2O_2. Most NOXes require additional subunits to be functional. Most NOXes, specifically NOX 1-3, bind to the transmembrane protein p22phox, which further recruits cytosolic regulatory subunits such as organizers (p47phox, p40phox, or NOXO1), activators (p67phox or NOXA1), and small GTPases (Rac1 or Rac2) [88, 89]. NOX4, being the exception, only needs to bind to p22phox and does not require cytosolic subunits for maximal oxidase activity. In addition, H_2O_2, not superoxide anion, seems to be the predominant species that is

detected in NOX4. NOX1-5 are mostly located at the plasma membrane of the cell, with NOX4 being additionally detected in the endoplasmic reticulum (ER), mitochondrial membrane, nuclear membrane, focal adhesions, and invadopodia [89]. Extensive details on the structure and activation of NOX isoforms have been reviewed elsewhere [4, 90, 91].

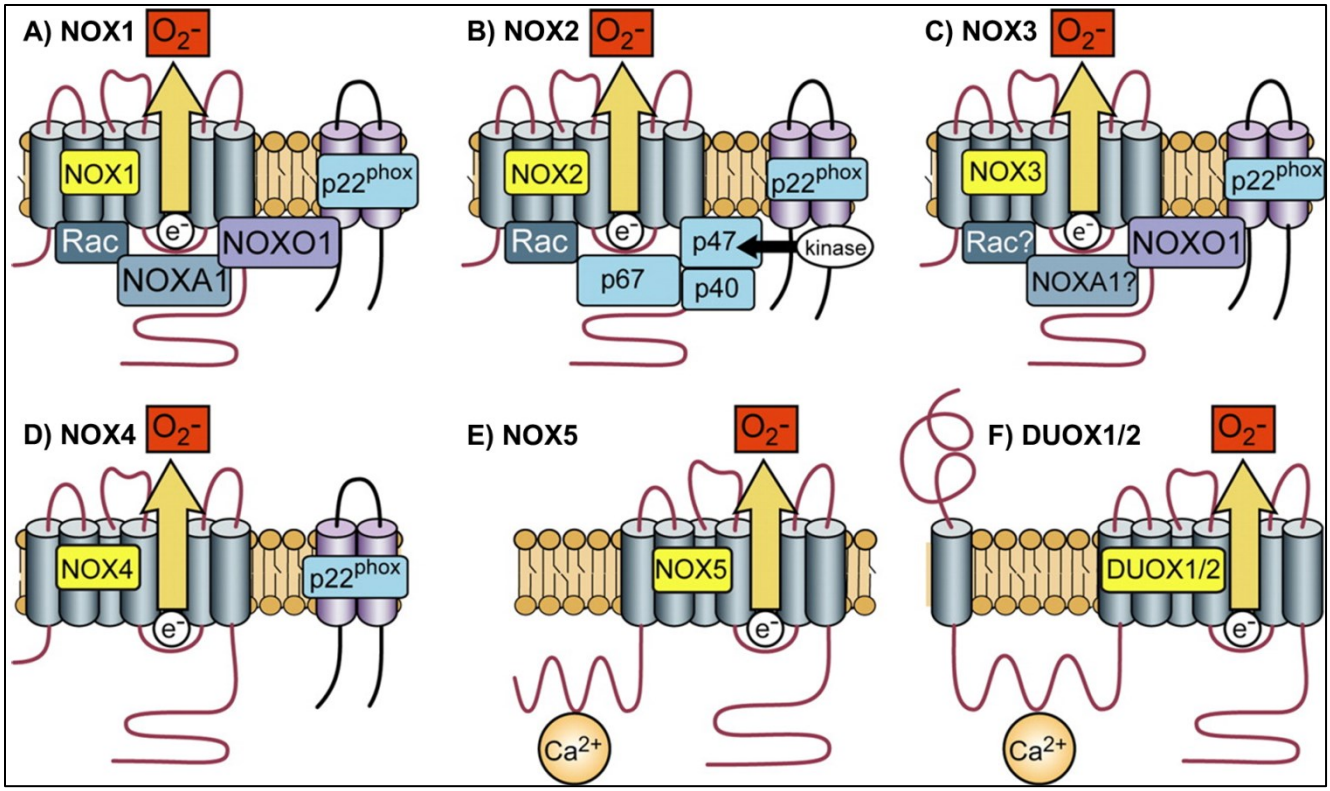

Figure 0.1. Structure of NADPH oxidase family.
A) NOX1 activity requires p22phox, NOXO1 and NOXA1, and the small GTPase Rac. B) NOX2 requires p22phox, p47phox, p67phox, and Rac. C) NOX3 requires p22phox and NOXO1. D) NOX4 requires p22phox, it is constitutively active without the requirement for other cytosolic subunits. E and F: NOX5, DUOX1, and DUOX2 are activated by Ca^{2+} and do not appear to require subunits. Adapted from Physiological Reviews [4].

High NOX4 expression in fibrosis. NOX4 mRNA expression has been found to be upregulated in both pulmonary fibroblasts isolated from idiopathic pulmonary fibrosis (IPF) patients [92] and skin fibroblasts from scleroderma patients [93], as well as in a number of *in vivo* fibrosis models, including liver fibrosis [94], pulmonary fibrosis [95, 96], diabetic neuropathy (kidney fibrosis associated with diabetes mellitus) [97].

As mentioned in the previous section (**section 1.1.2**), TGF-β signaling is the major contributor to fibrogenesis. TGF-β upregulates NOX4 expression through 2 major pathways: the canonical SMAD2/3 [92, 98] and non-canonical PI3K pathways [99, 100]. Inhibition of TGF-β signaling using pharmacological inhibitors for SMAD3 or PI3K abrogated NOX4 expression, suggesting that NOX4 expression is downstream of SMAD [101] and/or PI3K [100] pathway. Suppression of NOX4 activity with a NOX inhibitor diphenyleneiodonium chloride (DPI), siRNA, or the antioxidant N-acetylcysteine (NAC), was shown to decrease the expression of alpha smooth muscle actin (α-SMA) and collagen I (COL I) in fibroblasts collected from pulmonary fibrosis patients and in a bleomycin-induced lung injury mouse model [92, 96].

High NOX4 expression in cancer. High expression of NOX4 has been detected in several cancer types including gliomas [89], melanoma [102], breast cancer [103], ovarian cancer [103], and pancreatic cancer [81]. In cancer cell lines, elevated levels of NOX4 are associated with PI3K/Akt-regulated cell proliferation and invasion [104], TGF-β/SMAD3-driven EMT and cell migration [101], as well as Tks5-dependent invadopodia formation [105]. Depletion of NOX4 with siRNA treatment significantly reduced tumor growth in the *in vivo* models of bladder cancer [82], renal cancer [106], and

glioblastoma [63]. These results suggest that NOX4-derived ROS is a potential target for pharmacological intervention for cancer treatment.

1.2 Strategies to suppress oxidative stress

Antioxidants have been commonly described as substances that can delay, prevent or remove oxidative damage to a target molecule [107]. Given that fibrotic and cancer cells generally present with higher oxidative stress levels than normal cells, it is believed that patients who suffers from those diseases will benefit from antioxidant supplementation.

1.2.1 Dietary antioxidant supplements

Dietary antioxidants including vitamin C (ascorbic acid), vitamin E (tocopherol), vitamin A (β-carotene), and selenium have the ability to counteract oxidative damage and can be obtained through food components such as fruits and vegetables.

Vitamin C is water-soluble and strong antioxidant. Vitamin C exists in two forms: L-ascorbic acid and the oxidized form, dehydro-L-ascorbic acid. It can directly react with hydroxyl and lipid peroxyl radicals to form H_2O and lipid hydroperoxides. Vitamin C can also neutralize vitamin E and glutathione radicals, and regenerate these antioxidants [108].

Vitamin E exists in at least 8 different isoforms (α-, β-, γ-, δ-tocopherols, and α-, β-, γ-, δ-tocotrienols), which differ only in the number of methyl groups and in the side chains of its aliphatic tails [109]. Only α-tocopherols isoform is the most retained in the body due to the preferential transfer of α-tocopherol to the lipid particles by a liver α-tocopherol transfer protein. The main role of vitamin E is to act as a chain-breaking antioxidant, which prevents the propagation of lipid peroxidation [110].

Vitamin A is a fat-soluble vitamin and usually found in the diet as preformed vitamin A from animal products such as meat and fish, and as pro-vitamin A from plant-based products such as fruits and vegetable. β-carotene has the highest provitamin A activity which is further metabolized to retinoic acid and retinol, the active form of vitamin A. β-carotene can physically quench $^1O_2$ and protect organisms from oxidative damage [111].

Selenium is an essential trace element which can be acquired from the diet by the consumptions of nuts, meats, and fish. It is co-translationally incorporated into amino acids such as selenocysteine and selenomethionine [112]. The selenium-containing amino acids act as antioxidants by scavenging free radicals and repairing oxidized selenium species.

A few clinical trials (summarized in **Table 1.1**) have been conducted, mainly using the synthetic form of these antioxidants on healthy and at-risk populations [113-122]. These observational studies were designed to provide evidence on the benefit of antioxidant supplementation for reducing or lowering the risk of patients developing or dying from cancer. However, most of the data were inconclusive, with the majority showing no

protection or exhibiting harmful effects in the patient cohort. It is possible that this lack of benefit is due to: 1) the difference in the chemical composition of antioxidants found in food compared to those in supplements, 2) the disease-specificity of certain antioxidants (i.e. some antioxidants are more effective than the others in protecting against certain types of diseases), or 3) due to the low bioavailability, these supplements could not reach sufficient intracellular levels to be effective [123]. Therefore, a more potent antioxidant that can be delivered to a specific diseased tissue and with improved bioavailability is thought to be more beneficial than these antioxidant supplements.

1.2.2 Enzyme related antioxidants

Glutathione (GSH), N-acetylcysteine (NAC), and superoxide dismutase (SOD) are enzyme related antioxidants that act as the first-line defense against cellular oxidants. The effects of these molecules have also been investigated in several clinical trials (see **Table 1.2**), and the results from these studies will be discussed in details below.

GSH and NAC. is the main non-protein thiol in cells which acts as a reducing agent and is essential in regulating cellular redox status. GSH is involved in cell protection against free radical and many other cellular functions [124]. GSH is also critical for the regeneration of other antioxidants such as tocopherols and ascorbate [125]. NAC is a cysteine precursor that replenishes the intracellular levels of GSH [126]. A few clinical trials have been conducted with either GSH or NAC as interventions for fibrotic diseases, such as liver fibrosis [127, 128] and lung fibrosis [129, 130], as well as cancers such as head and neck cancer or lung cancer [118]. However, the data have been largely

disappointing, with most of them showing no beneficial effects. This is mostly contributed to the low bioavailability of GSH and NAC. GSH is known to be poorly absorbed when ingested due to the action of the intestinal enzyme, γ-glutamyl transpeptidase which degrades GSH [131]. High dose of NAC is impossible to achieve *in vivo* without toxicity concerns. For instance, an estimated 5010 mg/kg loading dose (within the first 60 min) and 2250 mg/kg maintenance dose (for the next 4 hr) are needed to reach 10 mM concentration in blood based on the pharmacokinetic data of NAC in human volunteers [132], but NAC is usually prescribed at a much lower dose of only 150 mg/kg loading dose and 50 mg/kg maintenance dose (i.v.) (NAC, Acetadote®, package insert) or 600-mg oral dose (three times daily) for pulmonary fibrosis patients in the PANTHER-IPF trial [133] .

SODs are metal-containing proteins that catalyze the conversion of superoxide to hydrogen peroxide. Three isoforms have been identified, namely, cytosolic Cu-Zn SOD (SOD1), mitochondrial Mn-SOD (SOD2), and extracellular SOD (SOD3). The cytosolic and mitochondrial SODs have been indicated in multiple studies as a tumor suppressor gene. Overexpression of MnSOD was able to suppress the malignancy of human breast cancer cells [134, 135], glioma cells [136], and melanoma cells [137]. In contrast, depletion of MnSOD resulted in increased cell proliferation *in vitro* and contributed to more aggressive tumor growth *in vivo* [138]. Similarly, overexpression of Cu-Zn-SOD could also decrease tumor growth in multiple cancer types [139].

SOD overexpression has been shown to confer protection against radiation and display chemopreventative effects in *in vivo* cancer models. Pre-clinical studies in mouse

models have shown that intraoral delivery of Mn-SOD2 plasmid/liposomes (MnSOD-PL) decreased irradiation-induced murine mucosal ulceration [140] as well as esophagitis [141]. Based on the results from these pre-clinical studies, the chemoprotective effects of MnSOD-PL were investigated in radiation/chemotherapy-induced esophagitis in NSCLC patients (see **Table 1.2**). Overall, in the phase I clinical trial study, the response rate for the chemoradiation regime was satisfying at 70% and the treatment was safe and well-tolerated [142]. Unfortunately, the Phase II study was later suspended (reason unknown). In another study, topical delivery of liposomal human recombinant Cu-Zn SOD1 (APN 201) was tested on 20 female breast cancer patients who received radiation therapy [143]. The goal of this study was to investigate the potential use of APN 201 in preventing radiation-induced dermatitis in breast cancer patients who undergo radiotherapy after surgery. The topical treatment of Cu-Zn SOD1 was able to reduce pain in the fibrotic region in more than 90% of the cases and decreased the fibrotic size by half in 30% of the patients [143].

Overall, these studies show some promising results in the chemoprotective effects of the SODs. That said, no clinical trial has been conducted so far to investigate the effectiveness of SODs in combatting cancer growth in humans; however, several SODs mimetics have been shown to be beneficial in the pre-clinical model of prostate [144] and breast cancer [145].

1.3 Inhibiting NOX enzymes

Currently, a few nonspecific NOX inhibitors have been identified (which target more than one NOX isoforms) [94, 146-151]. Some issues with specificity, potency, and toxicity of these inhibitors have limited the value of these compounds to be used in clinical studies [152]. Gene silencing of NOXes has been carried out with shRNA and siRNA [82, 104, 153] but primarily as a proof-of-concept in *in vivo* studies without using suitable delivery agents such as liposomes or nanoparticles to safely and efficiently deliver these molecules to the right target. The different types of NOX inhibitors as well as NOX gene therapeutics, and their potential applications from the in-vivo studies are summarized in **Table 1.3**.

Diphenyleneiodonium (DPI) is a nonspecific inhibitor for NOX enzymes. It inhibits a number of flavoproteins including eNOS, xanthine oxidase, and cholinesterases and the internal calcium pump [154]. Although at least two pre-clinical studies using DPI have shown positive results on lung cancer inhibition [146] as well as skin fibrosis reduction [147], the off-target effects of DPI against other flavoproteins will prevent its translation into clinical use.

Fulvene-5 is a water-soluble small molecule inhibitor for NOX2 and NOX4 enzymes. It has an aromatic structure which allows electron delocalization. Treatment of Fulvene-5 on bEnd.3 endothelioma cells (hemangioma) *in vivo* significantly reduced tumor growth and was largely attributed to NOX4 inhibition [148]. Hemangioma is the most common type of benign tumors which occurs in approximately 5-10% infants [155] .

Celastrol is a compound extracted from Thunder God Vine (Tripterygium wilfordii Hook F.) which could inhibit NOX1, 2, 4, and 5 [149]. Treatment of celastrol on mouse melanoma B16F10 and human lung cancer 95-D cells inhibits cell migration as well as invasion in a dose-dependent manner, without affecting cell viability [150]. The anti-metastatic effect of celastrol was further demonstrated in the B16F10 experimental metastasis model in mice with the reduction in pulmonary nodules.

Imipramine blue is an organic triphenylmethane blue dye which has been used as a derivative for the antidepressant drug, imipramine. It has been shown to target NOX4, however there was insufficient characterization data provided regarding its selectivity on other NOX isoforms. One study has hypothesized that due to its cationic charge, it is likely that imipramine blue exerts its NOX inhibition extracellularly [156]. Treatment with imipramine blue *in vivo* resulted in tumor inhibition of human glioma cells as well as enhance treatment efficacy in combination with chemotherapy, doxorubicin [157]. In another study, imipramine blue treatment in head and neck squamous cell carcinoma (HNSCC) tumor in mice inhibited tumor invasion and metastatic colonization in the lungs [158].

GKT136901 and GKT137831 are both small molecule inhibitors developed by the French biotech company, Genkyotex. Both compounds have high specificity to NOX1 and 4 (and less for NOX2 and 5). Both compounds show therapeutic potential in reducing liver fibrosis and tumor growth in mice [94, 151, 159]. GKT137831 is currently a lead compound undergoing Phase II clinical trials in diabetic kidney disease (NCT02010242). The preliminary results from this clinical trial showed that patients receiving treatment for 12 weeks had few adverse effects than placebo. However, the

primary efficacy endpoint was not achieved due to negligible change in albuminuria (Genkyotex press release, September 2015).

NOX4 shRNA/siRNA. NOX4 gene silencing using siRNA or shRNA has shown good results in terms of tumor reduction in multiple cancer types including NSCLC, hepatocarcinoma, and bladder cancer [82, 104, 153] as well as reduction in pulmonary fibrosis [96]. However, delivering siRNA into the target cells requires a delivery agent, such as atelocollagen [82], since siRNA is unstable under physiological conditions.

Table 0.1. Antioxidant supplementation in clinical trials

Name of trials	Type of antioxidants	Target population	Length of study	Conclusion of the study	Ref
Linxian general population nutrition intervention trial	15 mg beta-carotene, 30 mg alpha-tocopherol, and 50 µg selenium daily	29,584 healthy Chinese men and women in North China at increased risk of developing esophageal cancer and gastric cancer were recruited	5 years	reduction in cancer mortality associated with gastric cancer, but not esophangeal cancer	[113]
Alpha-Tocopherol/Beta-Carotene Cancer Prevention Study (ATBC)	alpha-tocopherol (50 mg/day) or beta-carotene (20 mg/day) or both	29,133 male smokers in Finland	5-8 years	no overall reduction in the incidence of lung cancer or in mortality in all treatment groups	[116]
Carotene and Retinol Efficacy Trial (CARET)	30 mg of β-carotene plus 25 000 IU of retinyl palmitate daily	816 men with substantial occupational exposures to asbestos and 1029 men and women who were either current or former cigarette smokers in United States	6-12 years	beta-carotene supplementation was associated with increased lung cancer incidence and all caused mortality which persisted up to 6 years after the supplementation was ended	[119]
				12 year study showed that beta-carotene had no effect on lung cancer incidence or mortality rate in smokers *vs*. non-smokers	[122]
Physicians' Health Study I (PHS I)	50 mg β-carotene every other day	22,071 male physicians between age of 40-84 years in the United States	12 years	supplementation did not reduce the incidence of prostate cancer or other cancers, including lymphoma, leukemia, melanoma, and cancers of the lung, bladder, pancreas, and colon and rectum	[120]

Table 1.1. (continued)

Name of trials	Type of antioxidants	Target population	Length of study	Conclusion of the study	Ref
Physicians' Health Study II (PHS II)	400 IU vitamin E every other day, 500 mg vitamin C every day, 50 mg β-carotene or in combination	14,642 male physicians older than 50 years old in the United States	8 years	daily multivitamin use was associated with a reduction in total cancer among 1312 men with a baseline history of cancer, but did not differ significantly from that among 13 329 men initially without cancer	[115]
Women's Health Study (WHS)	50 mg β-carotene every other day, vitamin E supplementation (600 IU every other day), and aspirin (100 mg every other day)	39,876 women aged 45 years or older	2 years	no benefit or harm associated with 2 years of beta-carotene supplementation	[121]
Selenium and Vitamin E Cancer Prevention Trial (SELECT)	daily supplementation with selenium (200 μg), vitamin E (400 IU), or both	35,533 men from 427 participating sites in the United States, Canada, and Puerto Rico	7 years	the use of supplements did not reduce the incidence of prostate or other cancers	[115]
			8.5 years	after 1.5 years post supplementation, the follow-up study found 17% increase in prostate cancer incidence among men taking vitamin E alone than among men taking a placebo	[114]

Table 0.2. Synthetic antioxidant in clinical trials

Drug name	Type	Disease	Sponsor	Phase	Study Outcome	Current status	Identifier/Ref
Glutathione (GSH)	GSH	Liver fibrosis	Royal Free Hospital London	N/A	no benefit in oral glutathione in hepatic cirrhosis patients	Completed	[127]
N-acetylcysteine (NAC)	Precursor of glutathione (GSH)	Idiopathic Pulmonary Fibrosis (IPF)	Zambon SpA	III	no increased survival and no significant difference between treatment arms at 12 months	Completed	NCT00639496 [130]
			Duke University	III	no benefit over placebo	Completed	NCT00650091 [133]
		Head and neck cancer, lung cancer	The Netherlands Cancer Institute, Amsterdam	N/A	no benefit shown in survival, event-free survival, or second primary tumors-for patients	Completed	[118]
MnSOD plasmid/liposome	Intraoral MnSOD-plasmid liposome (PL) gene therapy	Radiation-induced esophagitis in Advanced Stage III Non-small cell lung cancer	University of Pittsburgh	I/II	oral administration of MnSOD PL was safe and tolerable	Suspended (reason unknown)	NCT0061897 [142]
APN201	Topical administration of Liposomal Recombinant Human Cu/Zn-Superoxide Dismutase	Radiation-induced Dermatitis in Women With Breast Cancer	Apeiron Biologics	I/II	topical treatment was well tolerated with lower pain score in 36/39 patients and decreased fibrotic size in 50% of the cases	Completed	NCT01513278 [143]

Table 0.3. NOX inhibitors and its pre-clinical applications

Type	Name	NOX specificity	*In vivo* Route	Application	Ref
small molecule	diphenyleneiodonium (DPI)	All types of NOX	i.v.	inhibition of A549 human lung cancer metastasis in mice	[146]
			i.p.	attenuation of skin fibrosis in bleomycin-induced mouse model	[147]
small molecule	Fulvene-5	NOX1, NOX4	i.p.	inhibition of hemangioma growth in mice	[148]
small molecule	Celastrol	NOX1, NOX2, NOX4, NOX5	i.p.	inhibition of B16F10 lung cancer metastasis *in vivo*	[149, 150]
small molecule	Imipramine blue	NOX4, insufficient characterization data for other NOXes	i.v.	inhibition of HNSCC cancer invasion in mice	[158]
				inhibition of RT2 glioma invasion in rats	[157]
small molecule	GKT136901	NOX1, NOX2, NOX4, NOX5	p.o.	inhibition of tumor growth in B16F0 melanoma and Lewis Lung Carcinoma (LLC1) xenograft in mice	[159]
small molecule	GKT137831	NOX1, NOX2, NOX4, NOX5	p.o.	reduction of liver fibrosis in CCL_4-induced and BDL mouse models	[94, 151]
shRNA	NOX4	NOX4	N/A	inhibition of tumor growth in NOX4-shRNA transfected NSCLC cells, A549 and H460	[104]
			N/A	inhibition of tumor growth in hepatocarcinoma (Hep3B) xenograft in mice	[153]
siRNA	NOX4	NOX4	single intravesical delivery (with Atelocollagen)	inhibition of tumor growth in orthotopic bladder carcinoma	[82]
			i.t.	attenuation of pulmonary fibrosis in bleomycin-induced mouse model	[96]

Note: intravenously (i.v.), intraperitoneally (i.p.), per os (p.o.), or intrathecally (i.t.)

1.4 Nanoparticles with intrinsic antioxidant properties

Nanotechnology has become a main focus of biomedical research in recent years. Several types of inorganic nanoparticles possess intrinsic antioxidant properties by scavenging free radicals and decreasing ROS concentrations. In this section, these inorganic nanoparticles will be discussed and summarized in **Table 1.4**.

1.4.1 Cerium oxide (CeO_2)

Cerium is a rare-earth element, which belongs to the lanthanide series in the periodic table. It can exist in both, Ce^{3+} and Ce^{4+} valence states which give it the unique ability as an antioxidant [160]. The ROS-scavenging capability of CeO_2 depends on the relative thermodynamic efficiency of redox cycling between Ce^{3+} and Ce^{4+} on the nanoparticle surface. Giri et al. reported that treatment of CeO_2 nanoparticles attenuated tumor growth in A2780 ovarian cancer mice and significantly inhibited the metastasis of these cancer cells into the lungs of mice [161]. They also found that angiogenesis in the tumor was reduced among treated mice as indicated by less CD31-positive staining. The same group also reported that surface-functionalization of CeO_2 nanoparticle with folic acid and its co-delivery with cisplatin could further decrease the tumor burden and angiogenesis [162]. In separate studies, CeO_2 nanoparticle administration to carbon-tetrachloride (CCl_4)-induced liver fibrosis mice was shown to inhibit oxidative [163, 164] and endoplasmic reticulum stress signaling pathways as well as reduction in inflammatory cytokines such as TNF-α and IL-1β [163].

1.4.2 Fullerene C60

Fullerene is a sphere-like molecule composed of 60 carbon atoms which are arranged in a hexagonal formation to form a hollow spherical structure. It is a powerful antioxidant due to the delocalization of the π-electrons over the carbon atoms which can readily react with free radicals [165]. Fullerene is also known to be capable of inactivating hydroxyl radicals via attachment to its double bonds [166]. Due to these attractive antioxidant properties, fullerenes and its derivatives have been studied in numerous biomedical applications including fibrosis and cancer. Prophylactic treatment of fullerene in CCl_4-induced hepatic injury rat model prevented damage in the liver and kidney of the rats [167]. Another study has also shown that co-treatment of Doxorubicin chemotherapy drug with fullerene resulted in inhibition of tumor growth and metastasis, and increased survival in LLC tumor-bearing mice [168].

1.4.3 Platinum nanoparticles (PtNP)

Platinum nanoparticles (PtNPs) are known to possess ROS scavenging ability due to the catalytic activity contributed by its high ratio of electrons to particle surface [169]. PtNPs have demonstrated its therapeutic potential in several pre-clinical applications such as treating aging-related skin disease in SOD1 knockout mice [170], protection against UV-induced apoptosis in HaCaT keratinocytes [171], and prevention of hepatic injury from hepatic ischemia/reperfusion injury in mice [169].

1.4.4 Mesoporous silica nanoparticles (MSNP)

Mesoporous silica nanoparticles (MSNP) have been reported to have reactive oxygen species (ROS), hydroxyl radical, and free radical scavenging capability [24, 25, 172]. ROS scavenging by MSNP also attenuates NOX4 mRNA expression in melanoma cells *in vitro* [25]. Thus, MSNPs have great potential in the treatment of oxidative-induced pathological conditions such as fibrosis and cancer.

1.5 Mesoporous silica nanoparticles as siRNA delivery agent

In recent years, the RNA interference strategy has attracted great interest due to its therapeutic potential in silencing disease-related genes with high specificity, thus minimizing off-target effects commonly associated with small molecule inhibitors. Although promising, the utility of siRNA as a therapeutic agent has been hindered by its poor cellular uptake and short half-life [21]. Recently, silica nanoparticles have emerged as one of the more promising gene delivery agents for treatment of various preclinical cancer disease models upon systemic siRNA delivery [22, 23].

MSNP delivery carriers have many favorable attributes, such as tailorable mesoporous structures, high surface areas, large pore volumes, ease of controlling size, and high scalability. MSNP is soluble in physiological pH to non-toxic silicic acid, which can be cleared by the kidneys [173]. MSNPs have been widely researched for drug and imaging agent delivery. Silica nanoparticles with PET tracers have also recently entered a clinical trial with a favorable safety profile (Cornell dots) [174].

In addition, MSNP have been widely researched for siRNA delivery *in vitro* and *in vivo*. We recently reported a MSNP-based platform, coated with cross-linked PEI, PEG, and conjugated with the antibody trastuzumab for targeted systemic delivery of HER2 siRNA (siHER2) to HER2+ breast cancer [175]. The results from this study suggested that the nanomaterial has the ability to systemically deliver the siHER2 effectively to its target cells, the HER2-positive breast cancer, and induce apoptosis to prevent tumor growth in the orthotopic mouse model. In addition, a number of *in vitro* studies with MSNPs have demonstrated its ability to decrease reactive oxygen species (ROS) [24, 25, 176] and attenuate NOX4 mRNA expression in melanoma cells *in vitro* [25]. Thus, MSNPs have great potential in the treatment of oxidative-induced pathological conditions such as fibrosis and cancer.

Furthermore, MSNPs have demonstrated an excellent safety profile compared to other types of nanomaterials. This is largely due to silica being an endogenous substance which is present in our tissues such as bone and cartilage. Silica is generally regarded as safe (GRAS) by the Food and Drug Administration (FDA) and is often used as excipient for drug formulations [177]. In addition, numerous studies have also shown great *in vitro* [175, 178] and *in vivo* [179-181] biocompatibility of silica nanoparticles. It has also been reported that injected MSNP could be degraded into nontoxic material such as silicic acid salts and excreted in the urine of animals [181, 182]. These features are desirable since it will prevent long-term toxicity issues of the nanomaterials *in vivo*.

Table 0.4. Summary of different nanoparticles with intrinsic antioxidant properties and their mechanism of action

Types of nanoparticles	Mode of actions	*In vivo* Route	Applications	Ref
Cerium oxide nanoparticle (CeO2)	regenerative capacity of the $Ce^{3+/}Ce^{4+}$ redox couple	i.p.	inhibition of tumor growth and metastasis in A2780 ovarian cancer in mice	[161, 162]
		i.v.	reduction of oxidative stress in CCl_4-induced liver fibrosis in mice	[163, 164]
Fullerene	presence of π-electrons over the carbon atoms	i.v. , i.p.	protection from liver injury in CCl_4-induced acute hepatoxicity and nephrotoxicity rat models	[167]
		i.p.	inhibition of tumor growth and metastasis in LLC xenograft mouse models (when co-delivered with doxorubicin)	[168]
Platinum nanoparticles (PtNP)	catalytic activity due to high ratio of electrons remaining on the particle surface	i.v.	prevention of hepatic injury after hepatic ischemia/reperfusion in mice	[169]
Mesoporous silica nanoparticles (MSNP)	free radical scavenger, reduction of NOX4 expression in cells	i.d.	attenuation of dermal fibrosis in bleomycin-induced scleroderma mouse model	[172]

Note: i.p. (intraperitoneal), i.v. (intravenous), i.d. (intradermal)

1.6 Scope of the dissertation

Our group has recently developed and optimized a polymer-coated mesoporous silica nanoparticle (NP) for siRNA and drug delivery. The platform consists of a 50-nm mesoporous silica nanoparticle (MSNP) core coated layer-by-layer with bioreducible cross-linked 10-kDa polyethyleneimine (PEI) for effective siRNA binding and endosomal escape, and polyethylene glycol (PEG) for preventing nanoparticle aggregation, minimizing enzyme degradation of siRNAs, shielding the toxic effect of PEI, and preventing recognition by the immune system.

The focus of this dissertation is to evaluate the antioxidant activity and siRNA delivery efficiency of our NP platform for the treatment of fibrosis and cancer metastasis. My first project is to investigate the intrinsic antioxidant property of our MSNPs and assess the added benefit of silencing heat shock protein (HSP47) as a gene target in a skin fibrosis model. HSP47 is a collagen-specific molecular chaperone that presides in the endoplasmic reticulum and binds to the procollagen molecule to ensure its proper assembly into triple helix structure before secretion into the extracellular space. Overexpression of HSP47 has been observed in fibrotic tissues of patients suffering from systemic sclerosis, dermal, kidney, lung and liver fibrosis. Thus, reducing HSP47 levels could potentially hinder collagen accumulation and halt the progression of fibrosis. This work is presented in **Chapter 2**. In this work, I describe the roles of ROS, NOX4 and HSP47 in fibrogenesis and applied the nanoparticle platform to modulate all three effectors in order to treat fibrosis. I also showed that the MSNP nanoparticles efficiently delivered siRNA to knock-down HSP47 expression *in vitro* and *in vivo*. In addition, the nanoparticle carrier itself reduced ROS and NOX4 production, owing to the antioxidant

property of the MSNP core that was far superior to the antioxidant NAC. The therapeutic impact of MSNP was further enhanced by the addition of siRNA against HSP47 as demonstrated in the bleomycin-induced skin fibrosis mouse model.

The second part of my project involves systemic delivery of polo-like kinase 1 (PLK1) siRNA with NP for the treatment of metastatic breast cancer. PLK1 was chosen as the gene target for this project due to its role as the key regulator in mitotic cell division and its implication in the initiation and progression of various cancer types, including triple negative breast cancer (TNBC). In adults, PLK1 is only expressed in fast proliferating cells which make it a potential gene target for cancer therapy. This work is presented in **Chapter 3**. My results demonstrate that MSNP treatment inhibits cellular migration and invasion, and attenuates outgrowth of 3-D organotypic cultures of TNBC cell lines *in vitro*. Targeted delivery PLK1 siRNA on our MSNP platform to the TNBC metastasis model impedes tumor proliferation and promotes cancer apoptosis in the lungs of mice.

Finally, in **Chapter 4**, I will summarize results of **Chapter 2** and **3**, propose future directions by providing some of the preliminary results pertaining to these projects, and discuss the future applications of the NP stemming from my work in this dissertation.

Chapter 2: Dermal delivery of HSP47 siRNA with NOX4-modulating mesoporous silica-based nanoparticles for treating fibrosis

This chapter describes the application of polymer-coated mesoporous silica nanoparticles as antifibrotic therapy in bleomycin-induced skin fibrosis mouse model. A version of this chapter has been previously published:

Morry J, Ngamcherdtrakul W, Gu S, Goodyear SM, Castro DJ, Reda MM, et al. Dermal delivery of HSP47 siRNA with NOX4-modulating mesoporous silica-based nanoparticles for treating fibrosis. Biomaterials 2015; 66:41-52.

2.1 Introduction

As mentioned in **Chapter 1**, fibrosis is a complex disease characterized by increased oxidative stress [183, 184], persistent inflammation [185, 186], elevated levels of profibrotic and proinflammatory cytokines [187-189], and an excessive synthesis and accumulation of extracellular matrices mainly consisting of collagen [188, 189]. Fibrosis can occur in a wide spectrum of organs (e.g., lung, liver, skin, heart), and if left untreated can result in organ failure and death [36]. Notably, nearly 45% of all naturally-occurring deaths in the western world are attributed to some form of fibrotic disease [36, 190]. Current approaches to treating fibrosis in patients have mainly focused on antagonizing fibrosis-associated inflammation using drugs such as corticosteroids which is often ineffective [191] and lead to unwanted side effects with long term use [192, 193]. Several clinical studies have focused on either suppressing oxidative stress (e.g., with

N-acetylcysteine (NAC) [133], α-tocopherol (vitamin E) [117]) or reducing pro-fibrotic cytokines/genes (e.g., with monoclonal antibody against TGF-β [194], tyrosine kinase inhibitor, imatinib [195]). However, these attempts have not provided a satisfactory therapeutic index.

I hypothesize that managing both pro-fibrotic genes along with oxidative stress may have greater impact for treating fibrosis than managing just one factor. A nanoparticle platform could be designed to accomplish both. Recently, several inorganic nanoparticles (nickel [196], platinum [197-199], ceria [200, 201], yttria [201] and mesoporous silica [25, 202]) have been shown to possess intrinsic antioxidant properties. Among them, mesoporous silica nanoparticles (MSNPs) are considered the most promising due to their high biocompatibility (low toxicity *in vivo* as well as the ability to be degraded into soluble silicic acid species and cleared by the kidneys) [26, 203, 204] and ease of surface modification. Furthermore, MSNPs have been shown to decrease reactive oxygen species (ROS) [25, 176, 202] and attenuate NOX4 mRNA expression in melanoma cells *in vitro* [25]. NOX4 is an enzyme which provides the endogenous source of ROS by catalyzing the reduction of oxygen in cells to hydrogen peroxide [205] (**Figure 2.1**) and has also been implicated in the pathogenesis of various organ fibroses such as liver [151], lung [92, 183, 206] and dermal fibrosis [207, 208]. NOX4 can also be generated downstream of the TGF-β pathway [209], activated in the presence of ROS-producing inflammatory cells (e.g., neutrophils, macrophages) [187] during fibrosis as shown in **Figure 2.1**. Suppression of NOX4 activity with a NOX inhibitor diphenyleneiodonium chloride (DPI) [92, 206], siRNA [92, 206] or the antioxidant N-acetylcysteine (NAC) [92], were shown to decrease the expression of

alpha smooth muscle actin (α-SMA), and collagen I (COL I) in fibroblasts collected from pulmonary fibrosis patients [92] and in a bleomycin-induced lung injury mouse model [206]. Thus, I hypothesize that MSNP can remove ROS from the vicinity of the fibrotic tissue and alleviate fibrosis by reducing NOX4-associated fibroblast activation and proliferation.

The other benefit of MSNPs is their versatility as a delivery platform for drugs and small interfering RNA (siRNA). Gene silencing using siRNA has long been employed to study the roles of genes in various biological pathways. Although promising, the utility of siRNA as therapeutic agents has been hindered by their poor cellular uptake and the short half-life of siRNA [21]. Multiple MSNP-based platforms for siRNA delivery have been tested for cancer treatment [22, 23, 210, 211]. We have constructed an MSNP-based platform with optimized particle size and chemical modification to overcome barriers of systemic siRNA delivery to solid breast tumors [175]. Specifically, we utilized a co-polymer of PEI-PEG coating on the surface of 50nm-MSNP core to create MSNP-PEI-PEG nanoparticles. The PEI layer electrostatically binds the negatively-charged siRNA and the PEG layer protects siRNA from enzymatic degradation. Antibody has been attached at the end of PEG for targeted delivery [175]. Because siRNA is loaded last and resides on the outer surface, we can tailor the nanoconstructs for any gene target deemed essential for disease progression, enabling personalized medicine.

In this study, we harness the intrinsic antioxidant property of the MSNPs while assessing the added benefit of a gene silencing strategy to combat fibrogenesis. We chose heat shock protein 47 (HSP47) as the initial siRNA target because it plays an important role in collagen homeostasis (**Figure 2.1**). HSP47 is a collagen-specific

molecular chaperone which presides in the endoplasmic reticulum and binds to procollagen molecules to ensure its proper assembly before secretion into the extracellular space [212]. Elevated levels of HSP47 have been particularly observed in fibrotic tissues of patients suffering from systemic sclerosis [213], dermal [214], kidney [215], lung [216, 217] and liver fibrosis [218]. Thus, reducing levels of HSP47 could potentially hinder collagen accumulation and halt the progression of fibrosis. Several preclinical studies have shown that treatment with siRNA against HSP47 could reduce the deposition of collagen into the extracellular matrices in *in vivo* models of liver [219], pancreatic [220], and peritoneal fibrosis [221]. One study showed that siRNA against HSP47 when delivered with vitamin A-coupled liposomes could yield promising results for treating liver fibrosis in an *in vivo* rat model [219], and is currently undergoing a Phase Ib/II clinical trial (NCT02227459, Nitto Denko Corp., no published clinical trial results yet). This provides evidence that HSP47 may be an excellent gene target for antifibrotic treatment.

Intradermal siRNA delivery is an attractive strategy for treating cutaneous pathological conditions due to the ease of self-administration and reduced risk of systemic toxicity. Two phase I clinical trials have been recently completed with encouraging results, one involving intradermal injections of siRNA against keratin 6a [222] to treat pachyonychia congenital (PC) and the other involving injection of siRNA against connective growth tissue factor (CTGF) to reduce dermal scarring in pre-existing hypertrophic scar patients undergoing scar revision surgery (RXI-109, RXi Phamaceuticals, Westborough, MA). However, local delivery of nanoparticle-based siRNA delivery system has not been attempted for treatment of fibrotic dermal diseases such as scleroderma.

I demonstrate for the first time a nanoparticle platform capable of delivering siRNA with intrinsic antioxidant properties for treating fibrosis. For efficacy evaluation, I exploit the well-established TGF-β-induced *in vitro* fibrosis model. I also utilize the dermal fibrosis mouse model developed by repeated injections of bleomycin to mouse skin [223], which mimics the pathologic process underlying scleroderma in human.

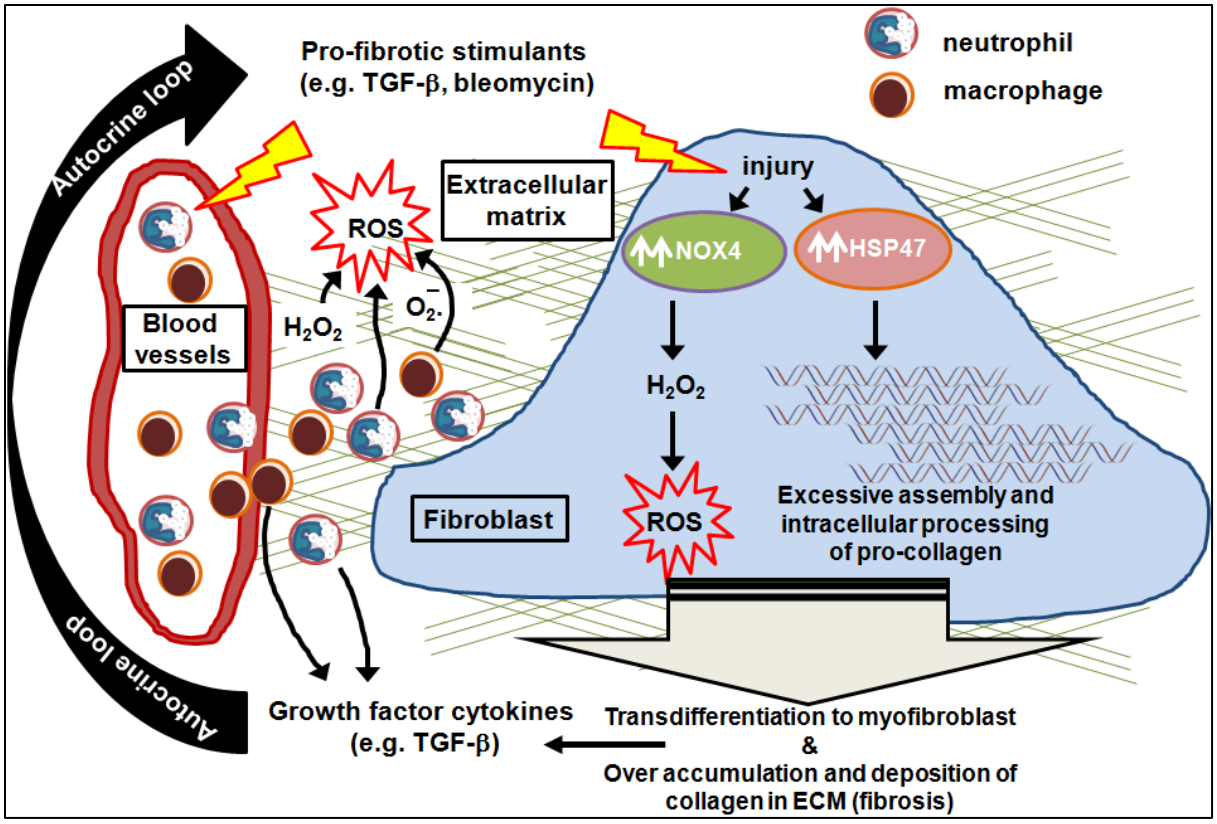

Figure 2.1. Schematic illustrating pathogenesis of fibrosis.
Pro-fibrotic stimulants (e.g., TGF-β or bleomycin) activate macrophages and neutrophils to secrete pro-fibrotic cytokines (e.g., TGF-β) and ROS (e.g., H_2O_2, superoxide) into the extracellular matrices (ECM) and surrounding cells. The presence of cytokines and ROS leads to up-regulation of profibrotic genes (NOX4, HSP47, α-SMA, and COL I) in fibroblast cells, transdifferentiation of quiescent fibroblast cells to myofibroblasts, and over-accumulation of collagen in the ECM, leading to fibrosis. Myofibroblasts will secrete more TGF-β, further inducing fibrogenesis in an autocrine loop. Reproduced with permission from Biomaterials[172].

2.2 Materials and Methods

2.2.1 Synthesis of MSNP-PEI-PEG Nanoparticles and siRNA Loading

Mesoporous silica nanoparticles (MSNPs) of 50nm in size were synthesized and surface modified as in our previous report [175]. Briefly, 0.15 M cetyltrimethylammonium chloride (CTAC) surfactant was mixed with 350 μL triethanolamine (TEA) in 125 mL of water at 95 °C. Then, 3 mL of tetraethoxysilane (TEOS) was added and the mixture was stirred for one hour. Nanoparticles were recovered from the suspension by centrifugation (60 min, 15 °C, 13,000 rpm), washed with ethanol twice and dried overnight in a desiccator. They were then re-suspended and refluxed in acidic methanol (0.6 M HCl in methanol) to remove CTAC. MSNPs were then washed with ethanol and dried in a desiccator. For PEI modification, PEI (branched, 10 kDa) was added into MSNP in absolute ethanol at a weight ratio of 1:4 of PEI per MSNP and the mixture was shaken at 300 rpm for 3 hr at room temperature. The MSNP-PEI was then centrifuged at 15,000 rpm for 30 min and resuspended in the ethanol solution containing free PEI and 0.2 mg dithiobis{succinimidyl propionate} (DSP, ThermoFisher, Waltham, MA) as a crosslinker. The solution was shaken for another 40 minutes. For PEG modification, 50 mg of mPEG-5kDa-NHS (JenKem, Plano, TX) was conjugated to the primary amines of MSNP-PEI (10 mg) in 1X PBS solution (pH 7.2) under stirred conditions overnight. The MSNP-PEI-PEG was then washed with the PBS solution and kept in this solution until use. The loading of siRNA onto MSNP-PEI-PEG was performed in the same PBS solution at room temperature under 1 hr of shaking. A nanoparticle to siRNA mass ratio of 25 (complete binding level) was used throughout the study. All reagents were from Sigma Aldrich (St. Louis, MO), unless specified otherwise.

2.2.2 Characterization of Nanoparticles

Mesoporous silica nanoparticle (MSNP) cores were measured for primary (dry) size by a Transmission Electron Microscope (Philips/FEI Tecnai TEM, Hillsboro, OR). After the chemical modification, the material was measured for hydrodynamic size in 10 mM NaCl with a Zetasizer (Malvern, Westborough, MA). PEI and PEG loadings were quantified by a thermogravimetric analyzer (TGA Q50, TA Instruments, New Castle, DE). siRNA loading was quantified by fluorescent detection of dye-tagged siRNA as well as gel electrophoresis.

2.2.3 Cell Culture and Primary Dermal Fibroblast Isolation

Primary murine dermal fibroblasts were harvested from 4 normal and 4 bleomycin-treated (as described in *section 2.2.9*) C3H/HeJ mice by using 6-mm (in diameter) skin biopsy punch following procedure described by Takashima et al. [224]. Excised skin was held on ice in Hank's buffered saline solution with 1% pen-strep while the fat tissues were removed prior to mincing the remaining skin into small pieces. 2 mL of 100 U/mL collagenase type I (Worthington Biochemical Corp., Freehold, NJ) was added into the minced tissues and the suspension was stirred at 37 ^{o}C for 1 hr. Dissociated fibroblast cells, designated "normal fibroblast" from normal skin and "bleo fibroblast" from bleomycin-treated skin, were pelleted at 1000 rpm for 5 min. The cell pellet was then re-suspended in warm DMEM (Cellgro, Manassas, VA) supplemented with 10% FBS and 1% pen-strep. The cell suspension was then filtered through a 40 μm cell strainer (BD Falcon, BD Biosciences, San Jose, CA) before plating in the same medium. The normal and bleo-fibroblast cultures were characterized by the mRNA level of HSP47, COL I and α-SMA and immunohistochemical staining of fibroblast-specific

marker, vimentin [225, 226], and myofibroblast marker, α-SMA (**Figure 2.2)**. The use of all of the fibroblast cultures was limited to passages between 3 and 9. In addition to the primary dermal fibroblast cell line, the murine embryonic fibroblast cell line, NIH/3T3, was also cultured in the same medium. Both cell lines were maintained at 37 ^{o}C and 5% CO_2 humidified incubator. 2-4 *in vitro* experimental replicates were performed for each experiment with at least 3 analytical replicates per each sample.

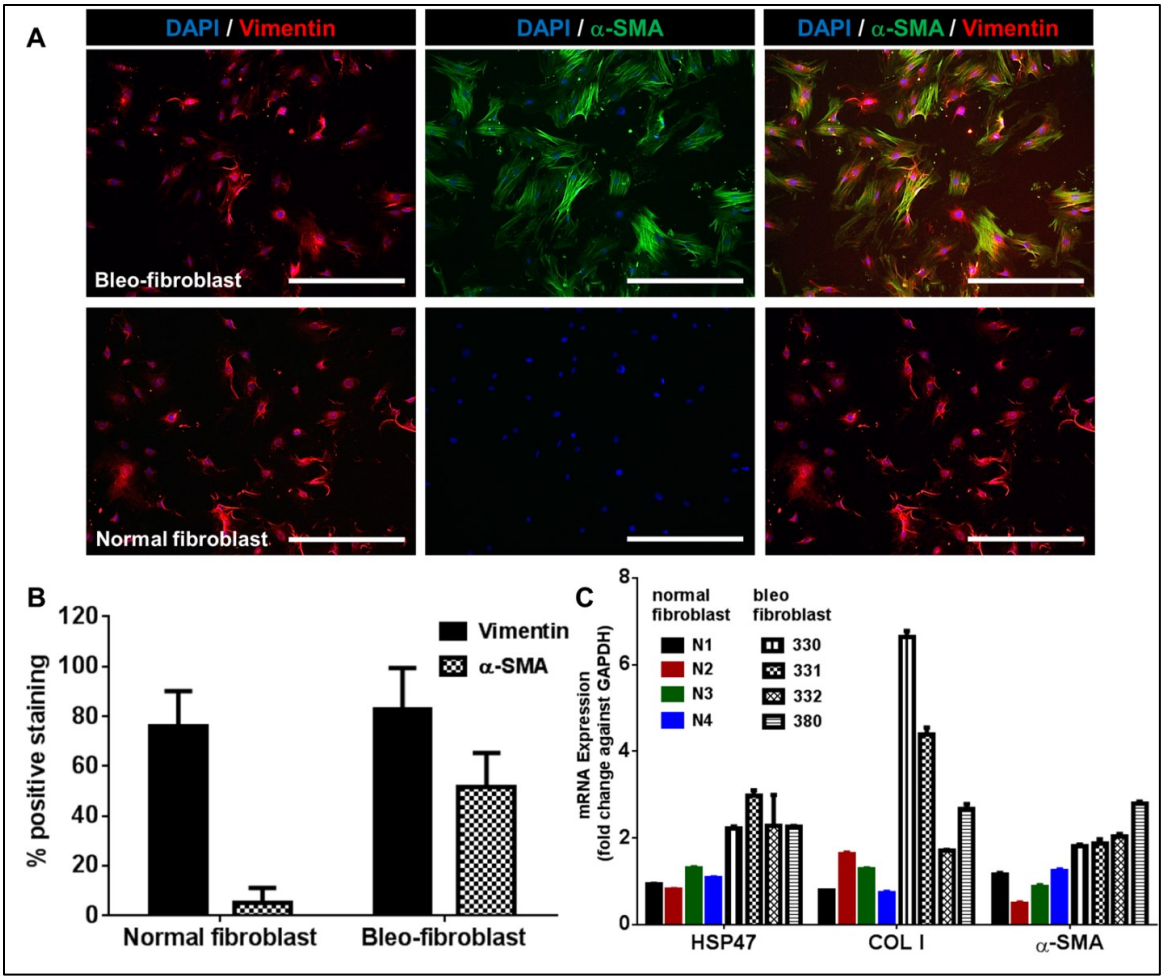

Figure 2.2. Primary dermal fibroblast cell characterization.
(A) Representative images of bleo-fibroblast and normal fibroblast stained with fibroblast-specific marker, vimentin, and myofibroblast marker, α-SMA (scale bar = 400 μm). (B) Quantitative analysis of vimentin-positive and α-SMA-positive fibroblast cells in (A). (C) mRNA expression of the individual fibroblast culture harvested from normal and bleomycin-treated mice (n=4). All bleo-fibroblast cultures obtained from the bleomycin-treated mice exhibit about 2-4-fold upregulation in the profibrotic markers (HSP47, COL I, and α-SMA) compared to the normal fibroblast cells. The normal fibroblast culture was pooled from 4 mice (N1-N4) since they exhibit similar cellular profile. However, the skin from mouse #380 grew robustly and, hence, was selected for subsequent studies.

2.2.4 Cellular Uptake of Nanoparticles

For cellular uptake experiments, primary murine dermal fibroblast cells (normal skin) were seeded at 8,000 cells/well on 96-well plates overnight in complete DMEM medium (DMEM + 10% FBS). The cells were then serum-starved in DMEM with 0.5% FBS on the next day prior to treatment with either 50 nM of non-targeting siRNA (siSCR, see **Table 2.1.** for siRNA sequence) conjugated with DyLight677 delivered by MSNP-PEI-PEG (17.5 μg/mL) or DharmaFECT (0.5 μL/well in 100 μL medium, DharmaFECT-1, Thermo Scientific, Lafayette, CO). After 24 hr of incubation, the cells were washed three times with PBS to remove non-internalized nanoparticles and stained with cell-permeant Hoechst dye at 37 ^{o}C for 30 min before fixation in 4% paraformaldehyde (PFA) for 15 min. Internalized DyLight677-siRNA were detected using a fluorescence microscope (EVOS FL, Life Technologies). Fluorescence intensity of DyLight677 was normalized over the total cell number (Hoechst-positive) and analyzed using Cell Profiler open-source image analysis software.

Table 2.1. Individual siRNA sequences used in the *in vitro* and *in vivo* experiments.

Type	Antisense
siHSP47 #1	5’ UUCUGCAUCUUUCCCAUCCUU 3’
siHSP47 #2	5’ AGUUGAUCUUGGAGUGUUCUU 3’
siHSP47 #3	5’ UCUUGGUCAAAGGGGUUGCUU 3’
siSCR (non-targeting)	5’ UUAGUCGACAUGUAAACCA 3’
siNOX #1	5’ CAGGAATAAATTAAAGCTTTA 3’
siNOX #2	5’ CAGATGGGATTCAGAAGATAA 3’
siNOX #3	5’ CACGGTGAGTTACTAGATTTA 3’
siNOX #4	5’ AAGGATCTATATGTTAAACAT 3’

2.2.5 Intracellular ROS Assay

To measure cellular ROS induction by nanoparticles, primary murine dermal fibroblast cells were pre-treated with either siSCR-MSNP-PEI-PEG, siSCR-DharmaFECT, (prepared in a similar manner as *2.4)*, or 2 mM of N-acetylcysteine (NAC, Sigma Aldrich) antioxidant. After 24 hr, 100 μM of menadione was added into each well for 1 hr to induce oxidative stress. At the end of the incubation period, the cellular ROS was assayed using CellROX® green reagent (Promega Corporation, Madison, WI) following the manufacturer's protocol. The fluorescence intensity of CellROX® green was normalized over the total cell number (DAPI-positive) and analyzed using Cell Profiler open-source image analysis software.

2.2.6 DPPH Free Radical Scavenging Assay

The 2, 2-diphenyl-1-picrylhydrazyl (DPPH, Sigma Aldrich) free radical scavenging assay was used to determine the antioxidant property of the nanoparticles. This assay is based on the reduction of the odd electron on the nitrogen atom in DPPH by antioxidants [227]. Briefly, various concentrations (from 0-500 μg/mL) of MSNP core, PEI, MSNP-PEI-PEG, and NAC were prepared in PBS solution and administered in triplicate in a 96-well plate (cell-free) followed by the addition of an equal volume of 0.5 mM DPPH (in ethanol). The mixture was then incubated in the dark at room temperature under shaking (300 rpm) for 15 min. Absorbance (abs.) was read at 517 nm using a TECAN spectrophotometer (TECAN US Inc., Research Triangle Park, NC). The percentage of DPPH scavenging radical was calculated as follows:

$$\%\ DPPH\ scavenging = (abs.of\ blank - \frac{abs.of\ sample}{abs.of\ blank}) \times 100$$

2.2.7 Screening of siHSP47 and siNOX4

For screening of siRNA against HSP47 (siHSP47), three individual siHSP47 sequences (Dharmacon, Lafayette, CO, see **Table 2.1.**) were transfected with DharmaFECT-1 (DharmaFECT) in NIH/3T3 murine embryonic fibroblast cells. Briefly, NIH/3T3 cells (300,000 cells/well) were seeded in a 6-well plate and transfected with 50 nM siRNA in DharmaFECT (0.5 μL/well) for 72 hr (media change at 24 hr post transfection). The cells were then lysed for subsequent mRNA and protein analysis by qRT-PCR and western blot, respectively. Likewise, for screening of siRNA against NOX4 (siNOX4), four individual sequences (Qiagen Valencia, CA) as summarized in **Table 2.1.** were transfected with DharmaFECT using the same transfection method but with primary murine dermal fibroblast cells.

2.2.8 In vitro Evaluation of siHSP47 and siNOX4

siRNA against HSP47 (siHSP47) and NOX4 (siNOX4) were screened from 3-4 sequences as summarized in **Table 2.1**. Once the best siRNA sequence was identified (**Figure 2.3**), it was used for *in vitro* gene silencing under TGF-β stimulation conditions as follows. Primary murine dermal fibroblast cells were seeded on a 96-well plate (8,000 cells/well) or on a 6-well plate (150,000 cells/well) overnight in complete medium. On the next day, the medium was replaced with DMEM with 0.5% FBS for 16 hr. Cells were then transfected with 50 nM siRNA on 17.5 μg/mL of MSNP-PEI-PEG or DharmaFECT (0.5 μL/well). After 24 hr, cells were washed once and the culture medium was replaced

with fresh medium (DMEM with 0.5% FBS) containing 10 ng/mL TGF-β (Peprotech Inc., Rocky Hill, NJ) and incubated either for another 24 hr (mRNA detection) or 72 hr (protein detection). For bleo-fibroblast cells, the MSNP-PEI-PEG and DharmaFECT treatments were done in similar manner as above, but without TGF-β stimulation. The HSP47, NOX4, COL I, and α-SMA protein expressions of the treated cells was quantified with either immunofluorescence imaging (IF) or Western Blot, while their mRNA levels were quantified with qRT-PCR.

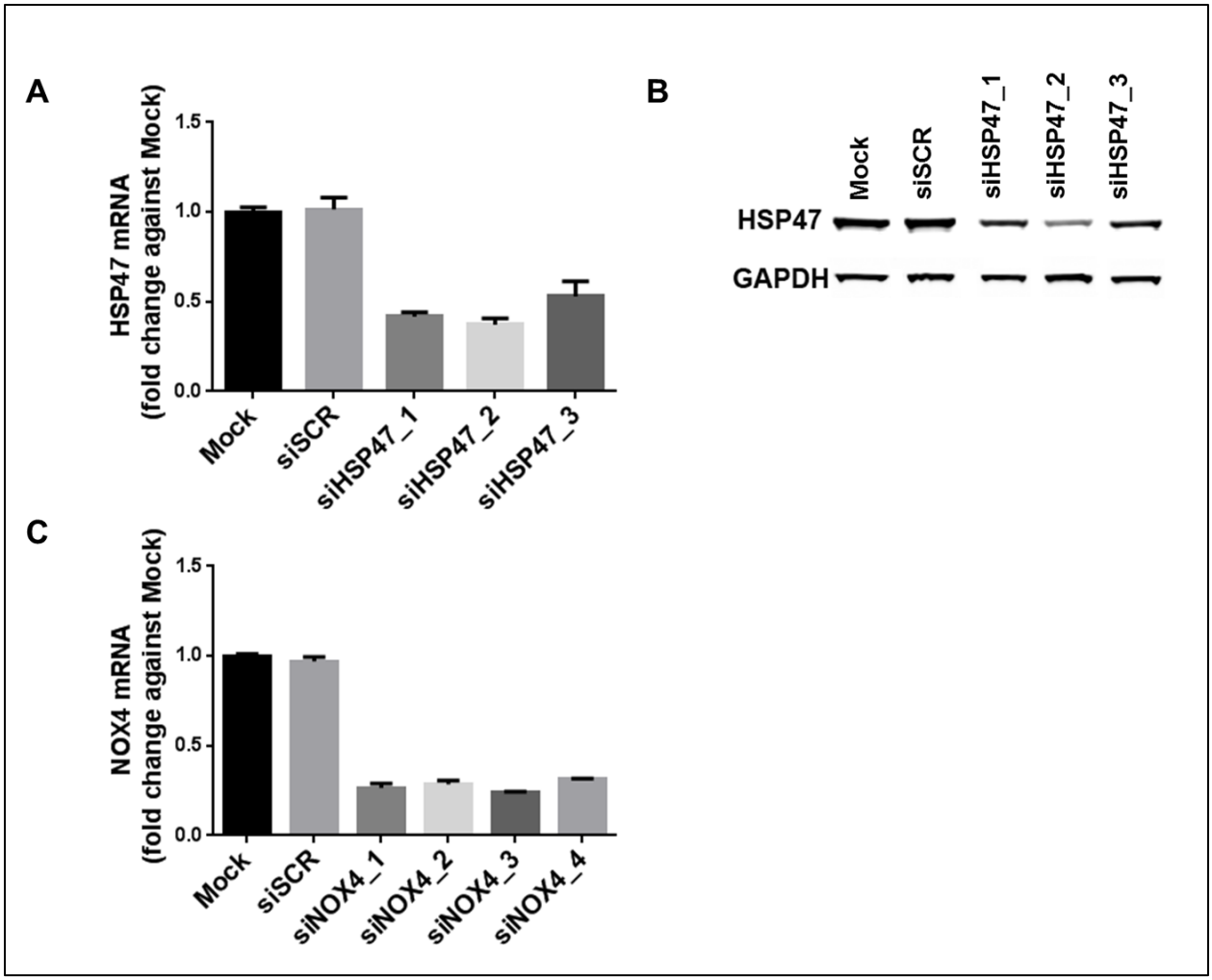

Figure 2.3. *In vitro* siRNA screening of siHSP47 and siNOX4.
(A) HSP47 mRNA (at 72 hr post-treatment) and **(B)** protein expressions (at 96 hr post-treatment) of NIH/3T3 cells transfected with various siHSP47 sequences (50 nM) in DharmaFECT. **(C)** NOX4 mRNA expression of primary murine dermal fibroblast cells transfected with various siNOX4 sequences (50 nM) in DharmaFECT at 48 hr post-treatment. The mRNA level was normalized against GAPDH and reported as fold change over mock (DharmaFECT alone). siHSP47_2 and siNOX4_3 sequence had the best silencing efficacy and were used throughout this work.

2.2.9 Cell Viability Assay

The viability of the cells treated as described in *2.7* was also determined at 96 hr post transfection using CellTiter-Glo® Luminescent Cell Viability Assay (Promega) following the manufacturer's protocol. The data were reported as the fold change against the untreated control.

2.2.10 SiHSP47-MSNP-PEI-PEG Nanoparticle Treatment of Bleomycin-Induced Scleroderma Mouse Model

The induction of dermal fibrosis (scleroderma) with bleomycin in mice followed the procedure described by Yamamoto et al. [223]. The experimental protocol was approved by the Institutional Animal Care and Use Committee (IACUC) of Oregon Health and Science University (OHSU). Specifically, 6-7 week old C3H/HeJ mice (Jackson Laboratories, Bar Harbor, ME) were intradermally injected with 100 μL of 0.5 mg/mL bleomycin in PBS (APP Pharmaceuticals) at the same location on the shaved back of mice every other day for 4 weeks (3 times weekly). Concurrently, mice (6-7 per group) were injected with 50 μL of PBS suspension containing siSCR- or siHSP47-MSNP-PEI-PEG at the dose of 220 μg nanoparticles and 0.65 nmol as siRNA. The siRNA dose was adapted from the reported intradermally injected siRNA doses to mice [228, 229]. Treatments were done twice a week on alternate days with bleomycin injection for a total of 8 treatments over 4 weeks. A positive control group received bleomycin and saline injections. All mice were sacrificed 4 days after the last injection with the siRNA-nanoparticle treatment.

2.2.11 Histological Analysis of Bleomycin-Induced Scleroderma Mouse Skin

Skin tissues from the region of injection (due to the small area of bleomycin injection (100 μL) and nanoparticle treatment (50 μL), only one 6 mm-biopsy punch was collected per animal) were collected and fixed in 4% PFA prior to processing and paraffin embedding. 5 μm-thick paraffin-embedded sections were used for H&E stain for determination of dermal thickness. Six images were taken per tissue section with the EVOS-XL microscope at x200 magnification. Dermal thickness was measured as the distance between the epidermal-dermal junction and the dermal-adipose layer junction and the data were presented as fold-change over untreated control.

2.2.12 Immunohistochemistry for Pro-fibrotic Markers on Skin Sections

Deparaffinized and rehydrated skin sections were subjected to heat-mediated antigen retrieval in citrate buffer (10 mM, pH 6.0) for 30 min. The tissue sections were blocked with 5% goat-serum (Vector Laboratories Inc., Burlingame, CA) for 1 hr at room temperature. Slides were then incubated with primary antibodies at 4 ^{o}C overnight, secondary antibodies for 1 hr at room temperature, and mounted with Prolong Gold Antifade reagent with DAPI (P-3691, Invitrogen). Six images were taken per tissue section per animal with the EVOS FL fluorescence microscope at x200 magnification. The total fluorescence intensity of the tissue sections were normalized over the total image area and analyzed using Cell Profiler open-source image analysis software. For the measurement of COL I and α-SMA positive area, the 'MeasureImageAreaOccupied' module in Cell Profiler software was used and calculated as the relative area occupied by the protein of interest (COL I or α-SMA) to the total area of the tissue.

2.2.13 Western Blot Analysis

Western blot analysis was performed for protein quantification of cell lysates as follows. Cell lysate (20 μg protein/lane) were electrophoresed with denaturing sodium dodecyl sulfate (SDS)-polyacrylamide NuPage Novex 4% to 12% gels (Invitrogen) and blotted on a PVDF membrane (Millipore, Temecula, CA). Mouse monoclonal anti-HSP47 and rabbit polyclonal GAPDH (Cell Signaling Technology, Danvers, MA) were used as primary antibodies. The HSP47 protein was visualized with Alexa Fluor 680-conjugated goat anti mouse IgG (Invitrogen) and the GAPDH protein was visualized with IRDye-800CW conjugated polyclonal goat anti-rabbit IgG (LI-COR Biosciences, Lincoln, NE) using the LI-COR Odyssey infrared imaging system.

2.2.14 Immunofluorescent Imaging (IF)

For IF assays, cells were washed twice in warm PBS, fixed with ice-cold methanol for 15 min and blocked with 5% goat serum in PBS for 1 hr (room temperature). Incubation with the primary antibody (1:100 dilution in blocking buffer) took place overnight at 4 ^{o}C. The following primary antibodies used were: Vimentin (5741, Cell Signaling Technology), HSP47 (NBP1-97491, Novus Biologicals, San Diego, CA), NOX4 (ab109225, Abcam), COL I (ab21286, Abcam), and α-SMA (ab7817, Abcam, Cambridge, MA). On the next day, the cells were washed three times with PBS (containing 0.1% Tween) and incubated with secondary antibodies; AlexaFluor®488-conjugated anti-mouse IgG (A-11001, Life Technologies), AlexaFluor®488-conjugated anti-rabbit IgG (A27034, Life Technologies), AlexaFluor®647-conjugated anti-rabbit IgG (A27018, Life Technologies), or AlexaFluor®647-conjugated anti-mouse IgG (A-21236, Life Technologies) for 1 hr (room temperature). Cells were imaged using EVOS FL fluorescence microscope and

the protein expression level was measured by normalizing fluorescence intensity to the total cell number (DAPI-stained nuclei) per image. For *in vitro* studies, protein quantification was done with 3 images per well and 3 replicate wells per treatment throughout. For *in vivo* assessment, quantification was done with 6 images per animal and 4-7 animals per treatment.

2.2.15 Real time quantitative PCR (qRT-PCR)

The RNA from the treated cells was isolated with the RNeasy Mini kit (Qiagen) following the manufacturer's protocol. The amount of RNA was quantified using NanoDrop 1000 spectrophotometer. Purified RNAs were reverse transcribed with EXPRESS One-Step SuperScript qRT-PCR kit (Invitrogen). Primer sequences chosen for qPCR (Life Technologies, Eugene, OR) are: HSP47 (Mm00438058_g1), α-SMA (Mm00725412_s1), NOX4 (Mm00479246_m1), COL I (Mm00801666_g1), and GAPDH (Mm99999915_g1). qPCR assays were performed in triplicate using an ABI 7500 Fast System (Applied Biosystems, Foster City, CA) under standard cycling conditions: 50 ^{o}C for 2 min, 95 ^{o}C for 10 min, 40 cycles of 95 ^{o}C for 15 s, and 60 ^{o}C for 1 min. Expression levels were analyzed using $2^{-\Delta\Delta C(t)}$ method using GAPDH as loading control.

For RNA isolation from skin tissue, the skin tissues harvested from each mouse were homogenized in RLT buffer using hand-held homogenizer and further lysed with 20G needle syringes. The total RNA was isolated using Rneasy Fibrous Tissue Mini Kit (Qiagen) following manufacturer's protocol. qPCR assays were performed in triplicate under the same conditions as the mentioned above and the expression levels were normalized against HPRT (Mm01545399_m1) as loading control.

2.2.16 2′,7′-Dichlorofluorescin diacetate (DCFA-DA) kinetic ROS assay

NIH/3T3 cells, seeded in 96-well plate (8000 cells/well) in DMEM + 10%FBS overnight, were stained with 50 μM DCFH-DA (Sigma-Aldrich) and treated with either 20 μg/mL MSNP-PEI-PEG or 2 mM NAC in combination with 100 μM H_2O_2. The fluorescence intensity of DCFH dye was read hourly with a TECAN spectrophotometer. DCFA-DA is a cell-permeable non-fluorescent probe. In the presence of pro-oxidant agent (such as H_2O_2), DCFH-DA de-esterified intracellularly and turns to highly fluorescent 2′,7′-dichlorofluorescein upon oxidation.

2.2.17 Transmission Electron Microscopy (TEM) on skin sections

Mouse skin tissues were fixed in 2.5% glutaraldehyde in pH 7.2, 0.1 M sodium cacodylate buffer (EMS, Hatfield, PA) overnight at 4 ^{o}C, rinsed with 0.15 M phosphate buffer, postfixed in 1% osmium tetroxide (EMS) for 1 hr and stained en bloc in 0.5% uranyl acetate (EMS) for 3 hr in the dark. The stained tissues were then dehydrated in graded acetone (diluted in 0.2 M sodium phosphate buffer (EMS), pH 7.2) for 15 minutes at each concentrations (50%, 75%, 95%, and 100%) and incubated in acetone-Araldite mixture (1:1 ratio, EMS) at room temperature overnight. On the next day, the skin samples were embedded in 100% Araldite resin (EMS) at 65 ^{o}C for 48 hr, sectioned, stained with lead citrate and uranyl acetate and imaged with Philips CM100 transmission electron microscope (Philips/FEI).

2.2.18 Statistical Analysis

Experiments were performed in triplicate with results presented as mean ± standard deviation. Data were analyzed using one-way ANOVA with post-hoc Dunnett's multiple

comparison test with significance set at p≤0.05. Graphpad Prism 6.0 software (GraphPad software Inc., San Diego, CA) was utilized for statistical analyses.

2.3 Results and Discussion

2.3.1 Synthesis and Characterization of Nanoparticles (MSNP-PEI-PEG)

Transmission electron micrograph (TEM, **Figure 2.4**) showed that the MSNP core had porous morphology with particle size of 47 ± 4 nm in diameter. Layer by layer coating with polyethyleneimine (PEI) and polyethylene glycol (PEG) (see schematic representation in **Figure 2.4B**) were confirmed by TGA. TGA analysis shows the amount of attached PEI and PEG on MSNP to be 13.5% and 18.2% by dry weight of whole nanoparticle, respectively. After the surface modification, MSNP-PEI-PEG has a hydrodynamic size of 104 ± 1.7 nm (**Figure 2.4C**) and zeta potential of 15.1 ± 0.7 mV (in 10 mM NaCl). The nanoparticle had a small polydispersity index (PDI) of 0.19, showing narrow size distribution. Even after siRNA loading, the particle size remains unchanged (**Figure 2.4C**). As shown in **Figure 2.4B**, the siRNA is bound to PEI, and is protected underneath the PEG layer. As a result, the siRNA was 100% protected against serum enzymes for at least 24 hr (measured in 50% human serum) [175].

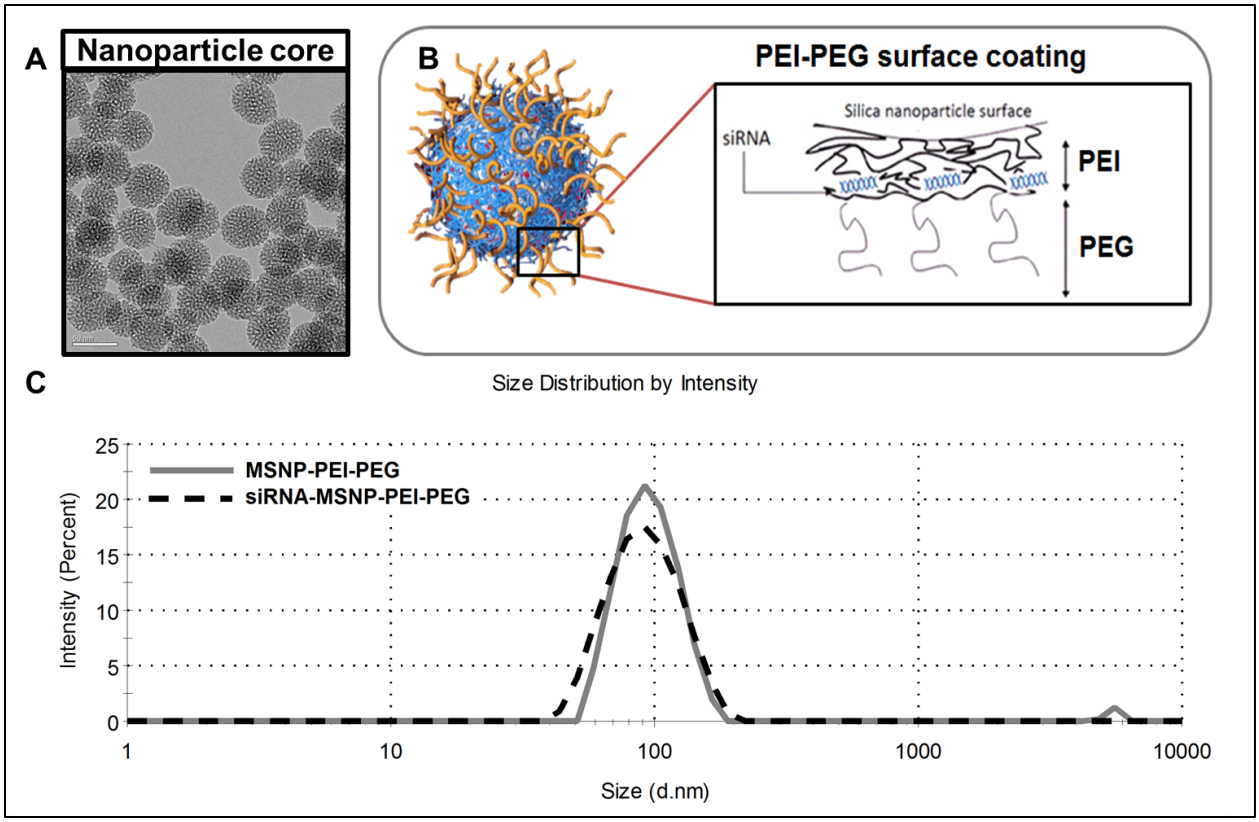

Figure 2.4. MSNP-PEI-PEG nanoparticle.
(A) TEM image of the mesoporous silica nanoparticle (MSNP) core (scale bar = 50 nm). (B) Schematic of surface modification of MSNP (layer-by-layer) with polyethyleneimine (PEI), polyethyleneglycol (PEG), and siRNA. (C) Hydrodynamic size distribution of MSNP-PEI-PEG (solid line) and with siRNA loading (dash line).

2.3.2 Cellular Uptake of siRNA-Nanoparticles (MSNP-PEI-PEG)

Results in the **Figure 2.5** demonstrate a greater cellular uptake distribution of DyLight677-siSCR (siSCR is a non-targeting siRNA) by DharmaFECT and a more uniform uptake of the DyLight677-siSCR delivered by MSNP-PEI-PEG nanoparticles in murine primary dermal fibroblasts after 24 hr (**Figure 2.5A**). Specifically, the cellular signal of dye-tagged siRNA increased by 76 ± 31% with nanoparticle delivery versus 49 ± 56% by DharmaFECT delivery (*vs*. the untreated control, **Figure 2.5B**). We attribute the non-uniform cellular uptake of the DharmaFECT to its large particle size of 446 nm (range from 190-955 nm) *vs*. 100 nm (range from 44-255 nm) of siSCR-MSNP-PEI-PEG as shown in **Figure 2.5C**.

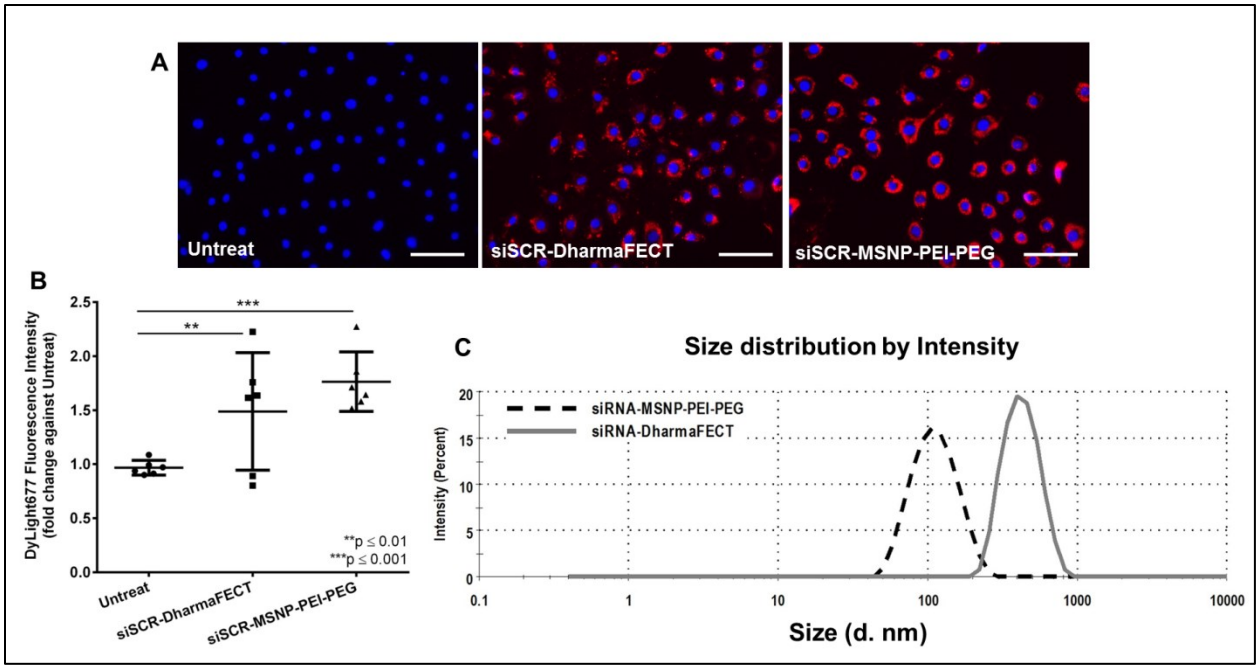

Figure 2.5. Cellular uptake of DyLight677-conjugated siSCR-MSNP-PEI-PEG in primary murine dermal fibroblast cells.

(A) Representative images of cells at 24 hr post-transfection with DharmaFECT (0.5 μL/well, 100 μL volume) or 17.5 μg/mL MSNP-PEI-PEG nanoparticles, both containing 50 nM DyLight677-siSCR, and untreated cells (scale bar = 100 μm). Red = DyLight677, blue = nuclei. (B) Corresponding DyLight677 fluorescence intensity. (C) Hydrodynamic size distribution of siRNA-DharmaFECT (solid grey line) compared with siRNA-MSNP-PEI-PEG (dashed line).

2.3.3 ROS Scavenging Ability of Nanoparticles (MSNP-PEI-PEG)

The antioxidant properties of bare MSNP (without chemical modification) in a human melanoma [25, 202] and mouse embryonic fibroblast [176] cell line have been reported as described previously. To assess the antioxidant property of MSNP-PEI-PEG in our cells of interest (murine dermal fibroblasts), we measured the ROS level after exposing the cells to MSNP-PEI-PEG overnight followed by 1 hr menadione-induced oxidative stress. Menadione (2-methyl-1,4-naphthoquinone) is a chemical compound known to generate intracellular ROS [230]. Such intracellular ROS could be measured by CellROX Green reagent as shown in **Figures 2.6A** and **B**. The cellular ROS was increased 7.6-fold after 1 hr of menadione exposure. However, pretreatment of the cells with MSNP-PEI-PEG, decreased ROS production to the non-menadione level, while DharmaFECT had little effect. The MSNP-PEI-PEG effect was similar to that obtained by an established antioxidant, NAC. Note that non-targeting siRNA (siSCR) was used on the nanoparticles to maintain similar surface charge of intended final nanoconstruct without imparting gene silencing effect.

Reduction of ROS by our nanoparticles was thought to be due to the MSNP core and not the cationic PEI coating. I confirmed this by measuring DPPH free radical scavenging ability of the materials in a cell free system. **Figure 2.6C** shows that bare MSNP displayed higher scavenging ability than MSNP-PEI-PEG, while PEI alone displayed very little effect. NAC was used as the positive control. In addition, I also observed a lower ROS activity when NIH/3T3 mouse embryonic fibroblast cells were exposed to the MSNP-PEI-PEG nanoparticles in the presence of H_2O_2 for up to 6 hr (**Figure 2.7**). Although MSNP-PEI-PEG had lower scavenging ability than bare MSNP,

the PEI-PEG layer is needed. PEI is needed for binding to siRNA, promoting cell entrance (via adsorptive endocytosis) and endosomal escape of siRNA via proton sponge effects [231], while PEG layer is needed for protecting siRNA from blood enzyme degradation [175].

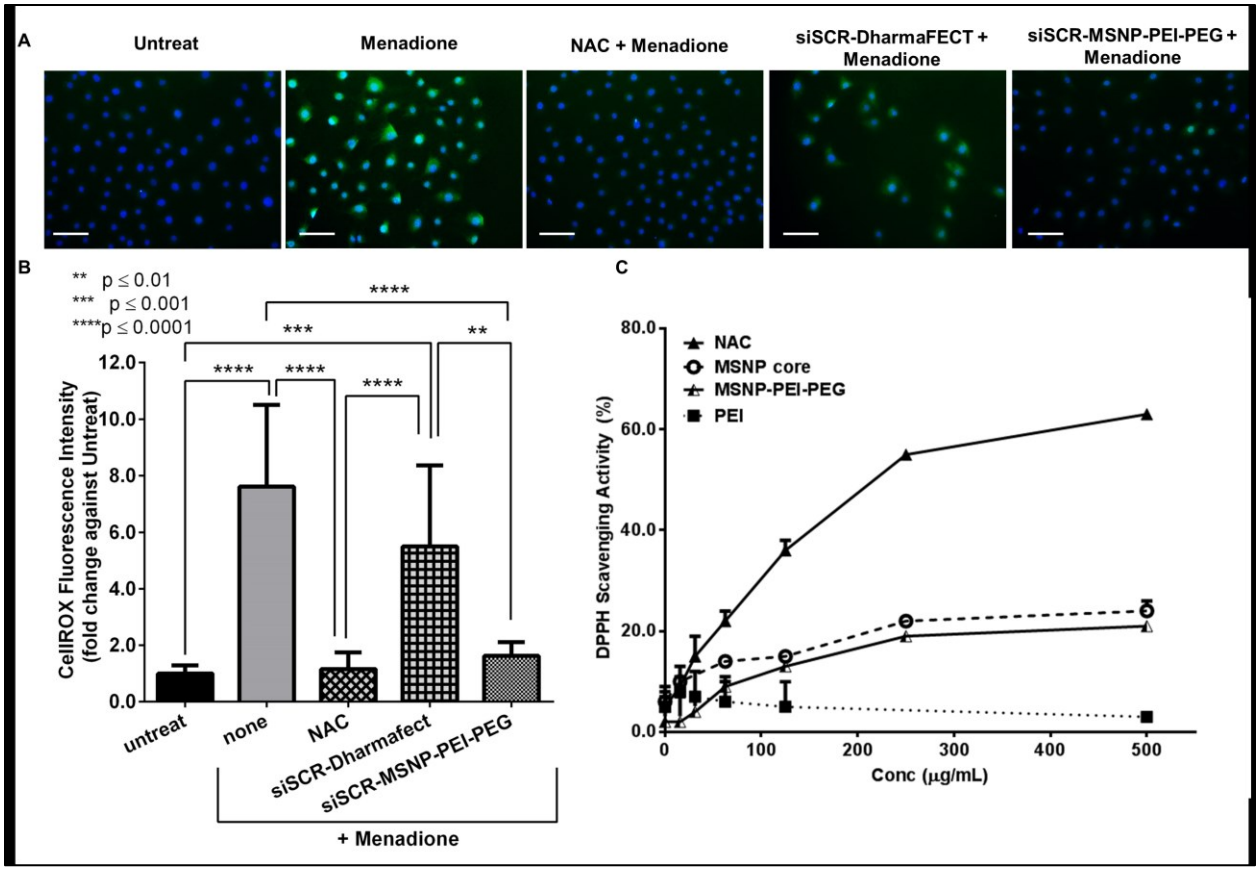

Figure 2.6. Intracellular ROS activity of primary dermal fibroblast treated for 24 hr with NAC (2mM), siSCR-MSNP-PEI-PEG or siSCR-DharmaFECT prior TGF-β stimulation.

(A) Representative images of cells (Hoechst dye, blue) stained with CellROX (green), scale bar = 100 μm. (B) Corresponding CellROX fluorescence intensity normalized by cell number (Hoechst-positive) and reported as fold-change against untreated control. (C) DPPH scavenging activity of various materials in a cell-free system.

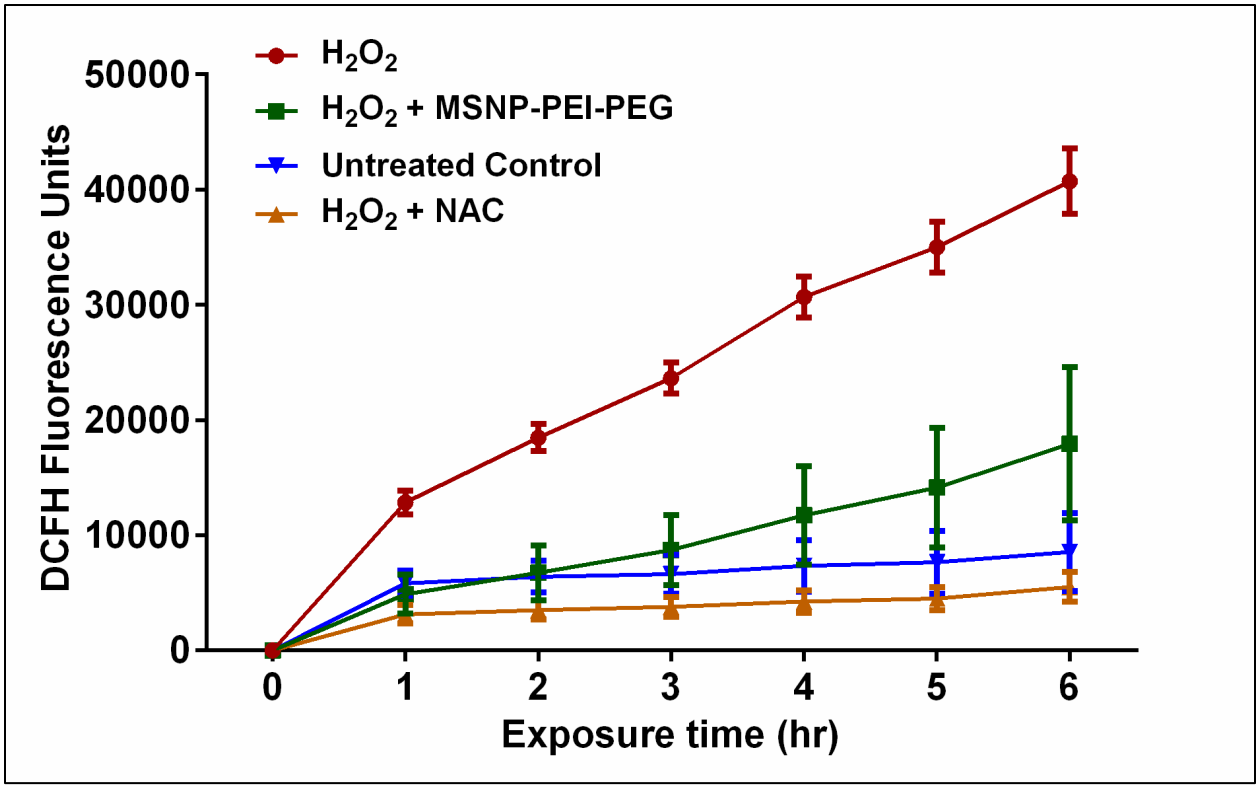

Figure 2.7. Kinetic analysis of ROS activity in murine fibroblast cells. Treatment of MSNP-PEI-PEG (20 μg/mL) or NAC (2 mM) in combination with the pro-oxidant, H_2O_2 (100 μM), resulted in lower ROS activity (reflected by lower fluorescence intensity of DCFH dye) at all time points up to 6 hr post-treatment in NIH/3T3 cells.

2.3.4 Effect of MSNP-PEI-PEG on TGF-β Stimulated Dermal Fibroblast Cells and Scleroderma-like Fibroblasts

In scleroderma patients, elevation of TGF-β [232], NOX4 expression [184, 208, 233], and ROS [208, 233] have been observed in dermal fibrotic lesions. In the previous section, MSNP-PEI-PEG nanoparticles were able to reduce cellular ROS. Next, I assess their ability to reduce NOX4 levels using an *in vitro* TGF-β–induced model. TGF-β is one of the major profibrotic growth factors and could stimulate fibroblast proliferation as well as its transdifferentiation to myofibroblast [189, 234, 235]. After TGF-β stimulation of primary murine dermal fibroblasts, a pronounced up-regulation of NOX4 by 2.2-fold, HSP47 by 1.5-fold, COL I by 2.5-fold, and α-SMA by 5.6-fold (*vs*. untreated control) was observed as shown in **Figures 2.8A and B**. Cell proliferation also increased by 1.9-fold. However, pre-treatment with siSCR-MSNP-PEI-PEG significantly decreased the expression of NOX4, HSP47, COL I and α-SMA, while siSCR-DharmaFECT had little effect. In particular, NOX4 and HSP47 protein expression was diminished to the level prior to TGF-β stimulation. Similar to section *3.3*, non-targeting siRNA (siSCR) was used to maintain similar surface charge of intended final nanoconstruct without imparting gene silencing effect as shown with DharmaFECT (**Figure 2.8**).

Next, I evaluated the ability of our nanoparticle to reduce NOX4 and other pro-fibrotic markers in scleroderma-like fibroblast cells harvested from skin of a mouse receiving intradermal bleomycin injections for 4 weeks, subsequently termed as “bleo-fibroblast”. This approach of treating already activated fibroblast will more closely mimic the current clinical situation. Evaluation of mRNA expression in these cells showed pronounced up-

regulation of genes including NOX4, COL I and α-SMA (**Figure 2.8C**) in a similar manner as the TGF-β stimulation model in **Figures 2.8 and 2.9**. This is because bleomycin injection in mouse skin has been shown to induce macrophage accumulation and local TGF-β production [236]. MSNP-PEI-PEG (with siSCR) treatment on these cells resulted in significant reduction in NOX4, COL I, and α-SMA mRNA expression ($p \leq 0.0001$) compared to the untreated counterpart (**Figure 2.8C**). NAC treatment at 2 mM could reduce NOX4 mRNA expression to the same extent as MSNP-PEI-PEG, but was unable to reduce the levels of COL I and α-SMA. A much higher dose of NAC (20 mM) was reported to be able to inhibit these pro-fibrotic markers [208, 233]. However, such high dose of NAC is impossible to achieve *in vivo* without toxicity concerns. An estimated 5010 mg/kg loading dose (e.g., first 60 min) and 2250 mg/kg maintenance dose (e.g., next 4 hr) are needed to reach 10 mM concentration in blood based on the pharmacokinetic data of NAC in human volunteers [132], but NAC is prescribed at only 150 mg/kg loading dose and 50 mg/kg maintenance dose (i.v.) (NAC, Acetadote®, package insert) or 600-mg oral dose (three times daily) for pulmonary fibrosis patients in the PANTHER-IPF trial [133]. This may be one of the reasons why oral monotherapy of NAC in pulmonary fibrosis patients did not show any beneficial effects and was also accompanied by a higher rate of cardiac events compared to the placebo treatment [133]. In short, much lower dose (17.5 mg/L) of MSNP-PEI-PEG was found to yield greater anti-fibrotic effects than NAC (~300 mg/L).

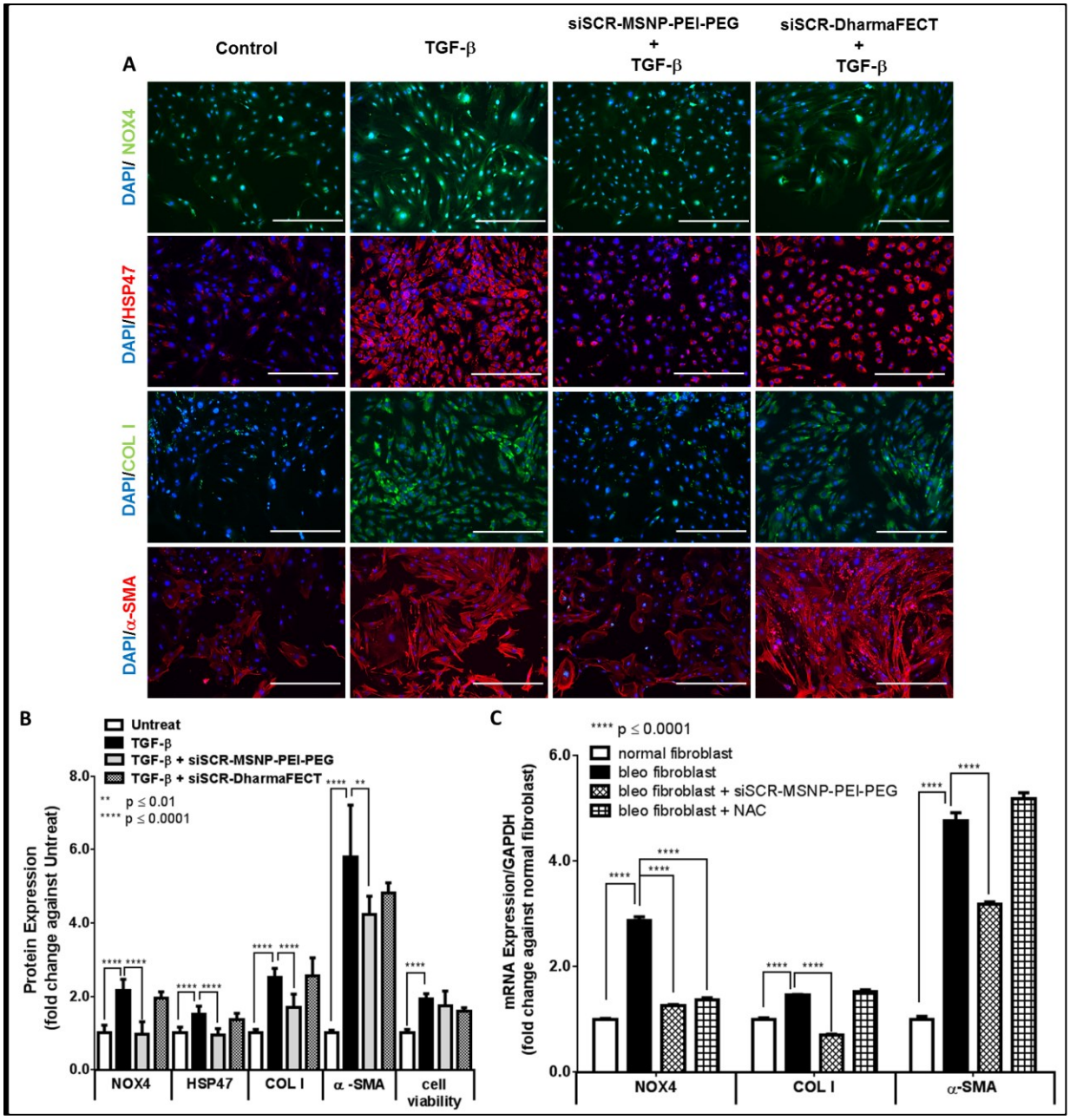

Figure 2.8. NOX4-modulating effects of MSNP-PEI-PEG on TGF-β stimulated and scleroderma-like dermal fibroblast cells.

(A) Representative images of the TGF-β stimulated cells stained for NOX4, HSP47, COL I, and α-SMA after 24-hr treatment with siSCR-MSNP-PEI-PEG or siSCR-DharmaFECT, followed by 72-hr treatment with 10 ng/mL TGF-β, scale bar = 400 μm. (B) Corresponding protein intensity normalized by cell number (DAPI), reported as fold-change against untreated control, and cell viability after each treatment. (C) mRNA expressions following 48 hr treatment with MSNP-PEI-PEG nanoparticles (17.5 μg/mL, 50 nM siSCR) *vs*. NAC (2 mM) on murine dermal fibroblasts harvested from bleomycin-induced scleroderma mouse model (bleo-fibroblast).

2.3.5 Role of NOX4 and HSP47 in Fibrogenesis

The involvements of both HSP47 and NOX4 in fibrogenesis are complex as summarized in **Figure 2.1**. Following tissue injury, the activated leukocytes (macrophages and neutrophils) induce ROS generation and secrete pro-fibrotic cytokines such as TGF-β [187]. The released TGF-β then triggers the synthesis and up-regulation of HSP47 [237] and NOX4 [209, 238, 239] in fibroblast cells. Overexpression of NOX4 induces intracellular ROS [205, 239], while the overexpression of HSP47 induces collagen synthesis (through excessive processing of pro-collagen molecules) [212]. Furthermore, NOX4 has been shown to induce the differentiation of fibroblasts to myofibroblasts [206, 240] and modulates collagen synthesis *in vitro* under TGF-β stimulation [238]. Myofibroblasts, in turn, secrete TGF-β in an autocrine fashion to further induce the activation and proliferation of the fibroblast cells [240].

MSNP-PEI-PEG treatment decreased not only NOX4 but also HSP47 protein expression (**Figure 2.8**). However, the relationship between NOX4 and HSP47 has not been clearly elucidated. In order to understand the relationship between these two genes, we exploited siRNA against NOX4 (siNOX4) or HSP47 (siHSP47) in separate studies without the use of nanoparticles. After the best sequence for siNOX4 or siHSP47 had been identified (see **Figure 2.3**), they were transfected using DharmaFECT in primary dermal fibroblast cells for 24 hr prior to TGF-β stimulation. As shown in **Figure 2.9A,** knocking down NOX4 by siNOX4 also resulted in down-regulation of HSP47. This is not the result of off-targeting effect of the siNOX4 sequence as both the antisense and sense strands do not show sequence homology to murine HSP47 mRNA sequence. In addition to NOX4 knockdown, COL I and α-SMA

was also down regulated. The data suggest that NOX4 may act as an upstream effector of HSP47. Oxidative stress could induce HSP47 production in several *in vitro* systems [241, 242], thus it is possible that silencing NOX4 reduces oxidative stress, which in turn lowers the HSP47 expression.

On the contrary, knocking down HSP47 by siHSP47 did not affect NOX4 level as shown in **Figure 2.9B**, but could significantly reduce COL I and α-SMA levels. Hence, I hypothesize that in addition to down-regulating NOX4 with our antioxidant nanoparticles, silencing HSP47 gene (with siHSP47) may have enhanced antifibrotic efficacy than managing the individual genes alone.

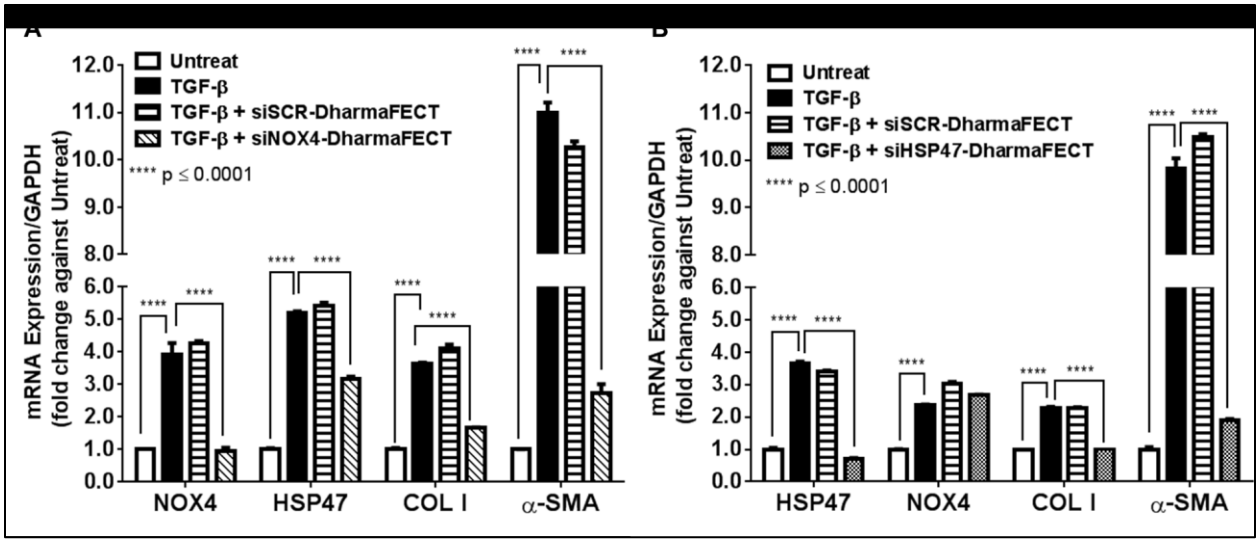

Figure 2.9. *In vitro* siNOX4 or siHSP47 transfection with DharmaFECT.
mRNA expression of primary dermal fibroblast cells treated for 24 hr with (A) siRNA against NOX4 (siNOX4) or (B) siRNA against HSP47 (siHSP47) *vs*. non-targeting siRNA (siSCR), followed by 24 hr of 10 ng/mL TGF-β stimulation. siRNA dose of 50 nM in 0.5 μL/well DharmaFECT.

2.3.6 In vitro HSP47 Gene Knock-down Efficacy by siHSP47-MSNP-PEI-PEG

To investigate the ability of MSNP-PEI-PEG nanoparticles in delivering siHSP47 in TGF-β stimulated dermal fibroblasts, I pre-treated the cells with siHSP47-MSNP-PEI-PEG or siHSP47 delivered with commercial transfection reagent, DharmaFECT. I observed 86 ± 16% knock-down in HSP47 protein expression, compared to the TGF-β alone group (**Figures 2.10A** and **B**). The knock-down efficacy was much greater than that by DharmaFECT (63 ± 18%). The qRT-PCR data also confirmed this finding where 95% mRNA knockdown was observed in siHSP47-MSNP-PEI-PEG *vs*. 81% in DharmaFECT compared to their respective non-targeting siRNA counterparts (**Figure 2.11**).Furthermore, the siSCR-MSNP-PEI-PEG also decreased the HSP47 expression by 21 ± 19% (72 ± 3% mRNA, **Figure 2.11**), demonstrating the ability of MSNP-PEI-PEG nanoparticles in reducing HSP47. In addition, I also performed similar experiment with the bleo-fibroblast cells. As shown in **Figure 2.12**, treatment of siHSP47-MSNP-PEI-PEG treatment resulted in more than 90% mRNA knock-down in bleo-fibroblast cells at 48 hr (as compared to siSCR-MSNP-PEI-PEG). The siSCR-MSNP-PEI-PEG treatment also resulted in about 20% decrease in HSP47 level as compared to the untreated bleo-fibroblast cells, which is in the same par as the siSCR-MSNP-PEI-PEG treated cells under TGF-β stimulation in **Figure 2.10**.

There was also no significant cytotoxicity associated with our nanoparticle treatment as shown in **Figure 2.10C**. Furthermore, cytotoxity study of the nanoparticles was also conducted in human dermal fibroblast, HDFa (**Figure 2.13**), which show no toxicity at efficacious dose after 24-48 hrs of exposure. Therefore, our nanoparticle can act as a safe and effective siRNA delivery system to the cells.

In summary, my *in vitro* findings so far have indicated that MSNP-PEI-PEG nanoparticle could serve as a superior siRNA carrier and can be therapeutic with regard to fibrosis treatment. The benefit of knocking down HSP47 with siHSP47 was also evident. These results prompted me to validate my *in vitro* finding with an *in vivo* mouse model.

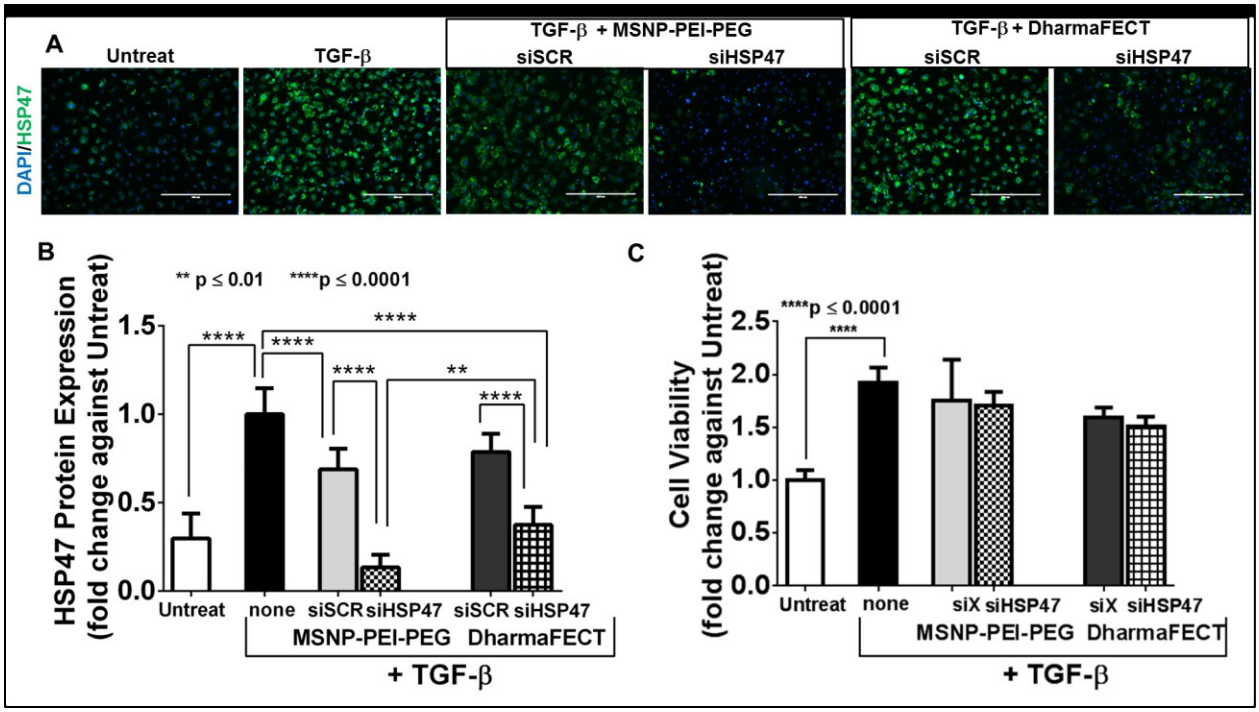

Figure 2.10. *In vitro* gene silencing efficacy with siHSP47-MSNP-PEI-PEG nanoparticles.

(A) Representative images of HSP47 stain on primary murine dermal fibroblast treated for 24 hr with siHSP47-MSNP-PEI-PEG or siHSP47-DharmaFECT, followed by 72 hr of 10 ng/mL TGF-β stimulation. Scale bar = 400 μm. (B) Corresponding HSP47 protein expression normalized by cell number (DAPI) and reported as fold-change against untreated control. (C) Relative cell viability upon the same treatments with (B).

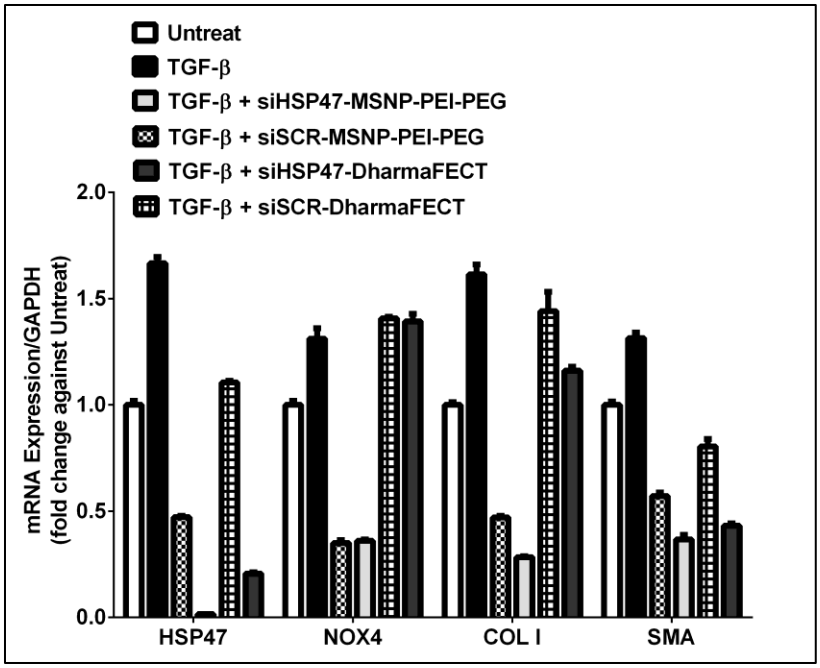

Figure 2.11. *In vitro* siHSP47 and siSCR transfection with MSNP-PEI-PEG or DharmaFECT.

mRNA expressions of primary dermal fibroblast cellstreated for 24 hr with either siSCR/siHSP47-MSNP-PEI-PEG nanoparticles (17 μg/mL, 50 nM siRNA) *vs*. siSCR/siHSP47-DharmaFECT (0.5 μL/well DharmaFECT, 50 nM siRNA), followed by 24 hr of 10 ng/mL TGF-β stimulation.

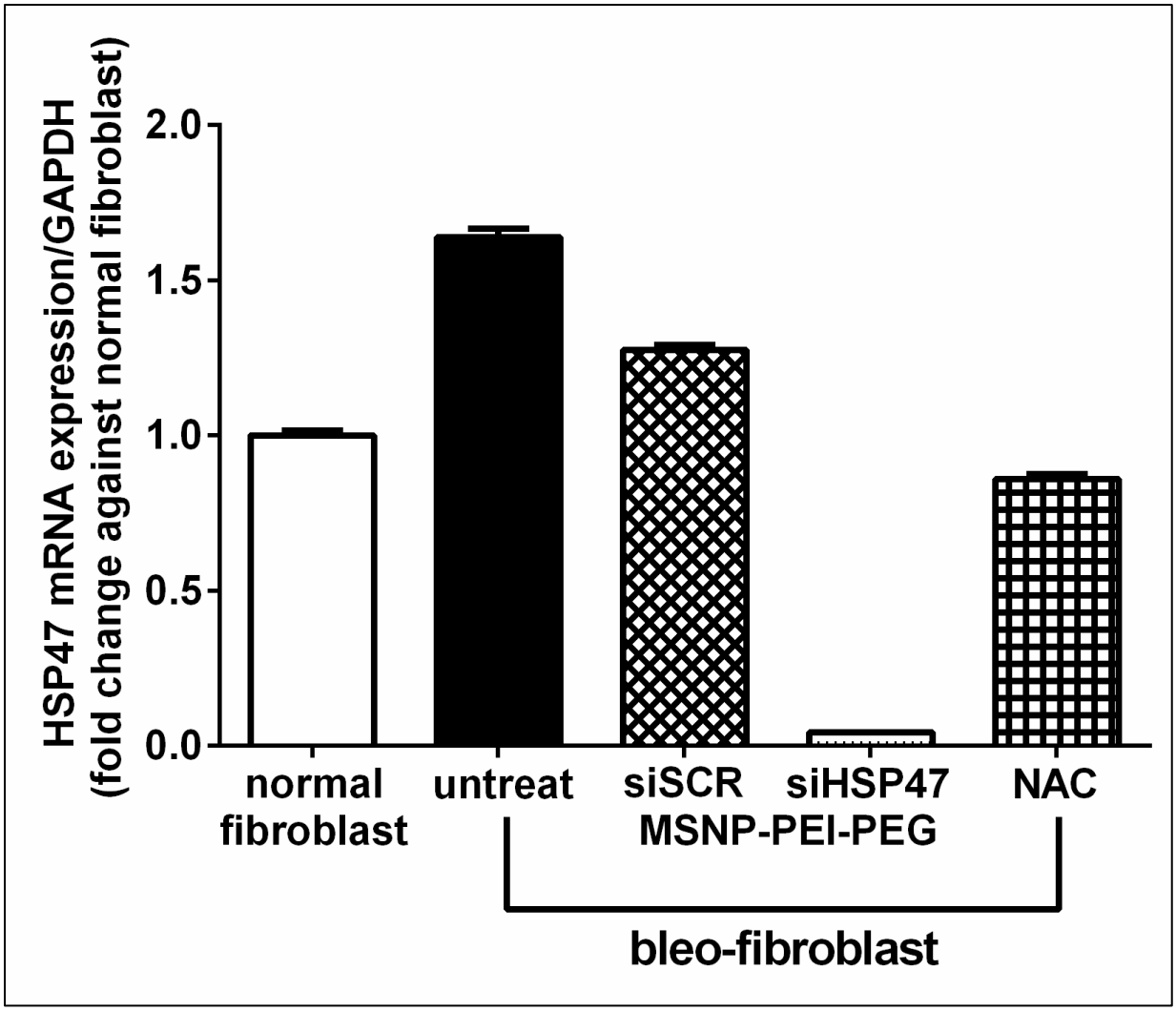

Figure 2.12. HSP47 mRNA expression in bleo-fibroblast cells treated with siHSP47-MSNP-PEI-PEG nanoparticles.
Bleo-fibroblast cells were treated with either 20 mM NAC or 17.5 μg/mL MSNP-PEI-PEG, loaded with siSCR or siHSP47 (50 nM siRNA) for 48 hr.

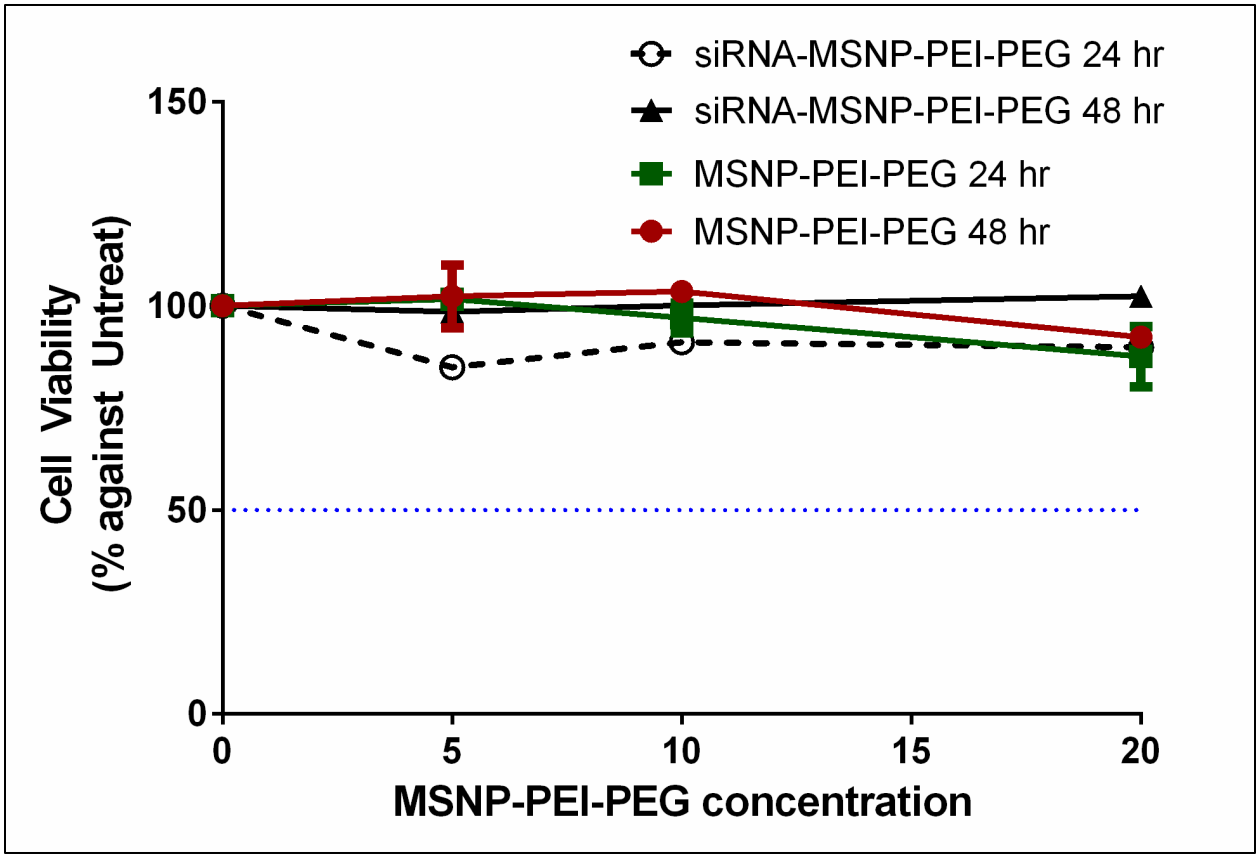

Figure 2.13. Cell viability of human dermal fibroblast cells (HDFa) with MSNP-PEI-PEG treatment.
HDFa cells were treated with increasing concentrations of MSNP-PEI-PEG nanoparticles with and without siRNA (nanoparticle to siRNA mass ratio of 25, siRNA dose of 50 nM) for 24 or 48 hr.

2.3.7 In Vivo Evaluation of siHSP47-MSNP-PEI-PEG: Skin Thickness

In order to further examine the therapeutic potential of our siHSP47-nanoparticles *in vivo*, I employed a well-accepted bleomycin-induced dermal fibrosis (scleroderma) mouse model [223]. Given intradermally, bleomycin induces toxicity (since skin lacks bleomycin hydrolase enzyme to metabolize bleomycin) and leads to the induction of ROS and pro-inflammatory cytokines (including TGF-β) to the skin [243].

I intradermally injected the siHSP47- or siSCR-MSNP-PEI-PEG nanoparticles to the shaved back of the mice on a twice-weekly schedule on alternate days of bleomycin administration over the course of 4 weeks as shown in **Figure 2.14A**. I also confirmed in a separate experiment that there was no binding of bleomycin onto the nanoparticles, which may have blocked the fibrogenesis effect of bleomycin (data not shown).

After the study was completed, H&E stains of skins were analyzed as shown in **Figures. 2.14B** and **C**. The bleomycin treatment increased the dermal thickness by 42% ($p \leq 0.001$ *vs*. untreat). Treatment of siHSP47-MSNP-PEI-PEG nanoparticles to the bleomycin-treated mice resulted in the reduction of dermal thickness by 19% ($p \leq 0.01$ *vs*. bleomycin alone), which brought the value down to the untreated level ($p=0.38$). Treatment of siSCR-MSNP-PEI-PEG nanoparticle could also decrease the dermal thickness by 7%, but not significantly different from bleomycin alone ($p=0.21$) and could not bring the value down to the untreated level ($p \leq 0.03$). These data indicated beneficial treatment of siHSP47-MSNP-PEI-PEG nanoparticle over MSNP-PEI-PEG alone.

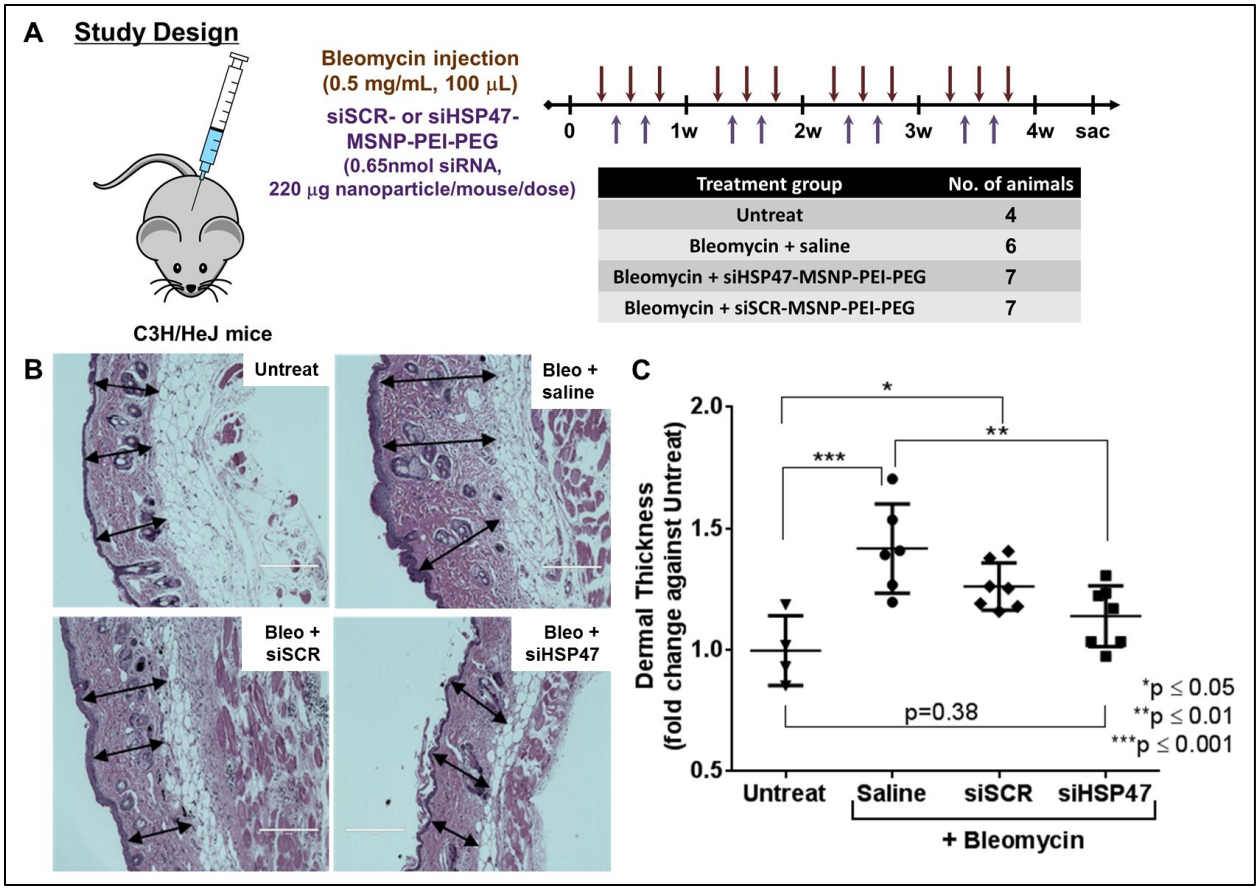

Figure 2.14. Effect of siHSP47-MSNP-PEI-PEG nanoparticles on dermal thickness in the bleomycin-induced scleroderma mouse model.
(A) Dosing scheme of bleomycin induction and the siHSP47-MSNP-PEI-PEG treatment. (B) Representative images of skin sections stained with hematoxylin and eosin (H&E), scale bar = 200 μm. (C) Dermal thickness measured from skin sections as in (C).

2.3.8 In Vivo Evaluation of siHSP47-MSNP-PEI-PEG: Protein Characterization

To examine whether siHSP47-MSNP-PEI-PEG can successfully silence HSP47 expression in the skin, we analyzed skin specimens harvested from mice treated as described in section *3.8*. Immunofluorescence technique was used for protein characterization as shown in **Figure 2.15A**, and quantified in **Figure 2.15B-E**. There was a clear up-regulation of HSP47 by 170% in the skin of mice treated with bleomycin (**Figure 2.15B**). The siHSP47-MSNP-PEI-PEG treatment was able to reduce bleomycin induced HSP47 expression to levels similar to the untreated control ($p=0.28$). The siSCR-MSNP-PEI-PEG treatment also decreased the HSP47 expression but to a much lesser extent and with less precision (larger standard deviation) than the siHSP47-MSNP-PEI-PEG counterpart. It could not bring the HSP47 level down to the untreated level ($p\leq0.0001$). As anticipated from the *in vitro* studies, the MSNP-PEI-PEG could reduce bleomycin induced NOX4 expression effectively to the untreated level regardless of siSCR or siHSP47 ($p\leq0.0001$) (**Figure 2.15C**). Bleomycin injection to the skin increased the α-SMA- and COL I-positive area by 2.7- and 1.6-fold compared to the untreated level, respectively.

With siHSP47-MSNP-PEI-PEG treatment, the area positive for α-SMA was reduced by 49% ($p\leq0.01$) as compared to the bleomycin group **(Figure 2.15D)**. Likewise, COL I-positive area for the siHSP47-nanoparticle treatment was reduced by 51% ($p\leq0.001$) compared to the bleomycin control (**Figure 2.15E**). Data also indicate that COL I-positive area was reduced to the normal level ($p=0.99$). The siSCR-MSNP-PEI-PEG effects on the reduction of the profibrotic markers (*vs*. bleomycin alone) were less substantial; 24% ($p=0.57$) for α-SMA and 19% ($p=0.25$) for COL I, respectively. In

addition, the mRNA analysis from the skin tissues collected from the siHSP47-MSNP-PEI-PEG treated mice also confirmed our findings in **Figure 2.15**. As shown in **Figure 2.16,** siHSP47-MSNP-PEI-PEG treatment showed significant reduction in HSP47 ($p \leq 0.05$), COL I ($p \leq 0.0001$) and α-SMA ($p \leq 0.0001$) levels as compared to the bleomycin-treated mice. Similar to the protein quantification data in **Figure 2.15**, the siSCR-MSNP-PEI-PEG treatment also showed significant reduction in COL I ($p \leq 0.0001$) and α-SMA ($p \leq 0.0001$) levels as compared to the bleomycin-treated mice. Thus, there is a clear advantage of siHSP47-MSNP-PEI-PEG nanoparticle over MSNP-PEI-PEG nanoparticle alone. Furthermore, I confirmed the cellular internalization of our nanoparticle in the skin by using transmission electron microscopy (TEM). As shown in **Figure 2.17**, the skin tissue of mouse injected with siSCR-MSNP-PEI-PEG + bleomycin showed intracellular localization of the nanoparticle in the dermis region.

In short, intradermal MSNP-PEI-PEG treatment could alleviate skin fibrosis by reducing ROS production and the antifibrotic effect could be further enhanced by the knocking down HSP47 expression with siHSP47.

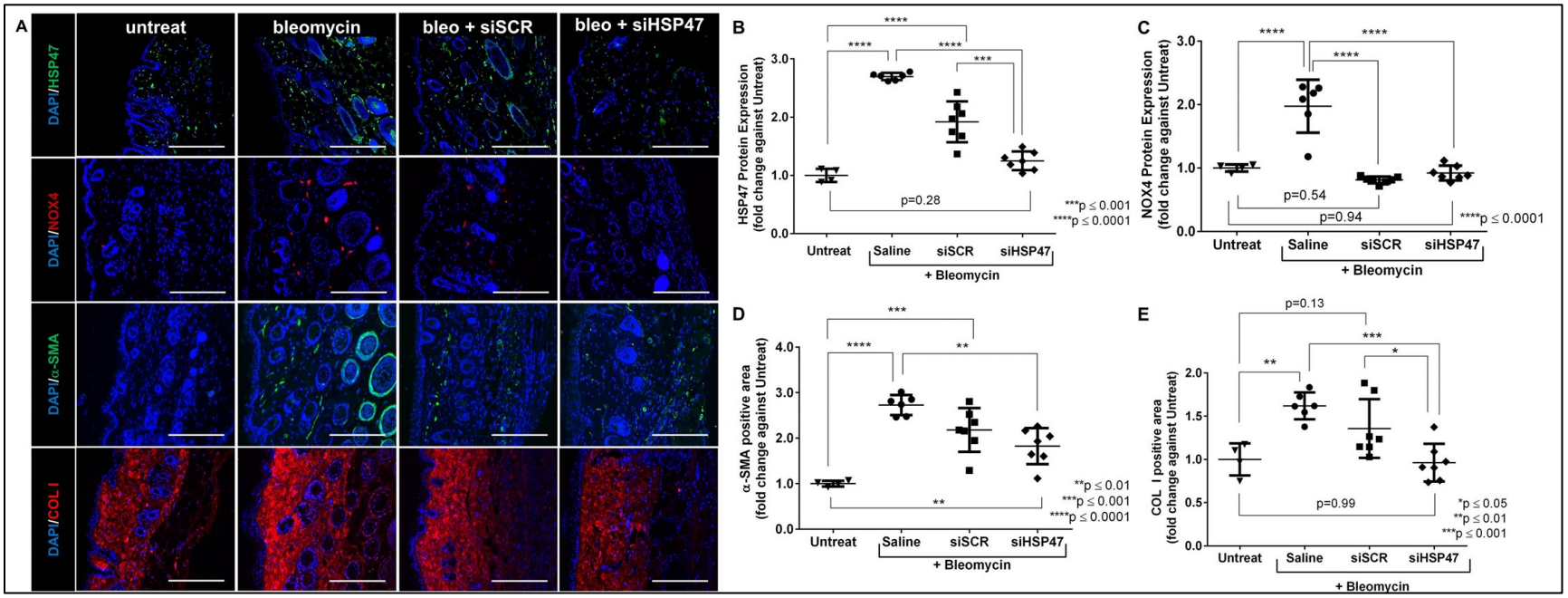

Figure 2.15. HSP47 silencing efficacy and anti-fibrotic effects of siHSP47-MSNP-PEI-PEG nanoparticles on bleomycin-induced scleroderma mouse model (dosing scheme as specified in Figure 2.14A).
(A) Representative images of skin sections stained with HSP47, NOX4, α-SMA, and COL I. Nuclei were stained with DAPI, scale bar = 200 μm. Expression levels of (B) HSP47 and (C) NOX4 proteins as well as (D) α-SMA- and (E) COL I-positive area were quantified by immunofluorescence analysis, normalized by that of untreated control.

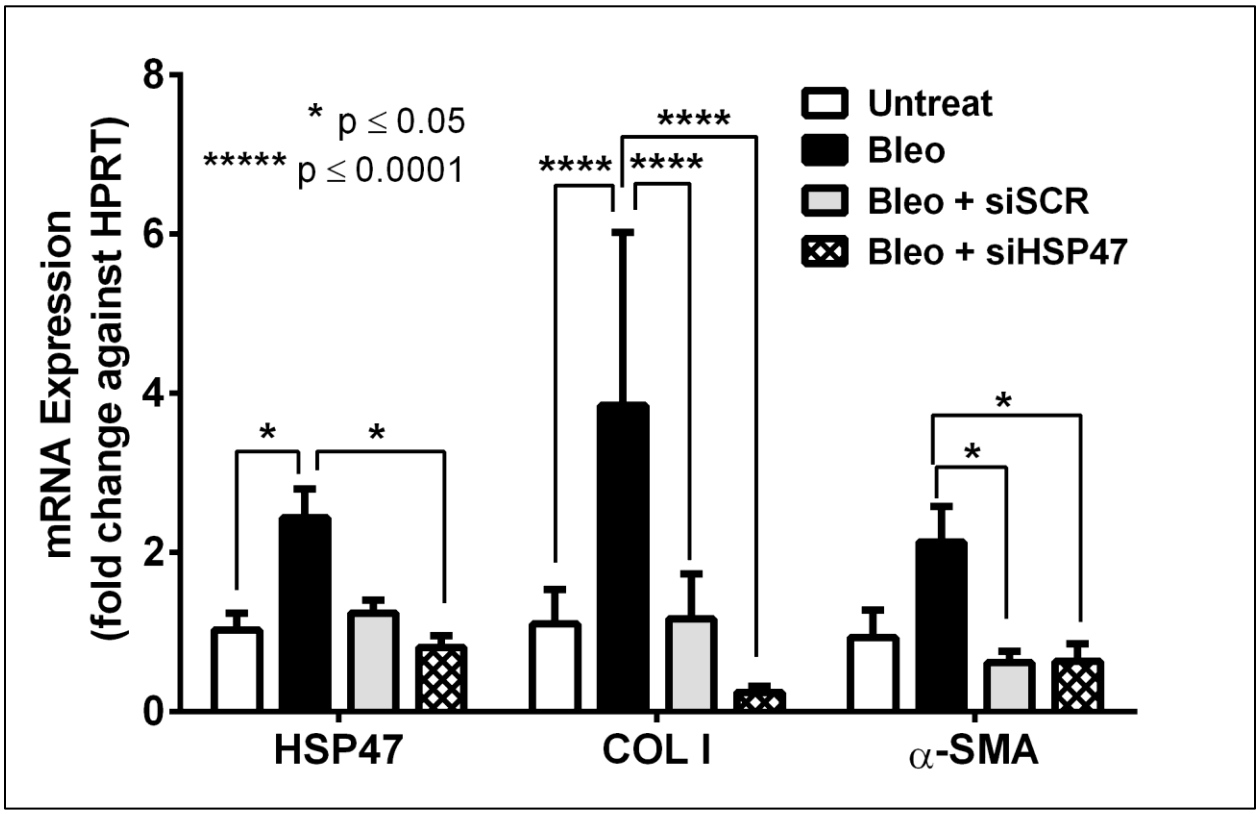

Figure 2.16. mRNA expression of the skin tissue in bleomycin-induced scleroderma mice treated with siHSP47-MSNP-PEI-PEG (n=4/treatment group).

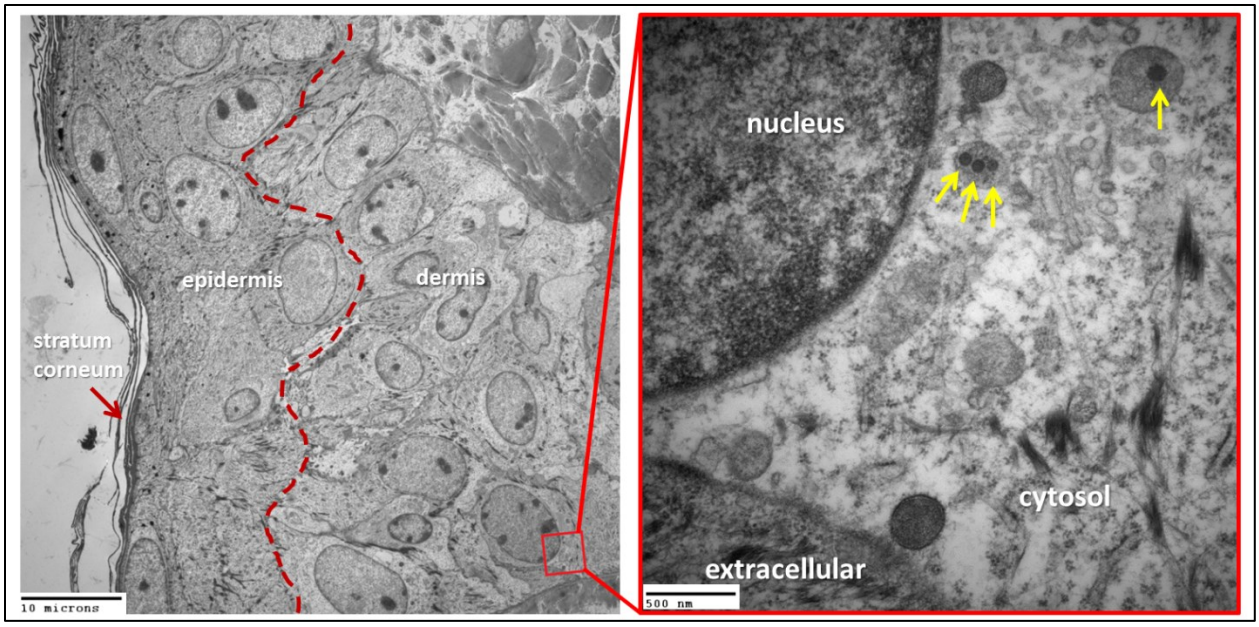

Figure 2.17. Transmission electron micrograph (TEM) of mouse skin receiving siSCR-MSNP-PEI-PEG treatment.
TEM showing intracellular localization of intradermally injected MSNP-PEI-PEG particles in the dermis layer of mouse skin collected 4 days post last treatment (treatment conditions as specified in Figure 2.14). Images were taken at low magnification (left) and high magnification (right). Yellow arrows represent nanoparticles.

2.4 Conclusions

In this work, we described the roles of ROS, NOX4 and HSP47 in fibrogenesis and developed a nanoparticle platform to modulate all three effectors in order to treat fibrosis. We show that our MSNP-PEI-PEG nanoparticles could efficiently deliver siRNA to knock-down HSP47 expression *in vitro* and *in vivo*. In addition, the nanoparticle carrier itself could reduce ROS and NOX4 production, owing to the antioxidant property of the MSNP core that is by far superior to NAC. We also elucidate for the first time that NOX4 may be an upstream effector of HSP47, which provides the explanation on how our nanoparticle carrier alone could also down-regulate HSP47 expression. The therapeutic impact of MSNP-PEI-PEG can be further enhanced by the addition of siRNA against HSP47 as demonstrated in a scleroderma mouse model. In addition to intradermal delivery reported herein, we have also shown in our most recent work [175] that the nanoparticles could be given intravenously, achieve excellent gene knock-down in solid tumors, and have excellent safety profile. Given the most optimal gene target, our nanoparticles will be able to provide combinatorial treatment for fibrotic diseases of other organs as well as inflammatory diseases.

2.5 Author contributions

The data presented in all figures were performed and analyzed by Jingga Morry, except for **Figure 2.4**. Data in **Figure 2.4** were collected by Worapol Ngamcherdtrakul, Moataz Reda, and Thanapon Sangvanich. The *in vivo* experiments were performed with the help of David Castro and Shaun Goodyear. All *in vivo* data were collected and analyzed by Jingga Morry. The manuscript was written by Jingga Morry and Wassana Yantasee.

2.6 Model limitations

In this chapter, I made use of a bleomycin-induced scleroderma mouse model as a proof-of-concept study for localized administration of our nanoparticles into the skin. The treatment was provided at the same time of bleomycin stimulation which primarily tested the anti-fibrotic effects of our nanoparticles to delay or inhibit fibrogenesis in the skin. To mimic the treatment in the clinical setting, the nanaoparticle should be given a several weeks after bleomycin stimulation to show the treatment efficacy in the established fibrosis model.

Chapter 3: Targeted treatment of metastatic breast cancer by PLK1 siRNA delivered by an antioxidant nanoparticle platform

3.1 Introduction

This dissertation chapter is focused on the application of MSNP in the treatment of breast cancer metastasis by harnessing its intrinsic antioxidant properties and taking advantage of its ability as a siRNA carrier for delivering polo-like kinase 1 (PLK1) siRNA. About 1.7 million new cases of breast cancer were diagnosed worldwide in 2012 [183] and around 250,000 are expected to be diagnosed in the US in 2016 [184], of which about 15% are triple negative breast cancer (TNBC) [185]. TNBC patients have one of the highest relapse and metastasis rates compared to other breast cancer subtypes [186, 187], with limited therapeutic options. Current treatment regimens may be new drugs not previously used in the primary setting, or re-challenged with a combination of the same drugs, mainly chemotherapeutics. Despite such treatments, median overall survival from metastasis to death is 9-13 months for all TNBC [188, 189].

Targeted delivery of siRNAs by nanoparticles holds great promise for cancer treatment since siRNA can target any gene deemed important to cancer progression, metastasis, and drug resistance with high specificity [188]. To that end, we have recently developed and optimized a polymer-coated mesoporous silica nanoparticles (NP) for siRNA delivery to treat trastuzumab-resistant HER2+ breast tumors [189]. The platform consists of a 50-nm mesoporous silica nanoparticle (MSNP) core coated layer-by-layer with bioreducible cross-linked 10-kDa polyethyleneimine (PEI) for effective siRNA binding and endosomal escape, and polyethylene glycol (PEG) for preventing nanoparticle aggregation, minimizing enzyme degradation of siRNAs, shielding the toxic

effect of PEI, and preventing recognition by the immune system. In addition, a targeting antibody can be attached to the PEG layer to act as a homing device for the nanoparticle. The siRNA is then loaded last onto the nanoparticle, passing the PEG layer (due to small size) and binding to the PEI layer due to charge preference (See **Figure 3.1**).

Herein, we report for the first time that the same platform can act as a targeted siRNA delivery system to metastatic breast tumors. For the siRNA target, we chose polo-like kinase 1 (PLK1), which is involved in cell division and DNA damage response and is found in actively dividing cancer cells [36]. There is strong association between elevated PLK1 levels in breast tumors and poor clinical outcome [190]. Moreover, a recent genome-wide kinase screen also identified PLK1 as the strongest kinase target as demonstrated by significant cell death in both cancer and tumor-initiating cells (TICs) in TNBC when either knocked down or inhibited [36]. PLK1 inhibitor, BI2536, had reached clinical trials but was terminated due to poor therapeutic index since the systemic delivery of PLK1 inhibitors was associated with increased incidence neutropenia and thrombocytopenia [191]. In addition, PLK1 inhibitors (e.g., BI2536, BI6727, GSK461364) can also inhibit other PLK family members PLK2 and PLK3, which may lead to unwanted off-target effects [192]. In contrast, siRNA can be designed to target only PLK1, and thus have less toxicity to non-cancer cells than BI2536 [193]. An siRNA against PLK1 (TKM-080301) was in clinical trials by Tekmira (now Arbutus Biopharma), but the delivery platform did not have a targeting agent and as a lipid-based platform it is only suitable for cancers with liver involvement. Although stable disease was achieved in 4 out of 9 patients, the therapeutic window was narrow due to toxicity [133].

We hypothesize that siRNA sequence specificity together with the delivery specificity to tumors achieved by our platform will improve both efficacy and safety.

Another unique feature of our platform is the inherent antioxidant activity of the mesoporous silica core. This antioxidant capability is shown herein to have pronounced effects both *in vitro* and *in vivo*, proven effective for inhibiting EMT and cellular invasion *in vitro*, and limiting metastatic spread of tumor cells in mice. ROS plays an important role in cancer metastasis [117]. ROS-generating NOX4 is crucial in redox-mediated signaling pathways, including Tks5-dependent invadopodia formation [194], TGF-β/SMAD3-driven EMT and cell migration [195], and PI3K/Akt-regulated cell proliferation and invasion [196]. Reduction of ROS using an antioxidant such as N-acetylcysteine (NAC) or the NOX inhibitor, Diphenyleneiodonium (DPI), successfully decreased cancer invasion and invadopodia formation [197]. Nevertheless, these agents are not used in clinics for such purposes due to the inability to achieve sufficient cellular NAC levels based on the current prescribed dose [198] and the challenge of getting specificity to particular NOX isoforms [199]. Thus, a material that can scavenge ROS at cellular levels can offer an effective therapy for metastatic breast cancer. Out of the 162 investigational new drugs (IND) in clinical trials for treating metastatic breast cancer, only one targets the cancers' ability to activate invasion and metastasis (a TGF-β inhibitor), and most target cancers' sustaining proliferative signaling [200]. Our material is uniquely targeting both cancer hallmarks, making it highly novel.

3.2 Materials and methods

3.2.1 Synthesis and characterization of nanoparticles and siRNA loading

Mesoporous silica nanoparticles (MSNPs) of 50 nm in size were synthesized and surface-modified as in our previous report [201]. MSNP cores were measured for primary (dry) size by a Transmission Electron Microscope (Philips/FEI Tecnai TEM, Hillsboro, OR). After chemical modifications, the material was measured for hydrodynamic size in PBS (pH 7.2) with a Zetasizer (Malvern, Westborough, MA). PEI and PEG loadings were quantified by a thermogravimetric analyzer (TGA Q50, TA Instruments, New Castle, DE). siRNA loading was quantified by fluorescence detection of dye-tagged siRNA as well as gel electrophoresis. The material contained 14 wt% 10-kDa PEI, 18 wt% 5-kDa PEG, 3 wt% antibody or no antibody, and 2 wt% siRNA. It is referred to as T-siRNA-NP with Trastuzumab (T) antibody, or siRNA-NP without [201]. The particle size in PBS was 104 ± 1.7 nm, and the charge in 10 mM NaCl was 8.10 ± 0.3 mV (within the neutral range as defined by Nanotechnology Characterization Lab of NCI [202]). Schematic illustration of the nanoconstruct can be found in **Figure 3.1**.

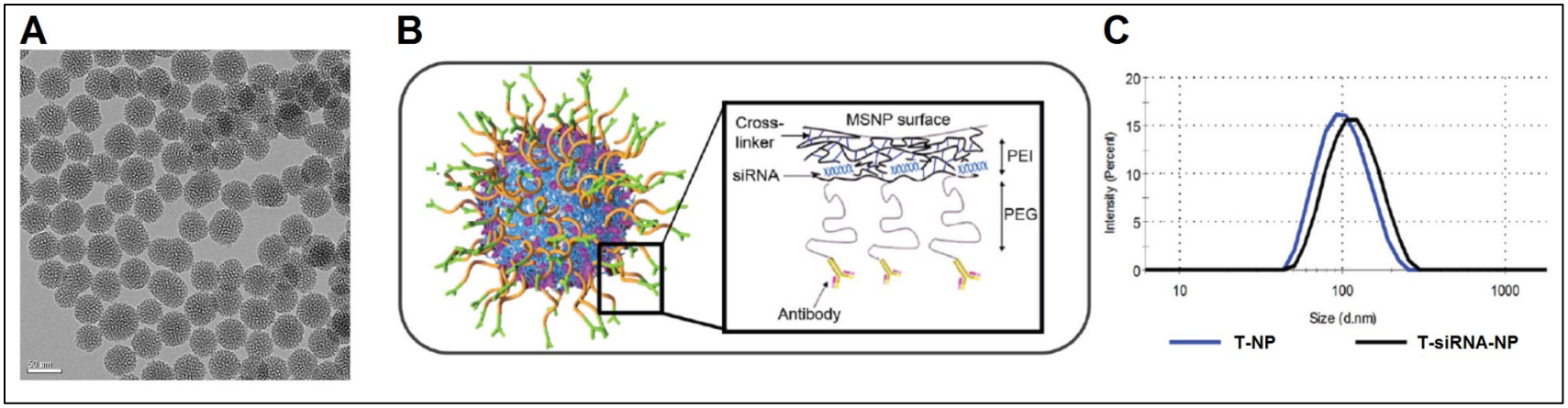

Figure 3.1. Mesoporous silica-based nanoconstruct for targeted delivery of siRNA.
(A) TEM image of mesoporous silica nanoparticle (MSNP), scale bar = 50 nm. (B) Schematic illustration of nanoconstruct (T-siRNA-NP), MSNP was coated layer-by-layer with cross-linked polyethylenimine (PEI), polyethyleneglycol (PEG), and trastuzumab. siRNA was loaded last and bound to the PEI layer due to charge preference, being protected under the PEG layer from enzyme degradation. (C) Hydrodynamic size of final nanoconstruct with and without siRNA, T-NP and T-siRNA-NP, respectively. Reproduced and modified with permission from John Wiley and Sons [175].

3.2.2 Cell culture and transfection

Human breast carcinoma cell lines, BT549 and MDA-MB-231, were obtained from American Type Cell Collection (ATCC) and maintained in RPMI with 10% FBS. LM2-4luc+/H2N [25], was a gift from Prof. Robert Kerbel (University of Toronto) and Prof. Giulio Francia (now at University of Texas at El Paso) and maintained in RPMI + 5% FBS. For NP transfection (loaded with siSCR or siPLK1), cells (3,000 cells/well in 96-well plates or 200,000 cells/well in 6 well plates) were seeded overnight in complete medium and transfected with NP for 24 h. The cells were washed once with PBS on the next day and incubated for another 24 – 72 h post-treatment depending on the type of the assays. Positive controls were carried out using DharmaFECT-1 transfection reagent (GE Dharmacon, Lafayettte, CO) diluted in OptiMEM medium (ThermoFisher Scientific, Eugene, OR). Unless stated otherwise, all experiments were performed with nanoparticle-to-siRNA mass ratio of 50 and 50 nM siRNA throughout the study.

3.2.3 siRNAs

Four different PLK1 siRNA sequences were purchased from Qiagen (cat. #1027416) for siRNA screening in the LM2-4luc+/H2N cell line. The *in vivo* grade siRNA was custom made by GE Dharmacon and identified as the sequence that yielded the highest PLK1 gene knockdown and cell death in LM2-4luc+/H2N cells (see **Figure 3.2**). The siRNA sequences were as follows: optimal PLK1 (antisense 5-‘UAUUCAUUCUUCUUGAUCCGG-3’); scrambled SCR (antisense 5’-UUAGUCGACAUGUAAACCA-3’). DY677-siSCR was custom made with DyLight 677 attached to the sense strand of the siSCR (GE Dharmacon).

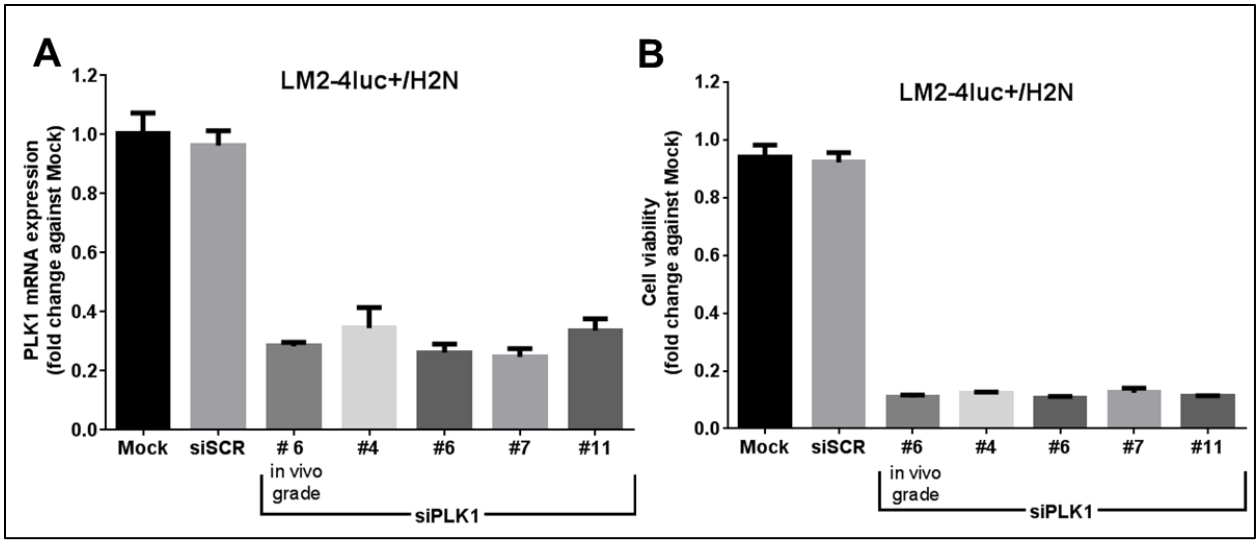

Figure 3.2. PLK1 siRNA screening on LM2-4luc+/H2N cells.
(A) PLK1 mRNA expression of LM2-4luc+/H2N transfected with various siRNA sequences against PLK1 using DharmaFECT transfection reagent at 10 nM siRNA concentration for 48 h. (B) Cell viability of LM2-4luc+/H2N cells treated with the same condition as (A) for 5 days. siPLK1 #6 is considered the best siRNA sequence and was custom-ordered for the *in vivo* grade. The *in vitro* silencing efficacy of the *in vitro vs*. *in vivo* grade siPLK1#6 were similar as shown above.

3.2.4 Intracellular ROS assay

To measure the impact of nanoparticles on cellular ROS induction, cells were pre-treated with siSCR-NP, siSCR-DharmaFECT (50 nM siRNA), 5 μM Diphenyleneiodonium chloride (DPI, Sigma Aldrich, St. Louis, MO), or 20 mM of N-acetylcysteine (NAC, Sigma Aldrich) antioxidant for 24 h. After 24 h, 100 μM of menadione was added into each well for 1 h to induce oxidative stress. At the end of the incubation period, cellular ROS was assayed using CellROX® deep red reagent (ThermoFisher Scientific) following the manufacturer's protocol using flow cytometry.

3.2.5 Cell viability assay

The viability of treated cells was determined 72 h post-transfection using CellTiter-Glo® Luminescent Cell Viability Assay (Promega, Madison, WI) following the manufacturer's protocol. The luminescent signal from CellTiter-Glo® assay was detected using Tecan Infinite M200 microplate reader and reported as fold change over the untreated control.

3.2.6 Cell-cycle analysis

After 24 h treatment with siSCR-NP, siPLK1-NP, or 10 nM BI2536 (Selleck Chemicals, Houston, TX), cells were washed once with PBS and stained with 10 μg/mL Hoechst 33342 (ThermoFisher Scientific) for 30 min at 37 ^{o}C. The cells were then trypsinized and spun down at 1000 rpm for 5 min. Cell pellets were washed twice in PBS and resuspended in 500 μL of FACS buffer (1X PBS (Ca/Mg^{2+} free), 1 mM EDTA, 25 mM HEPES pH 7.0, 1% FBS) and analyzed by flow cytometry (Guava Millipore Easycyte, EMD Millipore, Billerica, MA).

3.2.7 Wound healing assay

The wound healing assay protocol was modified from Liang *et al.* [92]. Briefly, 70-80% confluent LM2-4luc+/H2N cells in 12-well plate were treated with siSCR-NP, siPLK1-NP, siSCR-DharmaFECT, or siPLK1-DharmaFECT (all with 50 nm as siRNA dose). After 24 h treatment, a wound was created by scratching each well (~100% confluency) with a 200 µL pipette tip, washed three times with warm PBS, and replaced with serum-free medium. Each well was imaged at time 0 and 24 h after scratching with EVOS FL microscope (ThermoFisher Scientific). The migration of cells into the cell-free gap was quantified using ImageJ (NIH, Bethesda, MA) wound healing tool macros.

3.2.8 Gelatin degradation assay

This assay was performed following the established protocol [206] with slight modification. Briefly, Oregon-green 488 conjugate gelatin (ThermoFisher Scientific) was evenly coated (in 2% sucrose PBS) on the 12 mm glass coverslips for 30 min in the dark, fixed with 0.5% glutaraldehyde on ice for 15 min and quenched with 5 mg/mL sodium borohydride (Sigma Aldrich) for 3 min. Coverslips were then incubated in complete media overnight before use.

LM2-4luc+/H2N, pre-treated with siSCR-NP or 5 µM DPI, were seeded on the gelatin-coated coverslips for 24 h at 50,000 cells/well density before fixation and immunostaining. Cells were fixed with 4% PFA, permeabilized with 0.1% Triton-X for 30 min, and stained with Alexa-Fluor 568 Phalloidin (Thermo Fisher Scientific). Quantification of gelatin degradation activity was performed at 20X magnification with at least 8 randomly chosen fields per well, representing a minimum of 300 total cells

scored per experimental point. The analysis of degradation area was performed with ImageJ software and calculated as the degraded area per field normalized to the number of cells in each field. Representative images were taken at 63X magnification with Zeiss Axioplan2 microscope equipped with Zeiss Axiocam HRm CCD camera using Zen software.

3.2.9 Matrigel invasion assay

LM2-4luc+/H2N cells (1 x 10^6 cells/dish) were seeded on a 10-mm petri dish and transfected with siSCR-NP overnight. Cells were then trypsinized and counted before being seeded onto the matrigel-coated invasion chambers in serum-free medium (125,000 cells/insert). DPI (5 μM) or NAC (2 – 30 mM) was added to the cells at the same time of cell plating on the upper chamber insert. After 48 h, the number of invaded cells were quantified according to the manufacturer's instructions of Chemicon® QCM™ 24-well Fluorimetric Invasion assay kit (ECM554, Chemicon, Millipore).

3.2.10 3D Matrigel culture and immunostaining

3D culture of LM2-4luc+/H2N cells were performed as described by Lee *et al.* [92] with slight modifications. Briefly, cells transfected overnight with DY677siSCR-NP were trypsinized and counted before being seeded onto matrigel-coated 4 well chamber slides (10,000 cells/well) and overlaid with complete medium containing 2% matrigel. Cells were grown on the slides for up to 5 days and imaged on alternate days starting from day 1 post seeding with the EVOS FL automated fluorescence microscope.

3.2.11 Real time quantitative PCR (qPCR)

The RNA from the treated cells was isolated with the RNeasy Mini kit (Qiagen) following the manufacturer's protocol. The amount of RNA was quantified using the NanoDrop 1000 spectrophotometer (Thermo Scientific). Purified RNAs (20 ng per reaction) were reverse transcribed with EXPRESS One-Step SuperScript qRT-PCR kit (ThermoFisher Scientific). Primer sequences chosen for qPCR (ThermoFisher Scientific) are: human PLK1 (Hs00983227_m1), human NOX4 (Hs01558199_m1), and human GAPDH (Hs02758991_g1). qRT-PCR assays were performed in triplicate using an ABI 7500 Fast System (Applied Biosystems, Foster City, CA) under standard cycling conditions: 50 ^{o}C for 2 min, 95 ^{o}C for 10 min, 40 cycles of 95 ^{o}C for 15 s, and 60 ^{o}C for 1 min. Expression levels were analyzed using $2^{-\Delta\Delta C(t)}$ method using GAPDH as loading control.

3.2.12 Western blot

Cell lysate (30 µg protein/lane) were electrophoresed with denaturing sodium dodecyl sulfate (SDS)-polyacrylamide NuPage Novex 4% to 12% gels (Invitrogen) and blotted on a PVDF membrane (Millipore). Primary antibody incubation was carried out overnight at 4°C on a rocking platform (anti-PLK1, ab17056, Abcam; β-Actin (8H10D10), Cell Signaling Technology; anti-NOX4, ab109225, Abcam). Secondary incubation with IRDye 800CW and IRDye 680RD conjugated secondary antibodies (Licor Biosciences) was carried out at room temperature (2 h) the next day prior to imaging with the LI-COR infrared imaging system (LI-COR, Lincoln, NE).

3.2.13 Animal studies

The experimental protocol was approved by the Institutional Animal Care and Use Committee (IACUC) of Oregon Health and Science University (OHSU). 6-8 week old SCID hairless SHO^{TM} (Crl:SHO-Prkdc^{scid}Hr^{hr}, Charles River, Wilmington, MA) mice received intravenous tail vein injections of 2 x 10^6 LM2-4luc+/H2N cells (suspended in 200 µL PBS) and were allowed to establish metastasis in lungs for 2 weeks before initiating the treatments. All mice were randomly divided into three treatment groups (n = 8/group): Saline control, T-siSCR-NP (0.5 mg/kg siSCR), and T-siPLK1-NP (0.5 mg/kg siPLK1), with a dosing schedule of twice weekly by intravenous injection (Figs. 4A). IVIS imaging was done once weekly starting from 1 week post-inoculation, following the protocol established by Caliper Life Sciences, MA. Briefly, each animal received intraperitoneal injection of 150 mg/kg of D-luciferin (Gold Bio Technology, Inc, St. Loius, MO) in 200 µL PBS, 10 minutes prior to imaging with IVIS spectrum Imaging system on prone and supine positions. The average photon flux (of prone and supine positions) for each mouse was quantified within the same area of interest in the thoracic region of each mouse. The flux was plotted as average fold-change (relative to the pre-treatment signals of each mouse) as a function of time. Body weight was measured twice weekly. All animals were sacrificed 2 days after receiving the 6th dose of treatment and their major organs (brain, heart, lung, liver, spleen, kidney, lymph nodes, and spine) were harvested and immersed in 300 µg/mL of D-luciferin (in PBS) in a 24-well plate for 5 minutes prior to *ex vivo* IVIS imaging and signal quantification. Organs with detectable IVIS signals compared to negative controls (i.e., the same organs from mice without tumor inoculation) were considered positive for the presence of cancer and included in

'incidence rate'. The tumor burden was calculated as the sum of all signals from each respective tumor-bearing organ.

For the long-term *in vivo* study, animals (8 animals per group) received the same dose and treatment schedule as the short term study but the study was extended to 2 months. Mice were monitored daily for signs of illness (hind limb paralysis from suspected spine metastasis, excessive weight loss (>10% body weight loss compared to the pre-inoculation weight), visible tumors (from lymph nodes, with size greater than 1500 mm^3), or labored breathing from lung metastasis) and were euthanized in accordance with IACUC ethical guidelines. All major organs were collected, weighed, and fixed for histological analyses.

3.2.14 Lung metastasis quantification

The lung tissues from each mouse were collected and fixed in 4% PFA and snap-frozen in OCT compound (#4583, Tissue-Tek) prior to processing. Tissue sections (6-μm thick) were stained with hematoxylin and eosin (H&E). To assess the metastatic area, 10 sections of the entire lung at 160 μm apart were scanned using ScanScope XT Digital Slide Scanner (Aperio), and the area of each metastatic lesion was measured relative to the total lung area.

For determination of the tumor burden and human PLK1 mRNA expression in mouse lungs, lung tissue from each mouse was homogenized and lysed in RLT buffer using QIA-shredder columns (Qiagen), and the RNA was isolated using RNeasy Mini kit (Qiagen) following the manufacturer's protocol. RT-PCR (100 ng RNA/sample per reaction) was performed to identify the ratio of human HPRT mRNA (Hs99999909_m1)

relative to mouse HPRT mRNA (Mm03024075_m1) for tumor burden or human PLK1 mRNA (Hs00983225_g1) relative to human HPRT mRNA to assess PLK1 gene knockdown as the result of the treatments.

3.2.15 Histology

All tissues were either fixed in 10% buffered formalin (Fisher Scientific) or snap-frozen in OCT compound (#4583, Tissue-Tek) prior to processing. For immunofluorescence staining, deparaffinized and rehydrated lung tissues were subjected to heat-mediated antigen retrieval in citrate buffer (10 mM, pH 6.0) for 30 min. The tissue sections were permeabilized with 0.25% Triton-X100 (PBS) for 30 min and blocked with 10% goat serum (Vector Laboratories Inc., Burlingame, CA) for 1 h at room temperature. Slides were then incubated with primary antibodies (5% goat-serum + 1% BSA in PBS) at 4 ^{o}C overnight (mouse monoclonal human vimentin, NCL-L-VIM-V9, Leica Biosystems; rabbit polyclonal Ki67, NCL-Ki67p, Leica Biosystems; rabbit polyclonal cleaved caspase-3, #9661, Cell Signaling Technology), washed, incubated with secondary antibodies (Alexa 647-conjugated anti-rabbit or anti-mouse Ab, Invitrogen) for 1 h at room temperature, and mounted with ProLong Gold Antifade reagent with DAPI (P-3691, Invitrogen). Images were taken with the EVOS FL fluorescence microscope at 20X magnification.

For quantification of Ki67 and cleaved-caspase 3, images from Ki67-immunostained lung sections were taken at 20X magnifications (five fields per section, 2 lesions per mouse). Percentage of Ki67-positive or cleaved-caspase3-positive cells within the

lesion relative to total number of cells within the same region was quantified. Total of five mice per each group were analyzed.

3.2.16 Statistical Analysis

In vitro experiments were performed in triplicates (experimentally and analytically), and results were presented as mean ± SD. *In vivo* experimental data were presented as mean ± SEM. Comparisons of all groups at a single time point were performed after testing for D'Agostino-Pearson omnibus normality tests (Graphpad Prism 6.0). Comparisons of two groups were performed either with Student's *t* tests (for normal distribution) or Mann-Whitney test (for nonparametric test, unpaired groups). For comparisons of more than three groups, statistical analysis was done either with one-way ANOVA with post-hoc Dunnett's multiple comparison tests (for normal distribution) or Kruskal-Wallis non-parametric test with post-hoc Dunnett's multiple comparison tests (for non-normal distribution). Two-way ANOVA followed by post-hoc Tukey's multiple comparison tests was performed to analyze the treatment effects over time in the photon flux measurement of the *in vivo* study. Graphpad Prism 6.0 software (GraphPad software Inc., San Diego, CA) was utilized for all statistical analyses. P-value < 0.05 was considered to be statistically significant.

3.3 Results

3.3.1 PLK1 knockdown efficacy and resultant apoptotic cell death

To investigate the silencing efficacy of siPLK1-NP *in vitro*, I treated three human TNBC cell lines, BT549, MDA-MB-231, and LM2-4luc+/H2N (HER2-expressing MDA-MB-231 metastatic variant [203]) cell lines with siPLK1-NP and measured the mRNA and protein expressions 24 and 48 h post-treatment, respectively. As shown in **Figure 3.3A-B**, siPLK1-NP efficiently reduced the PLK1 mRNA by 69-87% and protein expressions by 64-91% in the three cell lines compared to the untreated control. Consequently, the siPLK1-NP treatment induced significant loss of cell viability measured at 3 days (**Figure 3.3C**). I also confirmed that the siPLK1-NP treatment caused G2/M cell cycle arrest at 24 h post treatment (**Figure 3.3D**). On the contrary, non-targeting siSCR-NP did not cause any significant reduction in the PLK1 expression (**Figure 3.3A-B**), was not toxic to the cells (~80% cell viability, **Figure 3.3C**), and did not alter cell cycle arrest compared to the untreat (**Figure 3.3D**). These results demonstrate that the NP is well tolerated, and can effectively deliver siPLK1 intracellularly, leading to apoptotic death of the TNBC cell lines.

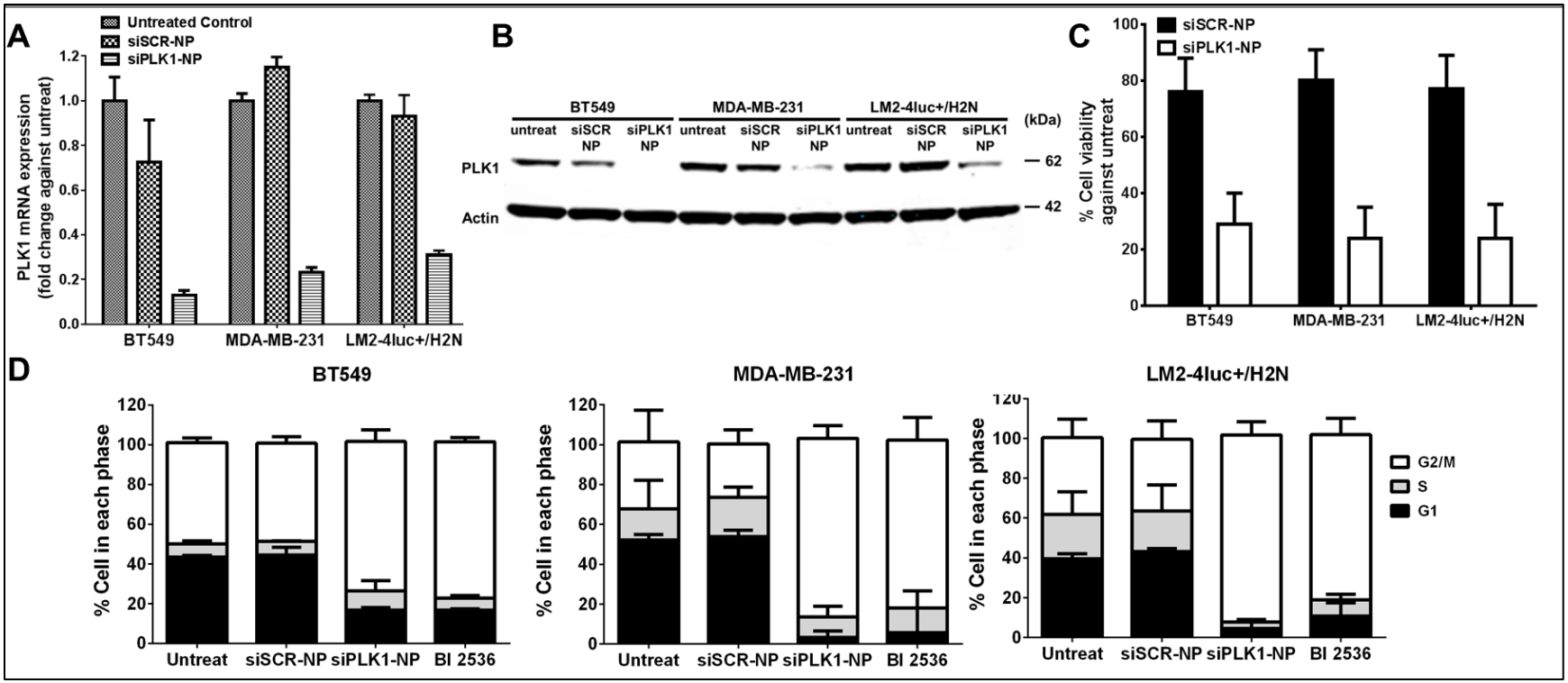

Figure 3.3. Effective knockdown of PLK1 with siPLK1-NP leads to G2/M cell cycle arrest and reduced viability of three TNBC cell lines (BT549, MDA-MB-231, and LM2-4luc+/H2N).
(A) Expression levels of PLK1 mRNA after treated with either siSCR- or siPLK1-NP for 24 h, as measured by qPCR, and normalized to GAPDH expression. (B) Protein expression of PLK1 after 48 h, as assessed by western blot with Actin as the loading control. (C) Cell viability after 72 h. (D) Cell cycle analysis after 24 h treatment with siSCR-, siPLK1-NP, or 10 nM of BI2536. All with siRNA dose of 50 nM. All data are presented as mean ± SD from 3 independent experiments.

3.3.2 Antioxidant and NOX4 reduction properties of NP in TNBC cell lines

From our recent report [204], the MSNP core of our NP had ROS scavenging and NOX4 reduction ability in TGF-β stimulated dermal fibroblast cells, yielding greater anti-fibrotic properties (e.g., reducing COL I and α-SMA) than observed with NAC treatment. Herein, I investigated the antioxidant effects of NP treatment on breast cancer cells. I included siSCR on the NP treatment in order to maintain similar size and charge of the nanoconstruct (and hence cellular uptake) as those of the siPLK1-NP. This siSCR does not have any significant sequence homology to known human or mouse genes. The ROS levels of all three TNBC cell lines were significantly higher (by 2-8 fold) than the non-tumorigenic breast epithelial cells line, MCF10A (**Figure 3.4A-B**). Pre-treatment of the breast cancer cell lines with siSCR-NP prior to ROS stimulation by menadione lowered the ROS levels by 60-84% compared to the menadione alone (**Figure 3.5A**). The NP performed in a similar manner as the antioxidant NAC, and NADPH oxidase (NOX) inhibitor DPI. Since NOX is a major source of ROS production, I measured the mRNA levels of NOX family members in the TNBC cell lines *vs.* those in the normal breast epithelial cell line, MCF10A. Out of the four NOX family members tested, NOX4 mRNA levels were significantly higher (than NOX1, NOX3, and NOX5) for all the TNBC cell lines compared to MCF10A (**Figure 3.4C**). In addition to its high level, NOX4 (and ROS) has been shown to play very important roles in cancer invasion and metastasis via invadopodia formation [26], thus I further focused on NOX4. Treatment of siSCR-NP for 24 h was able to significantly reduce NOX4 mRNA in the TNBC cell lines by 37-56% compared to the untreated cells (**Figure 3.5B**), similar to NAC and DPI. Interestingly, in terms of NOX4 protein reduction, siSCR-NP lowered NOX4 expression better than NAC

and DPI after 72 h treatment (**Figure 3.5C**), suggesting that NP may have more sustainable effect than NAC and DPI. Taken together, these results proved that NP, indeed, possessed ROS-scavenging ability. The NP ability to reduce NOX4 expression upon ROS scavenging also indicates a positive feedback loop between ROS and NOX4.

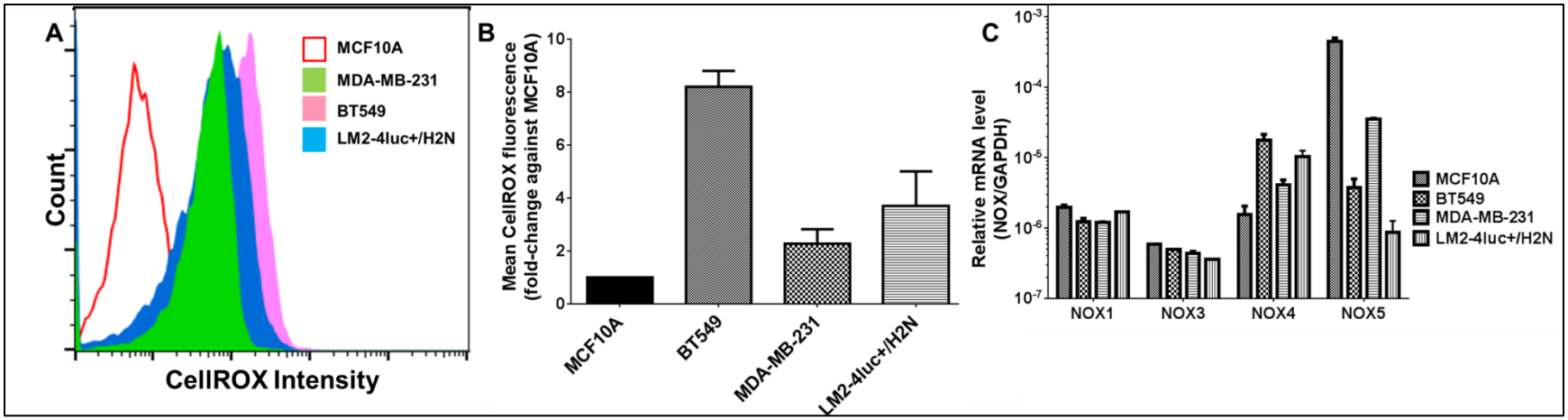

Figure 3.4. ROS intensity of TNBC cell lines measured against the non-tumorigenic cell line, MCF10A.
(A) CellROX deep red intensity of untreated MDA-MB-231, BT549, and LM2-4luc+/H2N cell lines against MCF10A. (B) Mean fluorescence quantification of (A), expressed as fold-change against MCF10A. (C) mRNA expression level of NOX family members in the three TNBC cell lines.

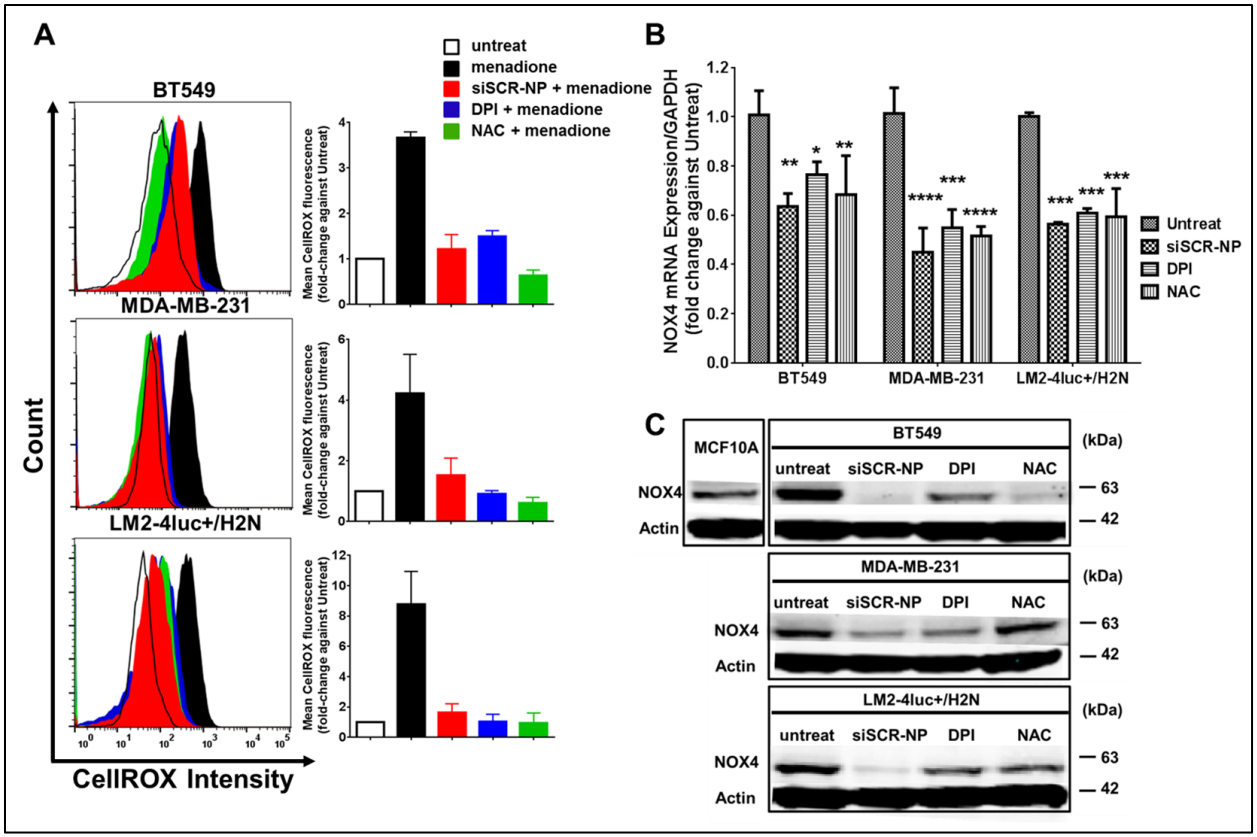

Figure 3.5. NP shows antioxidant activity and NOX4 reduction in three TNBC cell lines (BT549, MDA-MB-231, and LM2-4luc+/H2N).

(A) ROS levels of the cells after 24 h treatment with siSCR-NP (50 nM), DPI (5 μM), or NAC (20 nM), followed by 1 h treatment with 100 μM of menadione, assessed by CellROX flow cytometry. (B) Expression levels of NOX4 mRNA at 24 h and (C) NOX4 protein at 72 h of the three cell lines after receiving similar treatments with (A) for 24 h but without menadione. All mRNA data were measured by qPCR and normalized to GAPDH expression. Data are presented as mean ± SD from 3 independent experiments. *P<0.05, **P<0.01, ***P<0.001, ****P<0.0001 *vs*. untreat.

3.3.3 NP treatment inhibits cellular migration and invasion, and attenuates outgrowth of 3D-organotypic cultures

Elevated levels of ROS have been known to promote cellular migration as well as invasion [202]. To investigate the effects of NP treatment on cellular migration, I performed a wound healing assay using the LM2-4luc+/H2N cell line. The cells were wounded [25] following a 24 h pre-treatment with siSCR- or siPLK1-NP. DharmaFECT commercial transfection reagent delivering both siRNAs was also used as controls. I monitored wound closure at 24 h and report it as the percent wound recovery relative to the wound size at t = 0 h. **Figure 3.6A** shows the representative wound recovery images, and **Figure 3.6B** shows the quantification. Cells treated with siSCR-NP and siPLK1-NP displayed the least wound recovery indicating slowest cell migration compared to the untreated control and DharmaFECT counterparts. This was not due to the siSCR or siPLK1, since when delivered with DharmaFECT, they showed no inhibitory effects on wound recovery. Moreover, I also delivered NP loaded with fluorescently-labelled siRNA, DyLight 677 (DY677siSCR-NP) to ensure the effect was attributed to the intracellular presence of NP and not a physical hindrance at the wound border (**Figure 3.6A**).

Next, I investigated the ability of cancer cells to migrate through the extracellular matrix (ECM) by forming the actin-rich protrusions known as invadopodia. Specifically, I cultured cells that were pre-treated with siSCR-NP or DPI on thin fluorescent gel matrices for 24 h and measured the area of gelatin degradation. Higher gelatin degradation indicates higher invadopodia formation which correlates to the cellular invasive potential. As shown in **Figure 3.6C-D**, siSCR-NP treatment reduced gelatin

degradation activity by ~42% compared to the untreated groups, indicating reduction of invadopodia formation by the NP. The effect is on par with DPI treatment (~46%). To confirm our finding, I also measured the invasive capacity of the cells in a Matrigel-coated Boyden chamber assay. NP treatment markedly reduced the invasiveness of the cells by ~65%, in a similar manner as DPI (~60%), as compared to the untreated control (**Figure 3.6E**). Interestingly, only the high dose of NAC (30 mM) produced inhibitory effects on the invasiveness of the cells in the same par with NP and DPI. This is in agreement with previous report demonstrating that only a high NAC dose (20-40 mM) was able to reduce cancer cell invasion [176]. Conversely, the observed increase in invaded cells at the low dose of NAC (2 mM, **Figure 3.6E**) is also in line with another observation [244, 245] showing that low levels of NAC increased cancer metastasis potential *in vivo*.

To study the effects of NP treatment in a 3D environment, I seeded cells (pre-treated with DY677siSCR-NP) on matrigel-coated plates and observed the cell phenotypes from day 1 to day 5 post-seeding. LM2-4luc+/H2N cells grown in 3D culture exhibited stellate structures (**Figure 3.6F**), which is typical for highly invasive cells such as its parental MDA-MB-231 cell line [151]. However, treatment with siSCR-NP inhibited the invasive growth patterns of these cells, resulting in more rounded spheroid structures. To ensure that NP was still present within the cells, I also imaged the cells in the fluorescence channel (for viewing DY677siSCR-NP) up to 5 days post seeding on matrigel (**Figure 3.6F**). These experiments demonstrate that NP treatment effectively reduced cellular migration and invasiveness of a highly invasive breast cancer cell line *in vitro*.

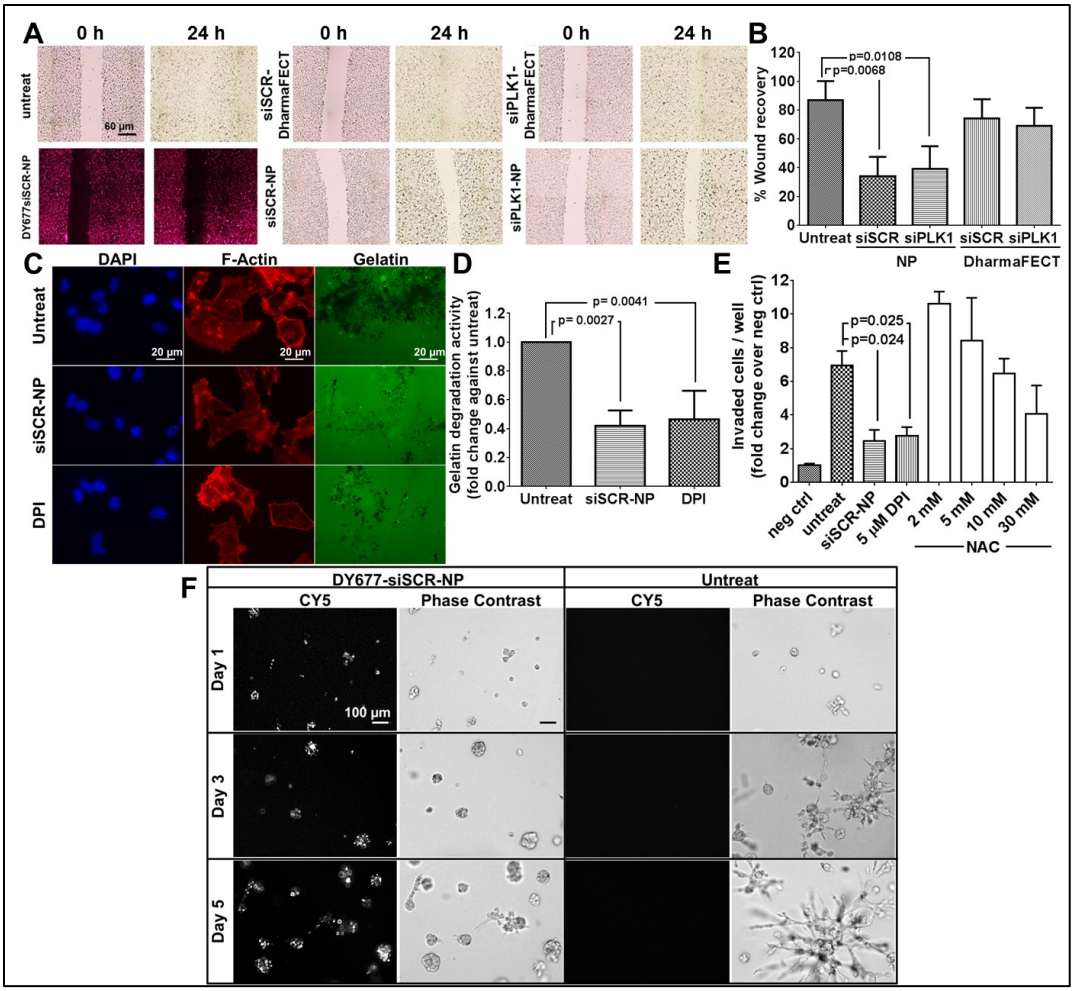

Figure 3.6. NP treatment impedes cellular migration and reduces cellular invasiveness of LM2-4luc+/H2N cell line.

(A) Representative images of wound healing assay with siSCR or siPLK1 on NP, or on DharmaFECT (all with 50 nM as siRNA). Cells were treated for 24 h prior to wound scratch and images were taken at 0 h and 24 h post wounding. (B) The percent wound recovery area from (A) using ImageJ. Data are presented as mean ± SD from 3 independent experiments (n=8-10 images/well, duplicate wells per experiment). (C) Representative images from gelatin degradation assay. Cells were pre-treated with 50 nM siSCR-NP or 5 μM DPI prior to seeding on the FITC-gelatin coated coverslips for 24 h. Cells were labeled with F-actin (red) and nucleus (blue). (D) The percentage of gelatin degradation per total number of cells in (C) by ImageJ. Data are presented as mean ± SD from 3 independent experiments (n = 5 images/well, >50 cells/field, duplicate wells per experiment). (E) Invasion of LM2-4luc+/H2N cells after 48 h treatment with 50 nM siSCR-NP, 5 μM DPI, or 2-30 mM NAC through Matrigel-coated Boyden chambers, normalized by negative controls (number of cells invaded through chambers with no serum added). Data are represented as mean ± SD from two independent experiments performed in duplicates. (F) Representative images of LM2-4luc+/H2N cells pretreated with 50 nM DY677siSCR-NP prior to seeding in 3D matrigel culture *vs*. untreat and imaged on day 1, 3, and 5 post seeding.

3.3.4 Ability of T-NP to deliver siRNAs and elicit therapeutic effects in a TNBC metastasis model

A breast cancer metastasis model was established upon tail vein injection of LM2-4luc+/H2N cells (from Dr. Robert Kerbel lab. University of Toronto) − a highly metastatic variant of MDA-MB-231 (TNBC), which were isolated from lung metastasis in mice [183] and has been shown to develop metastasis in multiple organs [92]. This cell line was later engineered to express luciferase and HER2 genes [206]. Despite overexpressing HER2, we found that this cell line behaved like its parental MDA-MB-231 cell in that it did not respond to trastuzumab (0-30 μg/ml) as a free drug or when conjugated to the NP (T-NP) *in vitro* (**Figure 3.7**). Thus, the HER2 protein can serve as the homing target receptor to facilitate targeted delivery of siPLK1 using our T-NP. siPLK1 was highly effective in killing this cell line (see **Figure 3.3**). In mice, tumors were allowed to establish for 2 weeks until luciferase signals were detected in lungs by IVIS (**Figure 3.8B**), followed by twice-weekly tail vein injections of T-siPLK1-NP. Dosing and schedule are shown in **Figure 3.8A**. After a total of 6 doses of 0.5 mg/kg siRNA, T-siPLK1-NP exhibited significantly reduced tumor burden in the lungs compared to the saline and T-siSCR-NP groups (**Figure 3.8C**). This was also reflected in the constant body weight of the animals treated with T-siPLK1-NP, while those treated with saline and T-siSCR-NP experienced weight loss likely due to advanced cancer metastases (**Figure 3.8D**). At 2 days post last dose, the study was concluded and the organs from each mouse were imaged *ex vivo* with IVIS (**Figure 3.8E**). Tumor incidence rates (organs with positive IVIS signals relative to the respective organs of normal mice) as well as tumor burden (photon flux relative to the respective organs of normal mice) were

tabulated in **Figure 3.8F**. The extent of tumor spreading was confined to fewer organs with the T-siSCR-NP treatment, with the least number of distant metastases observed with T-siPLK1-NP (**Figure 3.8F**). These findings are consistent with our *in vitro* data which demonstrated that siPLK1-NP inhibited cancer cell growth and that NP (with just siSCR) treatment reduced metastatic potential (e.g., spreading of cancer from the initial site, lungs, to other organs).

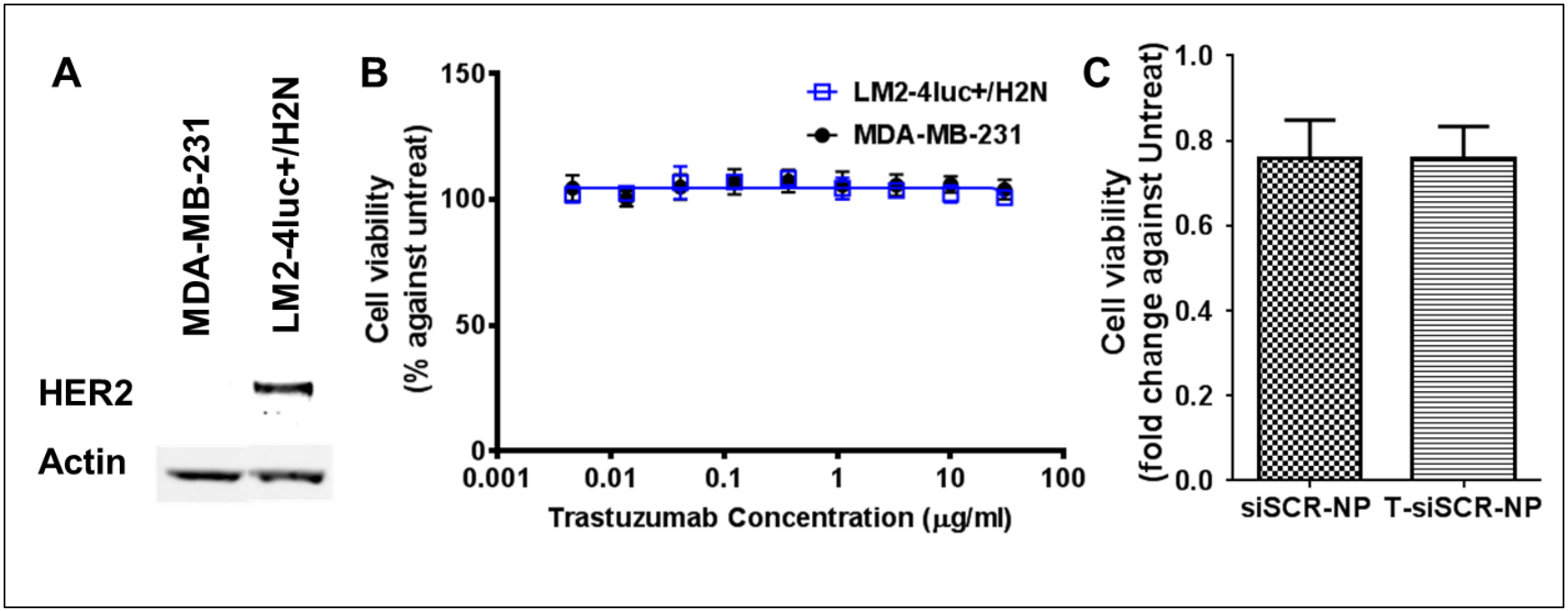

Figure 3.7. LM2-4luc+/H2N cells dependency on HER2 expression.
(A) Western blot data on the HER2 expression on LM2-4luc+/H2N cells as compared to its parental cell line, MDA-MB-231. (B) Dose response curve on the cell viability of LM2-4luc+/H2N treated with trastuzumab for 5 days, as compared to MDA-MB-231. (C) Cell viability of LM2-4luc+/H2N cells treated with siSCR-NP and T-siSCR-NP (50 nM as siRNA) at 5 days post treatment.

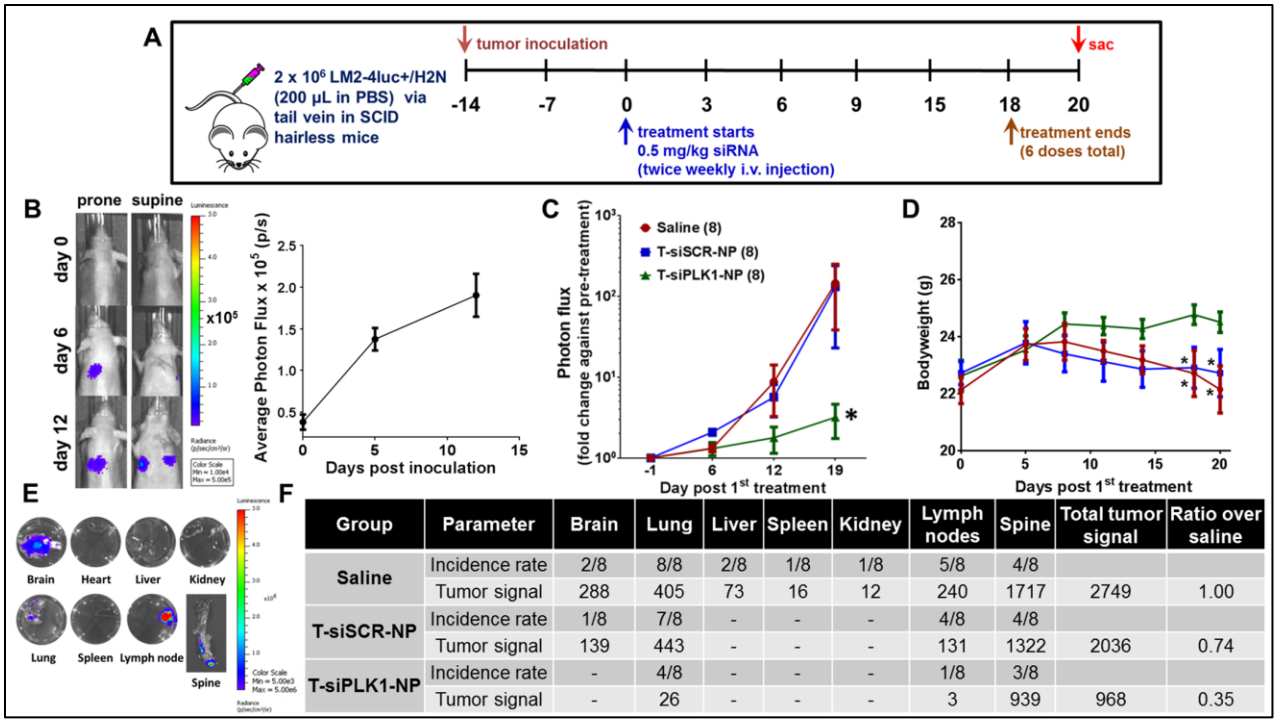

Group	Parameter	Brain	Lung	Liver	Spleen	Kidney	Lymph nodes	Spine	Total tumor signal	Ratio over saline
Saline	Incidence rate	2/8	8/8	2/8	1/8	1/8	5/8	4/8		
	Tumor signal	288	405	73	16	12	240	1717	2749	1.00
T-siSCR-NP	Incidence rate	1/8	7/8	-	-	-	4/8	4/8		
	Tumor signal	139	443	-	-	-	131	1322	2036	0.74
T-siPLK1-NP	Incidence rate	-	4/8	-	-	-	1/8	3/8		
	Tumor signal	-	26	-	-	-	3	939	968	0.35

Figure 3.8. T-siPLK1-NP treatment reduces LM2-4luc+/H2N tumor burden in lungs and prevents spread of the cancer to other organs in the *in vivo* experimental metastasis model.

(A) Schematic representation of the study design. (B) Representative whole body bioluminescent IVIS imaging of a mouse injected intravenously with 2 x 10^6 LM2-4luc+/H2N cells on both, prone and supine, positions on day 0, 6, and 12 post-inoculation (left). The average photon flux measured from thoracic region of mice up to two weeks post inoculation (right). (C) Quantification of lung photon flux (by weekly IVIS) normalized to pre-treatment flux from each individual mouse in the same treatment groups. (D) Average body weight of mice in each treatment groups during the study period. (E) Representative images of *ex vivo* bioluminescent IVIS imaging of the organs collected from a mouse sacrificed on day 20 of saline treatment. (F) Incidence rate of LM2-4luc+/H2N metastasis in various organs of mice receiving a total of 6 doses of either siPLK1- or siSCR-NP, as quantified by *ex vivo* IVIS imaging as shown in (E). The tumor signal in each organ is reported as fold-change over the signal from the same organ of normal mice (n=4 for normal mice, n=8 mice/treatment group). Data are presented as mean ± SEM (n=24 for Fig. B and n=8/group for Fig. C&D). *p<0.05 from Two-way ANOVA followed by Dunnett's multiple comparison tests.

3.3.5 T-siPLK1-NP impedes tumor proliferation and promotes cancer apoptosis in the lungs

In addition to metastasis incidence rate and tumor burden, we carefully characterized the cancer in lungs of mice to confirm the treatment efficacy of T-siPLK1-NP. T-siPLK1-NP treatment significantly reduced the tumor lesion area (by H&E, which was confirmed by human vimentin staining) in lungs by 91% and 89% compared to the saline and T-siSCR-NP groups, respectively (**Figure 3.9A-B**). The extent of human cancer in mouse lungs was also quantified by the relative levels of human HPRT (*h*HPRT) mRNA to mouse HPRT mRNA (*m*HPRT). In agreement with the histological data, T-siPLK1-NP decreased *h*HPRT mRNA by 84% and 79% compared to the saline and T-siSCR-NP groups, respectively (**Figure 3.9C**). Lastly, we confirmed that the therapeutic effect was the direct result of RNAi by assessing the level of PLK1 knockdown. T-siPLK1-NP treatment effectively depleted PLK1 gene expression by 84% and 81% compared to the saline and T-siSCR-NP groups, respectively (**Figure 3.9D**). Immunostaining for Ki-67 and cleaved-caspase 3 also confirmed that T-siPLK-NP caused a significant reduction in overall proliferation (**Figure 3.9E**) and increase in apoptosis (**Figure 3.9F**). Taken together, these experiments showed that our nanoparticle effectively delivered PLK1 siRNA to metastatic tumors upon systemic delivery, which resulted in reduced tumor growth and increased cancer death.

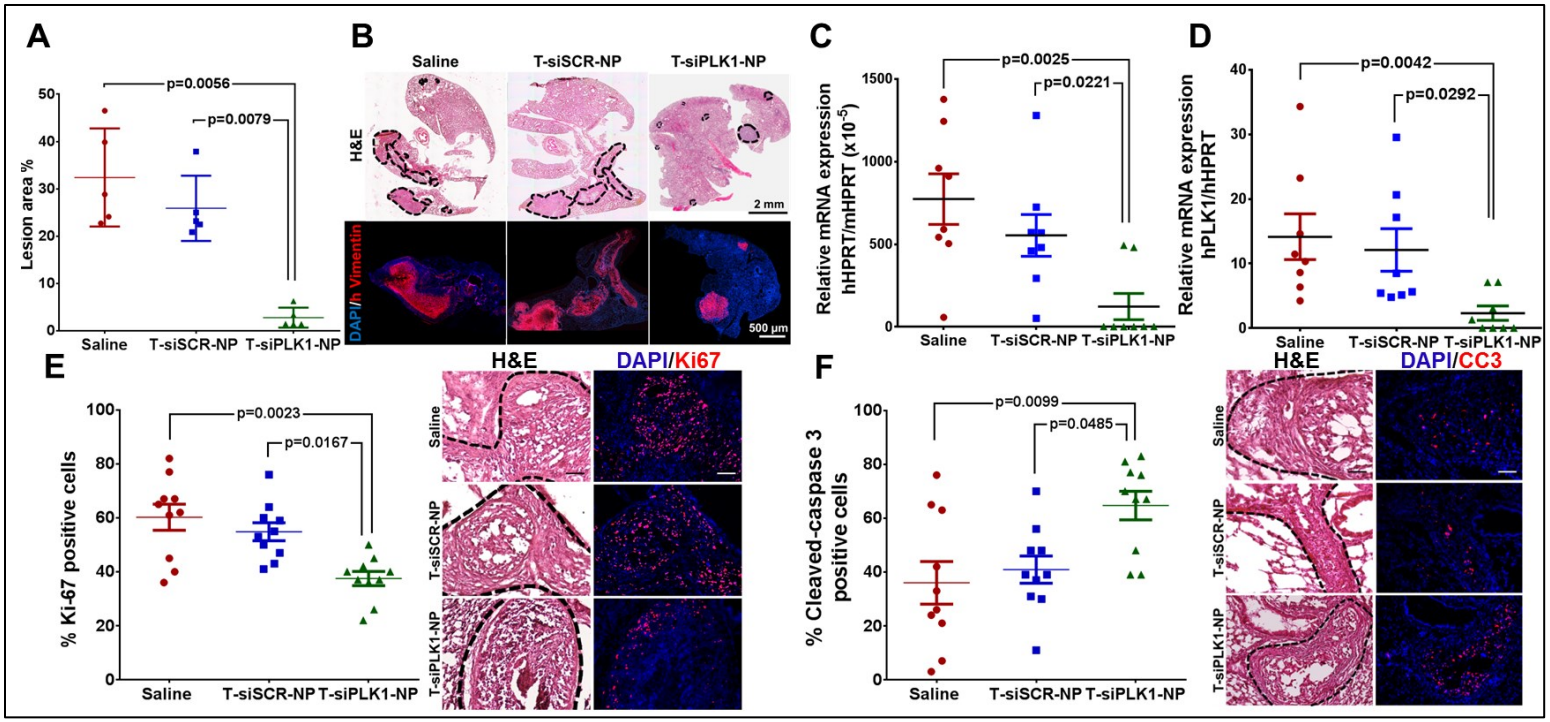

Figure 3.9. T-siPLK1-NP treatment inhibits tumor growth in lung by silencing the PLK1 gene, reducing proliferation, and promoting apoptosis.

(A) Percent lesion area per total lung area in LM2-4luc+/H2N experimental metastasis mice from the *in vivo* study as shown in **Figure 3.8A**. (B) Representative images of the lung tissues isolated from mice from each treatment groups, stained with H&E and anti-human vimentin (red) over DAPI (blue). (C) Tumor burden in LM2-4luc+/H2N mice as quantified by qPCR analysis of human HPRT (*h*HPRT) mRNA relative to mouse HPRT (*m*HPRT) in mouse lungs. (D) *h*PLK1 mRNA expression in the lung tissues relative to *h*HPRT mRNA. (E) Quantification and representative images of Ki-67 positive cells in the lung nodes. Scale bar = 100 µm. (F) Quantification and representative images of Cleaved-caspase 3 (CC3) positive cells in the lung nodes. Scale bar = 100 µm. Dotted lines in the images in (B, E&F) mark the boundary between the tumor and surrounding normal lung tissue. All data are represented as average ± SEM. Each dot in (A, C&D) represents value from one mouse, and in (E&F) represents one tumor node in the lungs of mice (n=2 nodes/mouse, 5 mice/group). P values as indicated on the graph from Kruskal-Wallis test, except in (A) from One way ANOVA, followed by Dunnett's multiple comparison tests.

3.3.6 Depletion of PLK1 by T-siPLK1-NP inhibits lung metastasis and prolongs overall survival in long-term *in vivo* study

To investigate the long-term therapeutic effect of T-siPLK1-NP treatment, we conducted a long-term study in which mice received the same dosing schedule as the short-term study but extended the study to 2 months (see dash lines in **Figure 3.10A** for injection days). Tumor burden was monitored up to day 32 post 1st treatment where >80% of mice were still alive. As expected, T-siPLK1-NP significantly reduced tumor burden in the lungs as measured by 1000-fold less of bioluminescence signal *vs*. saline (**Figure 3.10A**). Also, the first incidence of death in the T-siPLK1-NP treatment was significantly delayed by 36 days and overall survival improved greatly compared to the siSCR and saline groups (**Figure 3.10B**). In addition, upon sacrifice/death I observed large axillary lymph node tumors (>1200 mm^3) in multiple mice from the saline and T-siSCR-NP groups (4 out of 8 in each group), whereas only 1 out of 8 mice in the T-siPLK1-NP group exhibited large lymph node tumors. T-siPLK1-NP treatment also yielded smaller lung lesions as compared to saline and T-siSCR-NP groups (**Figure 3.10C**), which is in agreement with the results from the short-term study. In summary, treatment with T-siPLK1-NP elicits anti-metastatic activity and extends overall survival in mice, which provides a novel potential therapeutic option for metastatic breast cancer disease.

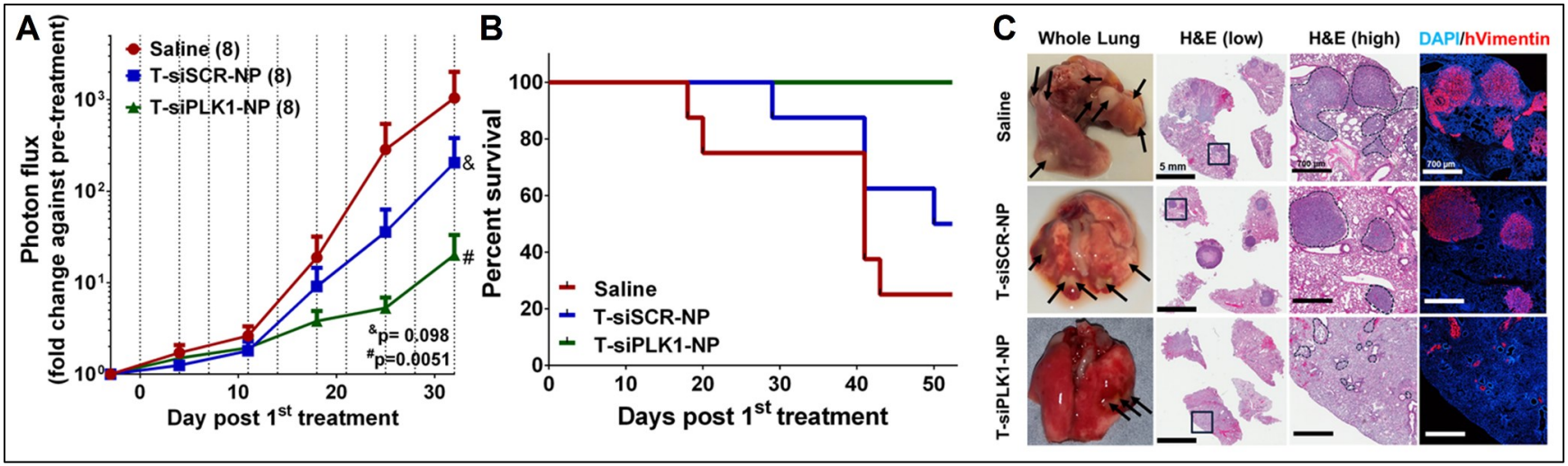

Figure 3.10. T-siPLK1-NP treatment improves overall survival of LM2-4luc+/H2N experimental metastasis mice. (A) Quantification of lung photon flux normalized to pre-treatment flux from each individual mouse in the treatment groups (n=8/group). IVIS imaging was performed on once per week basis. Data are presented as mean ± SEM. P values as indicated on the graph. Vertical dashed lines represent injection days. Two-way ANOVA followed by Dunnett's multiple comparison tests. (B) Kaplan-Meier survival analysis of the experimental metastasis study mice up to day 50 post treatment (n=8/group). Data are presented as mean ± SEM. *P=0.0251 between T-siPLK1-NP *vs* Saline. Mantel-Cox Log rank test. (C) Representative images of the whole lung, H&E, and anti-human vimentin staining on the NP-treated mice *vs* saline. (from left to right: whole lung image (unfixed tissue); low magnification of the entire lung H&E (each lobes were separated for better visualization of the tumor nodes); high magnification of the "boxed" area in the H&E (low magnification) panel; immunofluorescence staining of anti-human vimentin (red) and nucleus (blue) of the same lung sections.

3.4 Discussion and Conclusion

Herein, we have shown for the first time that mesoporous silica nanoparticles can scavenge intracellular ROS, modulate NOX4 activity, and in turn inhibit cellular invasion and migration in cancer cells *in vitro*. This intrinsic property of mesoporous silica nanoparticles hence further promotes its use as a therapeutic delivery platform for cancer treatment. We believe this finding is impactful as it may inspire new platforms that are not only passive carriers but also therapeutics.

By utilizing a HER2-expressing metastatic MDA-MB-231 cell line, LM2-4luc+/H2N [207], for the *in vivo* experimental metastasis model we demonstrated that silencing the PLK1 gene with T-siPLK1-NP impedes metastasis and tumor growth *in vitro* and *in vivo*. We used HER2 overexpressed TNBC as a cancer model to demonstrate effective targeted delivery. Our future work will focus on the most aggressive TNBC, basal-like TNBC, which is categorized as those with EGFR+ and/or CK5/6+. From a study that monitored 3,726 early stage BC patients for 15 years [208], basal-like TNBC was diagnosed in the youngest women and was most aggressive. The overall survival from metastasis to only 6 months compared to 9-13 months for all TNBC. The majority (>80%) of basal-like TNBC is EGFR+ [187, 206, 209], representing an attractive homing target for therapeutic delivery.

In conclusion, we have successfully developed a nanoparticle platform that is effective in treating metastatic breast cancer by simultaneously reducing metastasis potential of cancer through the intrinsic antioxidant property of the nanoparticle, while delivering siPLK1 to metastatic tumors to promote apoptosis through PLK1 gene silencing mechanism. As previously discussed, PLK1 inhibitors have shown to impart adverse

effects and siPLK1 on lipid nanoparticles without a targeting agent only provided a narrow therapeutic window in clinical trials. The sequence specificity of siPLK1 combined with the tumor target specificity of our nanoparticle platform will potentially improve both efficacy and safety for treating metastatic breast cancer. The unique antioxidant features and the versatility of our nanoparticles will potentially be beneficial in the treatment of not only cancer but also other inflammatory diseases.

3.5 Author contributions

All *in vitro* data collection and analysis were done by Jingga Morry, except for **Figure 3.1**. Worapol Ngamcherdtrakul and Moataz Reda synthesized and characterized materials presented in **Figure 3.1**. The western blot data in **Figure 3.3** was collected by Shenda Gu. The *in vivo* experiments were performed with the help of Brandon Beckman and Thanapon Sangvanich. All of the *in vivo* data presented in **Figure 3.8 - 3.10** were collected and analyzed by Jingga Morry.

3.6 Model limitations

In this chapter, a HER2-positive TNBC cell line was used to show the effect of targeted delivery of nanoparticle conjugated with the anti-HER2 antibody, trastuzumab, in an *in vivo* experimental metastasis model. However, most TNBC lacks HER2 expression, thus HER2-targeted therapy, in this case, can only be used as a proof-of concept study. Another targeting antibody has to be used to show efficacy in the treatment for TNBC, such as conjugation with anti-EGFR antibody. Another limitation of this study was the ability to only investigate the post-extravasation step of the metastatic cascade, since the early steps of metastasis was eliminated in the experimental metastasis model. In

order to examine the treatment efficacy at all stages of the metastatic cascade, a spontaneous metastasis model might be a better option.

Chapter 4: Summary, Conclusion, and Future Directions

4.1 Summary and conclusions

The work presented in this dissertation was a thorough evaluation of the antioxidant activity and siRNA delivery efficiency of a NP platform for inhibiting in two disease processes, skin fibrosis (scleroderma) and cancer metastasis. As mentioned in **Chapter 1**, increases in oxidative stress have been linked to various steps involved in fibrogenesis as well as carcinogenesis. Current antioxidant treatments are not effective due to low bioavailability which results in the inability to achieve a therapeutic level in the target tissues. Inorganic nanoparticles with intrinsic antioxidant properties such as mesoporous silica nanoparticles (MSNPs) have great potential to be used not only as an antioxidant therapy, but also as a carrier for siRNA gene delivery. Compared with other inorganic nanoparticles with antioxidant properties, MSNPs are safer and more biocompatible for *in vivo* applications. Furthermore, not only are MSNPs effective antioxidants, with the right surface modification as accomplished in our lab, the material (namely “NP”) can also effectively deliver siRNAs to the target cells, making it highly promising in treating diseases involving oxidative stress and gene abnormality such as fibrosis and cancer.

In **Chapter 2**, I investigated the intrinsic antioxidant property of the NPs and assessed the gene silencing effects of HSP47 in a bleomycin-induced scleroderma mouse model. In this study, I showed that MSNP was efficiently transported into the cells without causing overt cytotoxicity. In addition, I also demonstrated that the MSNP imparted an

antioxidant property by scavenging free radicals in both an acellular DPPH system as well as intracellularly via a CellROX assay. This reduction of ROS subsequently lead to the downregulation of NOX4 in the dermal fibroblast cells which also contributed to the reduction of profibrotic markers (COL I and α-SMA). Silencing of HSP47 was subsequently explored as a strategy to further inhibit fibrogenesis in both *in vitro* and *in vivo* models of fibrosis. Delivery of HSP47 siRNA into the TGF-β stimulated cells efficiently knocked down more than 90% HSP47 mRNA expression *in vitro*. Furthermore, with this model I was also able to elucidate a novel relationship between NOX4 and HSP47 signaling by demonstrating that NOX4 acts upstream of HSP47 under TGF-β stimulation. More importantly, the *in vitro* efficacy translated well to *in vivo* efficacy in a mouse model of skin fibrosis. In fact, intradermal administration of siHSP47-NP to the bleomycin-induced scleroderma mice decreased the skin thickness and significantly reduced pro-fibrotic markers (i.e., NOX4, COL I, and αSMA) through effective HSP47 gene silencing in addition to the ROS-scavenging properties of MSNP in the skin.

In **Chapter 3**, I evaluated the *in vitro* and *in vivo* efficacy of siPLK1 delivered by our NPs for treating metastatic breast cancer. I showed that siPLK1-NP treatment effectively silenced PLK1 gene expression and induced G2/M cell cycle arrest and concomitant apoptotic cell death in multiple TNBC cell lines. Treatment of NPs in TNBC cells could cause inhibition of cancer cell migration and invasion through ROS-scavenging ability of the MNSP core.

In addition, I also showed that treatment of NAC on breast cancer cells was ineffective in reducing cellular invasion at low dose and only showed increased inhibition at high

dose. Low dose of NAC (typically below 10 mM) prevent p53 activation by reducing oxidative DNA damage caused by high ROS levels (produced intracellularly by the cancer cells), which lead to increased tumor cell proliferation as well as invasiveness [244, 245]. NAC at high concentration (>10 mM) has inhibitory effects on matrix metalloproteinase activities due to the direct interference at the MMP catalytic domain by excess sulfhydryl residues [246]. At concentration above 10 mM, NAC treatment has been shown to reduce matrix metalloproteinase-9 (MMP-9) secretion in human corneal epithelial cells [247], transformed mouse fibroblasts [248], human bladder carcinoma [249], and murine melanoma cells [250]. MMP9 is the key enzyme for the proteolytic degradation of ECM during tumor invasion and metastasis [251]. High levels of MMP9 are expressed in basal-like and HER2-positive breast cancer patients as well as TNBC cell line, MDA-MB-231 [252].

By using a HER2-expressing metastatic MDA-MB-231 cell line, I showed that targeted delivery of siPLK1 on the NP conjugated with anti-HER2 antibody (trastuzumab, T; the nanoconstruct was named T-siPLK1-NP) could be achieved in an *in vivo* experimental metastasis model following intravenous. The mice receiving T-siPLK1-NP had effective PLK1 gene knockdown in the lung nodules with significantly fewer proliferative Ki-67^+ cells and more apoptotic cleaved-caspase 3^+ cells. In addition, these mice also showed significantly less metastasis to other organs and have increased survival compared to the saline and scrambled siRNA control groups.

In order to tailor the medical treatments to target the specific disease characteristics of individual patients, nanomaterials such as our nanoparticle could be applied advantageously to treat metastatic breast cancer disease. Since our NP has the intrinsic

antioxidant properties, it will be beneficial for treating patients with high ROS level in their tumor. The ROS level of the tumor could be measured from the tumor biopsy samples or non-invasively by using imaging system. For instance, the ratio of reduced glutathione (GSH) to oxidized glutathione (GSSG) may be used as a marker for oxidative stress in the tumor samples of the cancer patients. Alternatively, the tumor redox status could also be measured noninvasively *in vivo* with the use of redox-sensitive contrast agents such as nitroxides [253] or chemical exchange saturation transfer (CEST) method [254] for magnetic resonance imaging (MRI). By selecting patients with high tumor ROS level, we could ensure that the nanoparticle treatment is only given to patients with tumors with enhanced oxidative levels. In addition, the redox status of the tumor should also be monitored throughout the treatment period for optimal treatment efficacy as well as lowering the risk of adverse effects.

4.2 Future directions

So far, I have evaluated the intrinsic antioxidant property and therapeutic benefit of our nanoparticles in fibrosis and cancer disease models. I have also determined that the ROS-scavenging ability of NP was, in part, attributed by the mesoporous silica core. However, the possible implications of the cationic polymer coating, PEI, −beyond facilitating siRNA binding and endosomal escape of NP− have not been described. In the following sections, I will show some of my preliminary results relating to PEI polymer and its copper-binding ability in mitigating oxidative stress in cancer cells.

4.2.1 Roles of copper in oxidative stress and cancer

Copper is an essential mineral required for many physiological functions including cellular respiration, formation of connective tissues, and iron metabolism [255]. Copper is also an important cofactor for several enzymes including cytochrome c [256], SOD1 [257], and lysyl oxidase [258]. Ceruloplasmin is the major copper-binding protein in blood. It is a ferroxidase enzyme synthesized and secreted by hepatocytes which is responsible for transporting 95% of total copper in the circulation [259]. In clinic, serum ceruloplasmin is used as a surrogate marker for total body copper [260].

During cancer progression, copper was found to be an essential component for activation of several pathways which play a critical role in angiogenesis and metastasis such as angiogenesis promotion through HIF-1α/VEGF-signaling [261, 262] and Memo/NOX-mediated cellular migration and invasion [263] as shown in **Figure 4.1**. In HIF-1α/VEGF-signaling, copper was found to be capable of stabilizing HIF-1α through inhibition of prolyl hydroxylases [262]. Copper is also required for the activation of the Memo protein which is involved in the localized ROS production in the cell protrusions during chemotaxis and cellular invasion. MacDonald et al. proposed that Memo is necessary for the sustained activation of NOX in cancer cells during cell motility, invasion, and metastasis [263].

Increase in serum copper concentration has been observed in various malignancies including breast cancer [264]. One clinical trial in breast cancer patients showed that depleting copper with copper chelator, tetrathiomolybdate (TM), prevented relapse in highly invasive triple negative breast cancer patients (only 2 relapsed in 11 TNBC patients) [265]. In addition, of the 75% patients who achieved the copper depletion

target, there was a statistically significant reduction in endothelial progenitor cells (EPC). Moreover, another clinical trial in ovarian cancer patients also found that chelating copper with trientine increased treatment efficiency of carboplatin by overcoming the platinum resistance in those patients [266]. These clinical trials demonstrated that copper chelation has favorable anti-cancer benefits and when given in conjunction with a platinum-based chemotherapy agent, it can reduce drug resistance in cancer patients. Thus, depleting copper may inhibit tumor cells from invading to other organs and prevent cancer relapse in patients.

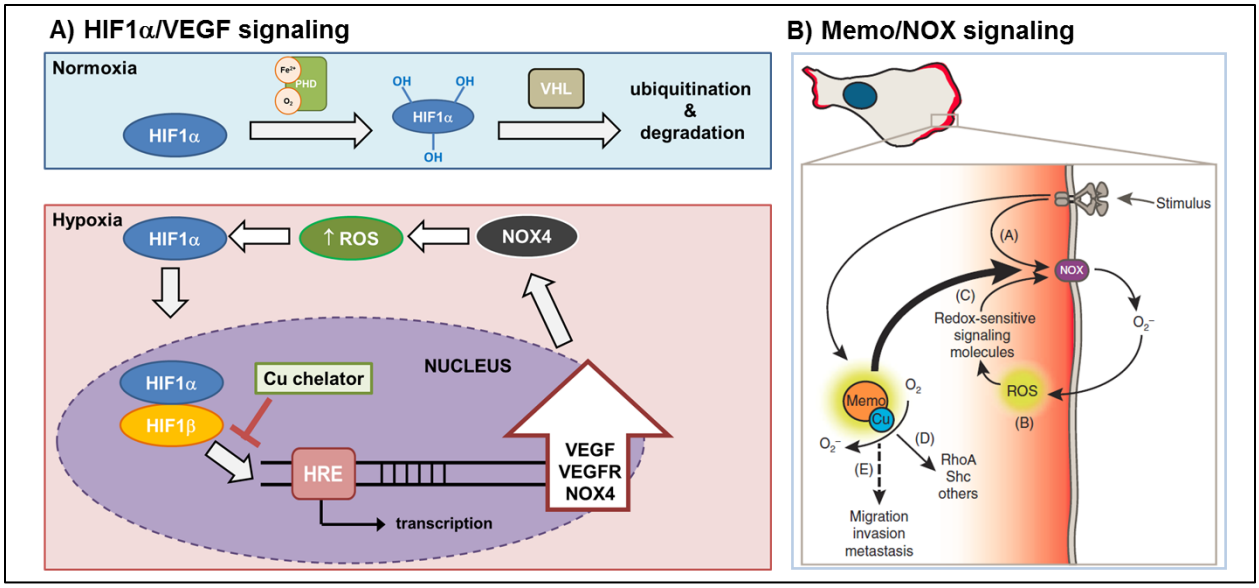

Figure 0.1. Copper involvement in major signaling pathways in cancer progression.

A) HIF is a heterodimer proteins consisting of an unstable alpha subunit (HIF-1α) and a stable subunit (HIF-1β) which binds to hypoxia response elements (HREs) on the DNA. In normoxic condition, HIF-1α is hydroxylated by prolyl hydroxylase domain (PHD) enzymes. The hydroxylated HIF-1α is then recognized by von Hippel-Liandau tumor suppresor gene product (pVHL) and degraded via ubiquitin-proteasome pathway. In hypoxic condition, the hydoxylation of HIF-1α is inhibited which prevents it from being degraded. The unmodified HIF-1α then dimerizes with HIF-1β and stimulates the transcription of its target genes such as VEGF and NOX4. In the presence of copper chelator, HIF-1α activation and accumulation is suppressed, thus preventing the transcription of its target genes. B) Copper is required for the activation of Memo. During metastasis, Memo is localized to the membrane protrusion upon stimulation with growth factors and is involved in sustaining superoxide production in response to NOX activation. Adapted from Science Signaling [263].

4.2.2 PEI on MSNP binds to copper ions

The polymer-coated mesoporous silica nanoparticle developed by our group is made up of multiple components consisting of two types of polymer, cationic polyethyleimine (PEI) and polyethylene glycol (PEG), coated on the surface of the mesoporous silica core. PEI has been long known to bind copper effectively by chelating Cu^{2+} ions through its amine groups [267]. PEI has mostly been investigated as a water-soluble copper-binding polymer for heavy metal removal from industrial wastewater [268] or as a chelating compound in copper detection assays [267, 269].

In one of our *in vivo* studies where we conducted trace element analysis using Inductively Coupled Plasma Mass Spectrometry (ICP-MS) in the blood plasma of the NP-treated mice, we observed that copper (Cu) and silicon (Si) levels were elevated in the NP-treated mice (**Figure 4.2**). The increase in copper metal levels alongside with silicon (from MSNP) might suggest copper binding to the nanoparticles in the blood. As the liver and kidney serum biomarker levels were normal for these mice (data not shown), the Cu increase is likely not attributed to nanoparticle toxicity. To further investigate this, we measured the amount of copper binding to NP in the acellular system by spiking 100 ppb of Cu (from $CuCl_2$) in three different matrices (water, RPMI media, or RPMI + 5% FBS) and found that NP (with PEI and PEG coating) with or without siRNA attachment could chelate at least 80% of the copper present in solution (**Table 4.1**). In addition, I also showed that pretreatment with NP prior to $CuCl_2$ stimulation on LM2-4luc+/H2N cells significantly reduced the ceruloplasmin and VEGF mRNA expression in a similar manner as the copper chelator, tetraethylenepentamine (TEPA). Collectively, these *in vitro* data support our hypothesis that PEI coating on NP

possesses copper-binding ability which might work in conjunction with the ROS-scavenging properties of the MSNP core in reducing cellular migration and invasiveness *in vitro* and lowering the metastasis rate *in vivo* as observed in **Chapter 3**.

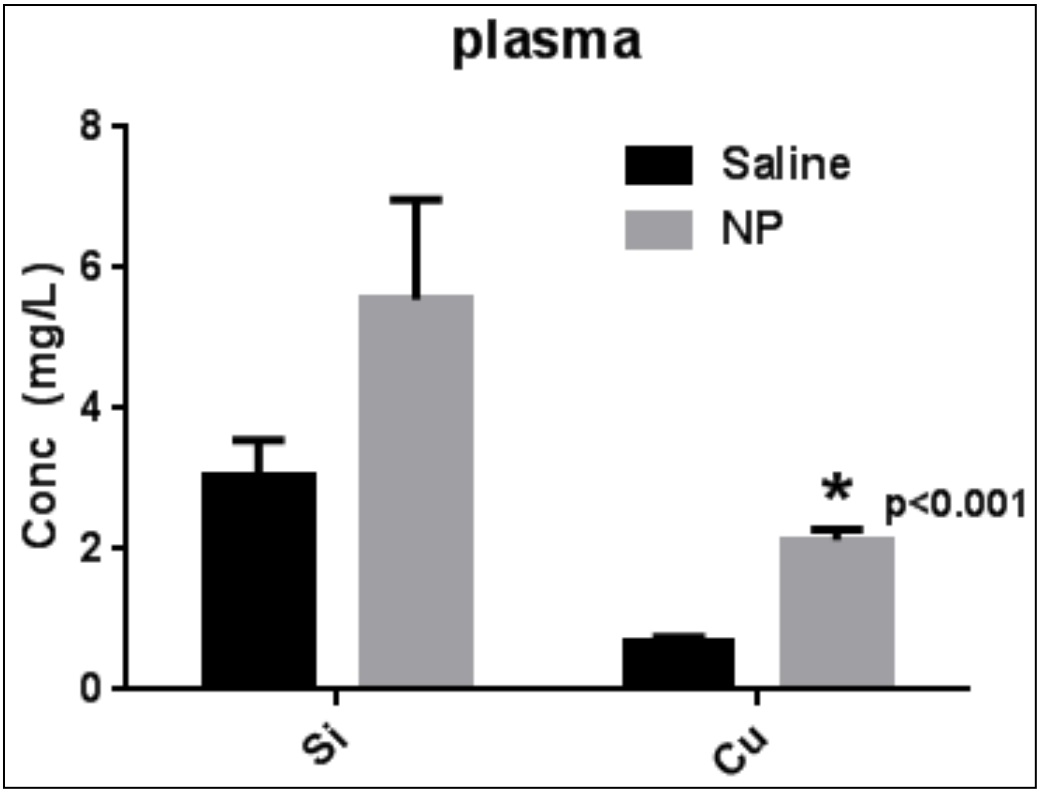

Figure 0.2. Silicon and copper plasma levels in HER2+ breast tumor xenograft in mice.
Orthotopic HCC1954 tumor-bearing mice were treated with 9 doses of 1.25 mg siRNA/kg of T-siHER2-NP or saline. The animals were sacrificed two days post last dose. (n=3 for Saline and n=5 for NP group)

Table 0.1. Percent Copper binding to NP or siSCR-NP in different matrices.

Material	Matrix	pH	% Cu binding	
			Average	SD
NP	Water	7.36	85.4	0.4
	RPMI	8.53	88.7	0.4
	RPMI+FBS	8.47	85.2	0.2
siSCR-NP	Water	7.02	85.8	0.7
	RPMI	8.53	88.6	1.5
	RPMI+FBS	8.49	85.8	0.8

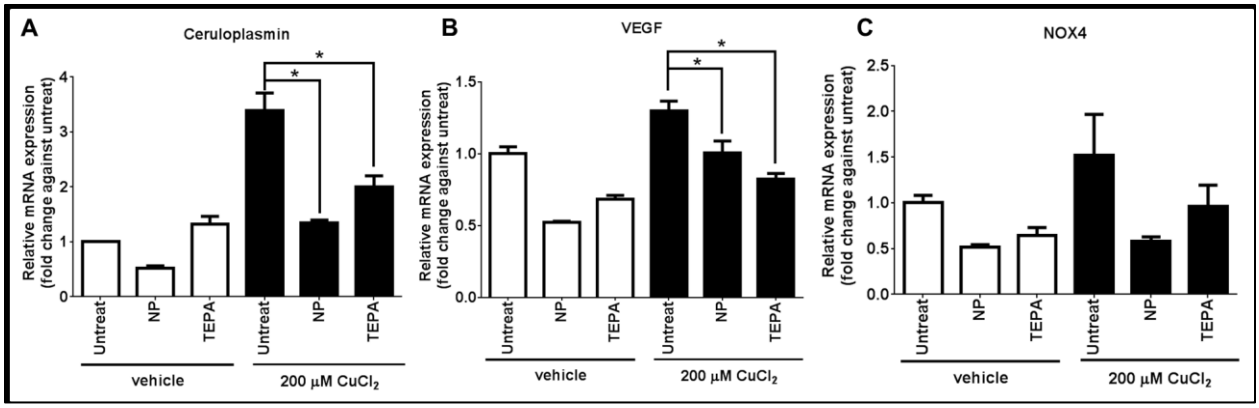

Figure 0.3. NP inhibits CuCl2 stimulation in LM2-4luc+/H2N cells.
mRNA expression of (A) ceruloplasmin, (B) VEGF, and (C) NOX4 in LM2-4luc+/H2N cells pre-treated with either 100 μM TEPA or siSCR-NP (50 nM siRNA, N/P ratio of 50 which is equivalent to 35 μg/mL NP) for 24 hr prior to 200 μM $CuCl_2$ stimulation. All mRNA data were measured by qPCR and normalized to GAPDH expression. Data are presented as mean ± SD from 3 technical replicates from a single experiment. *P<0.05 *vs* untreat.

4.3 Conclusions

In conclusion, in this dissertation I have shown that our NP platform has great potential for the treatment of fibrosis and cancer. Taking advantage of the intrinsic antioxidant properties of the MSNP core and the NP's ability to effectively deliver siRNA to target cells, our nanoparticle platform provided multi-functional treatment not only for fibrosis and cancer, but also for other types of oxidative-induced inflammatory diseases. In addition, I have also demonstrated a role of PEI in copper-binding which may contribute to additional benefit for the cancer therapy. Further investigation is warranted to assess the benefits of the inherent copper-chelating ability of our NPs in animal models of cancer disease.

References

[1] D.I. Brown, K.K. Griendling, Regulation of signal transduction by reactive oxygen species in the cardiovascular system, Circulation research 116(3) (2015) 531-549.

[2] G.-Y. Liou, P. Storz, Reactive oxygen species in cancer, Free radical research 44(5) (2010) 10.3109/10715761003667554.

[3] Y. Liu, G. Fiskum, D. Schubert, Generation of reactive oxygen species by the mitochondrial electron transport chain, J Neurochem 80(5) (2002) 780-7.

[4] K. Bedard, K.H. Krause, The NOX family of ROS-generating NADPH oxidases: physiology and pathophysiology, Physiol Rev 87(1) (2007) 245-313.

[5] F.C. Fang, Antimicrobial Actions of Reactive Oxygen Species, mBio 2(5) (2011).

[6] L.A. Rowe, N. Degtyareva, P.W. Doetsch, DNA Damage-induced Reactive Oxygen Species (ROS) Stress Response in Saccharomyces cerevisiae, Free radical biology & medicine 45(8) (2008) 1167-1177.

[7] M. Schieber, Navdeep S. Chandel, ROS Function in Redox Signaling and Oxidative Stress, Current Biology 24(10) R453-R462.

[8] G. Waris, H. Ahsan, Reactive oxygen species: role in the development of cancer and various chronic conditions, Journal of Carcinogenesis 5 (2006) 14-14.

[9] O. Babalola, A. Mamalis, H. Lev-Tov, J. Jagdeo, NADPH oxidase enzymes in skin fibrosis: molecular targets and therapeutic agents, Arch Dermatol Res 306(4) (2014) 313-30.

[10] L. Hecker, J. Cheng, V.J. Thannickal, Targeting NOX enzymes in pulmonary fibrosis, Cell Mol Life Sci 69(14) (2012) 2365-71.

[11] S. De Minicis, D.A. Brenner, NOX in liver fibrosis, Archives of Biochemistry and Biophysics 462(2) (2007) 266-272.

[12] C.E. Holterman, N.C. Read, C.R. Kennedy, Nox and renal disease, Clin Sci (Lond) 128(8) (2015) 465-81.

[13] K. Roy, Y. Wu, J.L. Meitzler, A. Juhasz, H. Liu, G. Jiang, J. Lu, S. Antony, J.H. Doroshow, NADPH oxidases and cancer, Clin Sci (Lond) 128(12) (2015) 863-75.

[14] M. Quintavalle, L. Elia, J.H. Price, S. Heynen-Genel, S.A. Courtneidge, A cell-based high-content screening assay reveals activators and inhibitors of cancer cell invasion, Science signaling 4(183) (2011) ra49.

[15] I.S. Okon, M.-H. Zou, Mitochondrial ROS and cancer drug resistance: Implications for therapy, Pharmacological research 100 (2015) 170-174.

[16] M. Nishikawa, Reactive oxygen species in tumor metastasis, Cancer letters 266(1) (2008) 53-9.

[17] B. Olsson, M. Johansson, J. Gabrielsson, P. Bolme, Pharmacokinetics and bioavailability of reduced and oxidized N-acetylcysteine, European journal of clinical pharmacology 34(1) (1988) 77-82.

[18] E.B. Souto, P. Severino, R. Basso, M.H. Santana, Encapsulation of antioxidants in gastrointestinal-resistant nanoparticulate carriers, Methods in molecular biology (Clifton, N.J.) 1028 (2013) 37-46.

[19] E. Sharpe, D. Andreescu, S. Andreescu, Artificial Nanoparticle Antioxidants, Oxidative Stress: Diagnostics, Prevention, and Therapy, American Chemical Society2011, pp. 235-253.

[20] R. Sandhir, A. Yadav, A. Sunkaria, N. Singhal, Nano-antioxidants: An emerging strategy for intervention against neurodegenerative conditions, Neurochemistry international 89 (2015) 209-26.

[21] D.M. Dykxhoorn, D. Palliser, J. Lieberman, The silent treatment: siRNAs as small molecule drugs, Gene Ther 13(6) (2006) 541-52.

[22] X. Li, Y. Chen, M. Wang, Y. Ma, W. Xia, H. Gu, A mesoporous silica nanoparticle--PEI--fusogenic peptide system for siRNA delivery in cancer therapy, Biomaterials 34(4) (2013) 1391-401.

[23] H. Meng, W.X. Mai, H. Zhang, M. Xue, T. Xia, S. Lin, X. Wang, Y. Zhao, Z. Ji, J.I. Zink, A.E. Nel, Codelivery of an optimal drug/siRNA combination using mesoporous silica nanoparticles to overcome drug resistance in breast cancer in vitro and in vivo, ACS nano 7(2) (2013) 994-1005.

[24] N. Hao, H. Yang, L. Li, L. Li, F. Tang, The shape effect of mesoporous silica nanoparticles on intracellular reactive oxygen species in A375 cells, New Journal of Chemistry 38(9) (2014) 4258-4266.

[25] X. Huang, J. Zhuang, X. Teng, L. Li, D. Chen, X. Yan, F. Tang, The promotion of human malignant melanoma growth by mesoporous silica nanoparticles through decreased reactive oxygen species, Biomaterials 31(24) (2010) 6142-53.

[26] T. Asefa, Z. Tao, Biocompatibility of Mesoporous Silica Nanoparticles, Chemical Research in Toxicology 25(11) (2012) 2265-2284.

[27] V. Sosa, T. Moliné, R. Somoza, R. Paciucci, H. Kondoh, M.E. Lleonart, Oxidative stress and cancer: An overview, Ageing Research Reviews 12(1) (2013) 376-390.

[28] K. Richter, A. Konzack, T. Pihlajaniemi, R. Heljasvaara, T. Kietzmann, Redox-fibrosis: Impact of TGFbeta1 on ROS generators, mediators and functional consequences, Redox Biol 6 (2015) 344-52.
[29] J.M. Robinson, Reactive oxygen species in phagocytic leukocytes, Histochemistry and Cell Biology 130(2) (2008) 281-297.
[30] T.A. Wynn, Common and unique mechanisms regulate fibrosis in various fibroproliferative diseases, Journal of Clinical Investigation 117(3) (2007) 524-529.
[31] J. Varga, D. Abraham, Systemic sclerosis: a prototypic multisystem fibrotic disorder, The Journal of Clinical Investigation 117(3) 557-567.
[32] G. Sebastiani, K. Gkouvatsos, K. Pantopoulos, Chronic hepatitis C and liver fibrosis, World Journal of Gastroenterology : WJG 20(32) (2014) 11033-11053.
[33] S.V. Siegmund, D.A. Brenner, Molecular pathogenesis of alcohol-induced hepatic fibrosis, Alcoholism, clinical and experimental research 29(11 Suppl) (2005) 102s-109s.
[34] A. Pellicoro, P. Ramachandran, J.P. Iredale, J.A. Fallowfield, Liver fibrosis and repair: immune regulation of wound healing in a solid organ, Nat Rev Immunol 14(3) (2014) 181-194.
[35] P.W. Noble, C.E. Barkauskas, D. Jiang, Pulmonary fibrosis: patterns and perpetrators, The Journal of Clinical Investigation 122(8) 2756-2762.
[36] P.B. Bitterman, C.A. Henke, Fibroproliferative disorders, Chest 99(3 Suppl) (1991) 81s-84s.
[37] C. Li, J.F. Kuemmerle, The mechanisms that mediate the development of fibrosis in patients with Crohn's Disease, Inflammatory bowel diseases 20(7) (2014) 1250-1258.

[38] R.T. Kendall, C.A. Feghali-Bostwick, Fibroblasts in fibrosis: novel roles and mediators, Frontiers in Pharmacology 5 (2014) 123.

[39] D. Pohlers, J. Brenmoehl, I. Löffler, C.K. Müller, C. Leipner, S. Schultze-Mosgau, A. Stallmach, R.W. Kinne, G. Wolf, TGF-β and fibrosis in different organs — molecular pathway imprints, Biochimica et Biophysica Acta (BBA) - Molecular Basis of Disease 1792(8) (2009) 746-756.

[40] O. Lepparanta, C. Sens, K. Salmenkivi, V.L. Kinnula, J. Keski-Oja, M. Myllarniemi, K. Koli, Regulation of TGF-beta storage and activation in the human idiopathic pulmonary fibrosis lung, Cell and tissue research 348(3) (2012) 491-503.

[41] S. Dooley, P. ten Dijke, TGF-β in progression of liver disease, Cell and tissue research 347(1) (2012) 245-256.

[42] S. Kanzler, A.W. Lohse, A. Keil, J. Henninger, H.P. Dienes, P. Schirmacher, S. Rose-John, K.H. zum Buschenfelde, M. Blessing, TGF-beta1 in liver fibrosis: an inducible transgenic mouse model to study liver fibrogenesis, The American journal of physiology 276(4 Pt 1) (1999) G1059-68.

[43] M. Corbel, S. Caulet-Maugendre, N. Germain, S. Molet, V. Lagente, E. Boichot, Inhibition of bleomycin-induced pulmonary fibrosis in mice by the matrix metalloproteinase inhibitor batimastat, The Journal of pathology 193(4) (2001) 538-45.

[44] G. Lakos, S. Takagawa, S.J. Chen, A.M. Ferreira, G. Han, K. Masuda, X.J. Wang, L.A. DiPietro, J. Varga, Targeted disruption of TGF-beta/Smad3 signaling modulates skin fibrosis in a mouse model of scleroderma, The American journal of pathology 165(1) (2004) 203-17.

[45] R.-M. Liu, L.P. Desai, Reciprocal regulation of TGF-β and reactive oxygen species: A perverse cycle for fibrosis, Redox Biology 6 (2015) 565-577.

[46] E.C. Chan, H.M. Peshavariya, G.S. Liu, F. Jiang, S.Y. Lim, G.J. Dusting, Nox4 modulates collagen production stimulated by transforming growth factor beta1 in vivo and in vitro, Biochemical and biophysical research communications 430(3) (2013) 918-25.

[47] H. Nakano, A. Nakajima, S. Sakon-Komazawa, J.H. Piao, X. Xue, K. Okumura, Reactive oxygen species mediate crosstalk between NF-kappaB and JNK, Cell death and differentiation 13(5) (2006) 730-7.

[48] D. Trachootham, W. Lu, M.A. Ogasawara, N.R.-D. Valle, P. Huang, Redox Regulation of Cell Survival, Antioxidants & Redox Signaling 10(8) (2008) 1343-1374.

[49] U.S. Cancer Statistics Working Group., United States Cancer Statistics: 1999–2013 Incidence and Mortality Web-based Report. . <www.cdc.gov/uscs>, 2016 2016).

[50] B.W. Stewart, C.P. Wild, World cancer report 2014, (2014).

[51] G.P. Gupta, J. Massagué, Cancer Metastasis: Building a Framework, Cell 127(4) 679-695.

[52] T.P. Szatrowski, C.F. Nathan, Production of Large Amounts of Hydrogen Peroxide by Human Tumor Cells, Cancer Research 51(3) (1991) 794-798.

[53] E. Panieri, M.M. Santoro, ROS homeostasis and metabolism: a dangerous liason in cancer cells, Cell Death Dis 7 (2016) e2253.

[54] M. Peiris-Pagès, Ubaldo E. Martinez-Outschoorn, F. Sotgia, Michael P. Lisanti, Metastasis and Oxidative Stress: Are Antioxidants a Metabolic Driver of Progression?, Cell Metabolism 22(6) (2015) 956-958.

[55] Paul T. Schumacker, Reactive Oxygen Species in Cancer: A Dance with the Devil, Cancer Cell 27(2) 156-157.

[56] P.A. Grimsrud, H. Xie, T.J. Griffin, D.A. Bernlohr, Oxidative Stress and Covalent Modification of Protein with Bioactive Aldehydes, The Journal of Biological Chemistry 283(32) (2008) 21837-21841.

[57] B. Liu, Y. Chen, D.K. St. Clair, ROS and p53: versatile partnership, Free radical biology & medicine 44(8) (2008) 1529-1535.

[58] Y.P. Lim, T.T. Lim, Y.L. Chan, A.C. Song, B.H. Yeo, B. Vojtesek, D. Coomber, G. Rajagopal, D. Lane, The p53 knowledgebase: an integrated information resource for p53 research, Oncogene 26(11) (2007) 1517-21.

[59] N. Rivlin, R. Brosh, M. Oren, V. Rotter, Mutations in the p53 Tumor Suppressor Gene: Important Milestones at the Various Steps of Tumorigenesis, Genes & Cancer 2(4) (2011) 466-474.

[60] D. Trachootham, J. Alexandre, P. Huang, Targeting cancer cells by ROS-mediated mechanisms: a radical therapeutic approach?, Nat Rev Drug Discov 8(7) (2009) 579-591.

[61] T.G. Graeber, C. Osmanian, T. Jacks, D.E. Housman, C.J. Koch, S.W. Lowe, A.J. Giaccia, Hypoxia-mediated selection of cells with diminished apoptotic potential in solid tumours, Nature 379(6560) (1996) 88-91.

[62] G.L. Semenza, Hypoxia-inducible factors: mediators of cancer progression and targets for cancer therapy, Trends in pharmacological sciences 33(4) (2012) 207-14.

[63] C.-H. Hsieh, W.-C. Shyu, C.-Y. Chiang, J.-W. Kuo, W.-C. Shen, R.-S. Liu, NADPH Oxidase Subunit 4-Mediated Reactive Oxygen Species Contribute to Cycling Hypoxia-

Promoted Tumor Progression in Glioblastoma Multiforme, PLoS ONE 6(9) (2011) e23945.

[64] W. Liu, S.-M. Shen, X.-Y. Zhao, G.-Q. Chen, Targeted genes and interacting proteins of hypoxia inducible factor-1, International Journal of Biochemistry and Molecular Biology 3(2) (2012) 165-178.

[65] L.E. Huang, Z. Arany, D.M. Livingston, H.F. Bunn, Activation of Hypoxia-inducible Transcription Factor Depends Primarily upon Redox-sensitive Stabilization of Its α Subunit, Journal of Biological Chemistry 271(50) (1996) 32253-32259.

[66] T.-C. Chang, C.-J. Huang, K. Tam, S.-F. Chen, K.T. Tan, M.-S. Tsai, T.-N. Lin, S.-K. Shyue, Stabilization of Hypoxia-inducible Factor-1α by Prostacyclin under Prolonged Hypoxia via Reducing Reactive Oxygen Species Level in Endothelial Cells, Journal of Biological Chemistry 280(44) (2005) 36567-36574.

[67] V. Srinivas, I. Leshchinsky, N. Sang, M.P. King, A. Minchenko, J. Caro, Oxygen Sensing and HIF-1 Activation Does Not Require an Active Mitochondrial Respiratory Chain Electron-transfer Pathway, Journal of Biological Chemistry 276(25) (2001) 21995-21998.

[68] Krsti, #x107, J. , Trivanovi, #x107, D. , Mojsilovi, #x107, S. , J.F. Santibanez, Transforming Growth Factor-Beta and Oxidative Stress Interplay: Implications in Tumorigenesis and Cancer Progression, Oxidative Medicine and Cellular Longevity 2015 (2015) 15.

[69] R. Hiraga, M. Kato, S. Miyagawa, T. Kamata, Nox4-derived ROS signaling contributes to TGF-beta-induced epithelial-mesenchymal transition in pancreatic cancer cells, Anticancer research 33(10) (2013) 4431-8.

[70] P.A.J. Muller, K.H. Vousden, p53 mutations in cancer, Nat Cell Biol 15(1) (2013) 2-8.

[71] J.-J. Lebrun, The Dual Role of TGF in Human Cancer: From Tumor Suppression to Cancer Metastasis, ISRN Molecular Biology 2012 (2012) 28.

[72] L. Gorelik, R.A. Flavell, Immune-mediated eradication of tumors through the blockade of transforming growth factor-[beta] signaling in T cells, Nat Med 7(10) (2001) 1118-1122.

[73] T. Sakurai, M. Kudo, Signaling pathways governing tumor angiogenesis, Oncology 81 Suppl 1 (2011) 24-9.

[74] C.-H. Heldin, M. Vanlandewijck, A. Moustakas, Regulation of EMT by TGFβ in cancer, FEBS Letters 586(14) (2012) 1959-1970.

[75] S. Nakajima, R. Doi, E. Toyoda, S. Tsuji, M. Wada, M. Koizumi, S.S. Tulachan, D. Ito, K. Kami, T. Mori, Y. Kawaguchi, K. Fujimoto, R. Hosotani, M. Imamura, N-cadherin expression and epithelial-mesenchymal transition in pancreatic carcinoma, Clinical cancer research : an official journal of the American Association for Cancer Research 10(12 Pt 1) (2004) 4125-33.

[76] S. Lamouille, J. Xu, R. Derynck, Molecular mechanisms of epithelial–mesenchymal transition, Nature reviews. Molecular cell biology 15(3) (2014) 178-196.

[77] I.K. Bukholm, J.M. Nesland, A.L. Borresen-Dale, Re-expression of E-cadherin, alpha-catenin and beta-catenin, but not of gamma-catenin, in metastatic tissue from breast cancer patients [seecomments], The Journal of pathology 190(1) (2000) 15-9.

[78] S. Kase, K. Sugio, K. Yamazaki, T. Okamoto, T. Yano, K. Sugimachi, Expression of E-cadherin and beta-catenin in human non-small cell lung cancer and the clinical

significance, Clinical cancer research : an official journal of the American Association for Cancer Research 6(12) (2000) 4789-96.

[79] M.L. Hermiston, M.H. Wong, J.I. Gordon, Forced expression of E-cadherin in the mouse intestinal epithelium slows cell migration and provides evidence for nonautonomous regulation of cell fate in a self-renewing system, Genes & Development 10(8) (1996) 985-996.

[80] R.B. Hazan, G.R. Phillips, R.F. Qiao, L. Norton, S.A. Aaronson, Exogenous Expression of N-Cadherin in Breast Cancer Cells Induces Cell Migration, Invasion, and Metastasis, The Journal of Cell Biology 148(4) (2000) 779-790.

[81] R. HIRAGA, M. KATO, S. MIYAGAWA, T. KAMATA, Nox4-derived ROS Signaling Contributes to TGF-β-induced Epithelial-mesenchymal Transition in Pancreatic Cancer Cells, Anticancer research 33(10) (2013) 4431-4438.

[82] K. Shimada, T. Fujii, S. Anai, K. Fujimoto, N. Konishi, ROS generation via NOX4 and its utility in the cytological diagnosis of urothelial carcinoma of the urinary bladder, BMC Urology 11(1) (2011) 1-12.

[83] N. Tobar, J. Guerrero, P.C. Smith, J. Martinez, NOX4-dependent ROS production by stromal mammary cells modulates epithelial MCF-7 cell migration, British journal of cancer 103(7) (2010) 1040-7.

[84] J.M. Seo, S. Park, J.H. Kim, Leukotriene B4 receptor-2 promotes invasiveness and metastasis of ovarian cancer cells through signal transducer and activator of transcription 3 (STAT3)-dependent up-regulation of matrix metalloproteinase 2, J Biol Chem 287(17) (2012) 13840-9.

[85] K.K. Nelson, J.A. Melendez, Mitochondrial redox control of matrix metalloproteinases, Free Radic Biol Med 37(6) (2004) 768-84.

[86] B. Diaz, G. Shani, I. Pass, D. Anderson, M. Quintavalle, S.A. Courtneidge, Tks5-dependent, nox-mediated generation of reactive oxygen species is necessary for invadopodia formation, Science signaling 2(88) (2009) ra53.

[87] E.C. Vaquero, M. Edderkaoui, S.J. Pandol, I. Gukovsky, A.S. Gukovskaya, Reactive Oxygen Species Produced by NAD(P)H Oxidase Inhibit Apoptosis in Pancreatic Cancer Cells, Journal of Biological Chemistry 279(33) (2004) 34643-34654.

[88] B. Diaz, S.A. Courtneidge, Redox signaling at invasive microdomains in cancer cells, Free Radic Biol Med 52(2) (2012) 247-56.

[89] K. Block, Y. Gorin, Aiding and abetting roles of NOX oxidases in cellular transformation, Nature reviews. Cancer 12(9) (2012) 627-37.

[90] M. Geiszt, NADPH oxidases: new kids on the block, Cardiovascular research 71(2) (2006) 289-99.

[91] J.D. Lambeth, T. Kawahara, B. Diebold, Regulation of Nox and Duox enzymatic activity and expression, Free Radic Biol Med 43(3) (2007) 319-31.

[92] N. Amara, D. Goven, F. Prost, R. Muloway, B. Crestani, J. Boczkowski, NOX4/NADPH oxidase expression is increased in pulmonary fibroblasts from patients with idiopathic pulmonary fibrosis and mediates TGFbeta1-induced fibroblast differentiation into myofibroblasts, Thorax 65(8) (2010) 733-8.

[93] T. Spadoni, S. Svegliati Baroni, D. Amico, L. Albani, G. Moroncini, E.V. Avvedimento, A. Gabrielli, A reactive oxygen species-mediated loop maintains

increased expression of NADPH oxidases 2 and 4 in skin fibroblasts from patients with systemic sclerosis, Arthritis Rheumatol 67(6) (2015) 1611-22.

[94] T. Aoyama, Y.H. Paik, S. Watanabe, B. Laleu, F. Gaggini, L. Fioraso-Cartier, S. Molango, F. Heitz, C. Merlot, C. Szyndralewiez, P. Page, D.A. Brenner, Nicotinamide adenine dinucleotide phosphate oxidase in experimental liver fibrosis: GKT137831 as a novel potential therapeutic agent, Hepatology (Baltimore, Md.) 56(6) (2012) 2316-27.

[95] E.R. Jarman, V.S. Khambata, C. Cope, P. Jones, J. Roger, L.Y. Ye, N. Duggan, D. Head, A. Pearce, N.J. Press, B. Bellenie, B. Sohal, G. Jarai, An inhibitor of NADPH oxidase-4 attenuates established pulmonary fibrosis in a rodent disease model, American journal of respiratory cell and molecular biology 50(1) (2014) 158-69.

[96] L. Hecker, R. Vittal, T. Jones, R. Jagirdar, T.R. Luckhardt, J.C. Horowitz, S. Pennathur, F.J. Martinez, V.J. Thannickal, NADPH Oxidase-4 Mediates Myofibroblast Activation and Fibrogenic Responses to Lung Injury, Nature medicine 15(9) (2009) 1077-1081.

[97] M. Sedeek, G. Callera, A. Montezano, A. Gutsol, F. Heitz, C. Szyndralewiez, P. Page, C.R.J. Kennedy, K.D. Burns, R.M. Touyz, R.L. Hébert, Critical role of Nox4-based NADPH oxidase in glucose-induced oxidative stress in the kidney: implications in type 2 diabetic nephropathy, American Journal of Physiology - Renal Physiology 299(6) (2010) F1348-F1358.

[98] C.D. Bondi, N. Manickam, D.Y. Lee, K. Block, Y. Gorin, H.E. Abboud, J.L. Barnes, NAD(P)H Oxidase Mediates TGF-β1–Induced Activation of Kidney Myofibroblasts, Journal of the American Society of Nephrology : JASN 21(1) (2010) 93-102.

[99] S. Ismail, A. Sturrock, P. Wu, B. Cahill, K. Norman, T. Huecksteadt, K. Sanders, T. Kennedy, J. Hoidal, NOX4 mediates hypoxia-induced proliferation of human pulmonary artery smooth muscle cells: the role of autocrine production of transforming growth factor-{beta}1 and insulin-like growth factor binding protein-3, American journal of physiology. Lung cellular and molecular physiology 296(3) (2009) L489-99.

[100] C. Michaeloudes, M.B. Sukkar, N.M. Khorasani, P.K. Bhavsar, K.F. Chung, TGF-β regulates Nox4, MnSOD and catalase expression, and IL-6 release in airway smooth muscle cells, American Journal of Physiology - Lung Cellular and Molecular Physiology 300(2) (2011) L295-L304.

[101] H.E. Boudreau, B.W. Casterline, B. Rada, A. Korzeniowska, T.L. Leto, Nox4 involvement in TGF-beta and SMAD3-driven induction of the epithelial-to-mesenchymal transition and migration of breast epithelial cells, Free radical biology & medicine 53(7) (2012) 1489-1499.

[102] M. Yamaura, J. Mitsushita, S. Furuta, Y. Kiniwa, A. Ashida, Y. Goto, W.H. Shang, M. Kubodera, M. Kato, M. Takata, T. Saida, T. Kamata, NADPH oxidase 4 contributes to transformation phenotype of melanoma cells by regulating G2-M cell cycle progression, Cancer Res 69(6) (2009) 2647-54.

[103] K.A. Graham, M. Kulawiec, K.M. Owens, X. Li, M.M. Desouki, D. Chandra, K.K. Singh, NADPH oxidase 4 is an oncoprotein localized to mitochondria, Cancer Biol Ther 10(3) (2010) 223-31.

[104] C. Zhang, T. Lan, J. Hou, J. Li, R. Fang, Z. Yang, M. Zhang, J. Liu, B. Liu, NOX4 promotes non-small cell lung cancer cell proliferation and metastasis through positive feedback regulation of PI3K/Akt signaling, Oncotarget 5(12) (2014) 4392-4405.

[105] B. Diaz, G. Shani, I. Pass, D. Anderson, M. Quintavalle, S.A. Courtneidge, Tks5-dependent, Nox-mediated Generation of Reactive Oxygen Species is Necessary for Invadopodia Formation, Science signaling 2(88) (2009) ra53-ra53.

[106] J.L. Gregg, R.M. Turner, G. Chang, D. Joshi, Y. Zhan, L. Chen, J.K. Maranchie, NADPH oxidase NOX4 supports renal tumorigenesis by promoting the expression and nuclear accumulation of HIF2α, Cancer research 74(13) (2014) 3501-3511.

[107] B. Halliwell, Biochemistry of oxidative stress, Biochemical Society transactions 35(Pt 5) (2007) 1147-50.

[108] V. Fuchs-Tarlovsky, Role of antioxidants in cancer therapy, Nutrition (Burbank, Los Angeles County, Calif.) 29(1) (2013) 15-21.

[109] L. Packer, S.U. Weber, G. Rimbach, Molecular Aspects of α-Tocotrienol Antioxidant Action and Cell Signalling, The Journal of Nutrition 131(2) (2001) 369S-373S.

[110] V. Thakur, S. Morley, D. Manor, The hepatic alpha tocopherol transfer protein (TTP): ligand-induced protection from proteasomal degradation, Biochemistry 49(43) (2010) 9339-9344.

[111] J. Fiedor, K. Burda, Potential Role of Carotenoids as Antioxidants in Human Health and Disease, Nutrients 6(2) (2014) 466-488.

[112] A.S. Rahmanto, M.J. Davies, Selenium-containing amino acids as direct and indirect antioxidants, IUBMB life 64(11) (2012) 863-71.

[113] W.J. Blot, J.Y. Li, P.R. Taylor, W. Guo, S. Dawsey, G.Q. Wang, C.S. Yang, S.F. Zheng, M. Gail, G.Y. Li, et al., Nutrition intervention trials in Linxian, China: supplementation with specific vitamin/mineral combinations, cancer incidence, and

disease-specific mortality in the general population, Journal of the National Cancer Institute 85(18) (1993) 1483-92.
[114] E.A. Klein, I.M. Thompson, Jr., C.M. Tangen, J.J. Crowley, M.S. Lucia, P.J. Goodman, L.M. Minasian, L.G. Ford, H.L. Parnes, J.M. Gaziano, D.D. Karp, M.M. Lieber, P.J. Walther, L. Klotz, J.K. Parsons, J.L. Chin, A.K. Darke, S.M. Lippman, G.E. Goodman, F.L. Meyskens, Jr., L.H. Baker, Vitamin E and the risk of prostate cancer: the Selenium and Vitamin E Cancer Prevention Trial (SELECT), Jama 306(14) (2011) 1549-56.
[115] S.M. Lippman, E.A. Klein, P.J. Goodman, M.S. Lucia, I.M. Thompson, L.G. Ford, H.L. Parnes, L.M. Minasian, J.M. Gaziano, J.A. Hartline, J.K. Parsons, J.D. Bearden, 3rd, E.D. Crawford, G.E. Goodman, J. Claudio, E. Winquist, E.D. Cook, D.D. Karp, P. Walther, M.M. Lieber, A.R. Kristal, A.K. Darke, K.B. Arnold, P.A. Ganz, R.M. Santella, D. Albanes, P.R. Taylor, J.L. Probstfield, T.J. Jagpal, J.J. Crowley, F.L. Meyskens, Jr., L.H. Baker, C.A. Coltman, Jr., Effect of selenium and vitamin E on risk of prostate cancer and other cancers: the Selenium and Vitamin E Cancer Prevention Trial (SELECT), Jama 301(1) (2009) 39-51.
[116] The effect of vitamin E and beta carotene on the incidence of lung cancer and other cancers in male smokers. The Alpha-Tocopherol, Beta Carotene Cancer Prevention Study Group, The New England journal of medicine 330(15) (1994) 1029-35.
[117] M.P. de la Maza, M. Petermann, D. Bunout, S. Hirsch, Effects of long-term vitamin E supplementation in alcoholic cirrhotics, Journal of the American College of Nutrition 14(2) (1995) 192-6.

[118] N. van Zandwijk, O. Dalesio, U. Pastorino, N. de Vries, H. van Tinteren, EUROSCAN, a randomized trial of vitamin A and N-acetylcysteine in patients with head and neck cancer or lung cancer. For the EUropean Organization for Research and Treatment of Cancer Head and Neck and Lung Cancer Cooperative Groups, Journal of the National Cancer Institute 92(12) (2000) 977-86.

[119] G.E. Goodman, M.D. Thornquist, J. Balmes, M.R. Cullen, F.L. Meyskens, Jr., G.S. Omenn, B. Valanis, J.H. Williams, Jr., The Beta-Carotene and Retinol Efficacy Trial: incidence of lung cancer and cardiovascular disease mortality during 6-year follow-up after stopping beta-carotene and retinol supplements, Journal of the National Cancer Institute 96(23) (2004) 1743-50.

[120] C.H. Hennekens, J.E. Buring, J.E. Manson, M. Stampfer, B. Rosner, N.R. Cook, C. Belanger, F. LaMotte, J.M. Gaziano, P.M. Ridker, W. Willett, R. Peto, Lack of effect of long-term supplementation with beta carotene on the incidence of malignant neoplasms and cardiovascular disease, The New England journal of medicine 334(18) (1996) 1145-9.

[121] I.M. Lee, N.R. Cook, J.E. Manson, J.E. Buring, C.H. Hennekens, Beta-carotene supplementation and incidence of cancer and cardiovascular disease: the Women's Health Study, Journal of the National Cancer Institute 91(24) (1999) 2102-6.

[122] M.L. Neuhouser, M.J. Barnett, A.R. Kristal, C.B. Ambrosone, I.B. King, M. Thornquist, G.G. Goodman, Dietary supplement use and prostate cancer risk in the Carotene and Retinol Efficacy Trial, Cancer epidemiology, biomarkers & prevention : a publication of the American Association for Cancer Research, cosponsored by the American Society of Preventive Oncology 18(8) (2009) 2202-6.

[123] V. Hajhashemi, G. Vaseghi, M. Pourfarzam, A. Abdollahi, Are antioxidants helpful for disease prevention?, Research in Pharmaceutical Sciences 5(1) (2010) 1-8.
[124] S. Chakravarthi, C.E. Jessop, N.J. Bulleid, The role of glutathione in disulphide bond formation and endoplasmic-reticulum-generated oxidative stress, EMBO Reports 7(3) (2006) 271-275.
[125] A. Meister, Glutathione, ascorbate, and cellular protection, Cancer Res 54(7 Suppl) (1994) 1969s-1975s.
[126] B. Schmitt, M. Vicenzi, C. Garrel, F.M. Denis, Effects of N-acetylcysteine, oral glutathione (GSH) and a novel sublingual form of GSH on oxidative stress markers: A comparative crossover study, Redox Biology 6 (2015) 198-205.
[127] G.C. Cook, S. Sherlock, Results of a controlled clinical trial of glutathione in cases of hepatic cirrhosis, Gut 6(5) (1965) 472-6.
[128] M. Khoshbaten, A. Aliasgarzadeh, K. Masnadi, M.K. Tarzamani, S. Farhang, H. Babaei, J. Kiani, M. Zaare, F. Najafipoor, N-Acetylcysteine Improves Liver Function in Patients with Non-Alcoholic Fatty Liver Disease, Hepatitis Monthly 10(1) (2010) 12-16.
[129] T.I.P.F.C.R. Network, Randomized Trial of Acetylcysteine in Idiopathic Pulmonary Fibrosis, New England Journal of Medicine 370(22) (2014) 2093-2101.
[130] J. Behr, M. Demedts, R. Buhl, U. Costabel, R.P. Dekhuijzen, H.M. Jansen, W. MacNee, M. Thomeer, B. Wallaert, F. Laurent, A.G. Nicholson, E.K. Verbeken, J. Verschakelen, C. Flower, S. Petruzzelli, P. De Vuyst, v.d.J. Bosch, E. Rodriguez-Becerra, I. Lankhorst, M. Sardina, G. Boissard, Lung function in idiopathic pulmonary fibrosis - extended analyses of the IFIGENIA trial, Respiratory Research 10(1) (2009) 1-9.

[131] H. Zhang, H.J. Forman, J. Choi, Gamma-glutamyl transpeptidase in glutathione biosynthesis, Methods in enzymology 401 (2005) 468-83.

[132] S.-Y. Hong, H.-W. Gil, J.-O. Yang, E.-Y. Lee, H.-K. Kim, S.-H. Kim, Y.-H. Chung, E.-M. Lee, S.-K. Hwang, Effect of High-Dose Intravenous N-acetylcysteine on the Concentration of Plasma Sulfur-Containing Amino Acids, The Korean Journal of Internal Medicine 20(3) (2005) 217-223.

[133] F.J. Martinez, J.A. de Andrade, K.J. Anstrom, T.E. King, Jr., G. Raghu, Randomized trial of acetylcysteine in idiopathic pulmonary fibrosis, The New England journal of medicine 370(22) (2014) 2093-101.

[134] H.J. Zhang, T. Yan, T.D. Oberley, L.W. Oberley, Comparison of effects of two polymorphic variants of manganese superoxide dismutase on human breast MCF-7 cancer cell phenotype, Cancer Res 59(24) (1999) 6276-83.

[135] C.J. Weydert, T.A. Waugh, J.M. Ritchie, K.S. Iyer, J.L. Smith, L. Li, D.R. Spitz, L.W. Oberley, Overexpression of manganese or copper–zinc superoxide dismutase inhibits breast cancer growth, Free Radical Biology and Medicine 41(2) (2006) 226-237.

[136] W. Zhong, L.W. Oberley, T.D. Oberley, D.K. St Clair, Suppression of the malignant phenotype of human glioma cells by overexpression of manganese superoxide dismutase, Oncogene 14(4) (1997) 481-90.

[137] S.L. Church, J.W. Grant, L.A. Ridnour, L.W. Oberley, P.E. Swanson, P.S. Meltzer, J.M. Trent, Increased manganese superoxide dismutase expression suppresses the malignant phenotype of human melanoma cells, Proceedings of the National Academy of Sciences 90(7) (1993) 3113-3117.

[138] Y. Hu, D.G. Rosen, Y. Zhou, L. Feng, G. Yang, J. Liu, P. Huang, Mitochondrial manganese-superoxide dismutase expression in ovarian cancer: role in cell proliferation and response to oxidative stress, J Biol Chem 280(47) (2005) 39485-92.
[139] Y. Zhang, W. Zhao, H.J. Zhang, F.E. Domann, L.W. Oberley, Overexpression of Copper Zinc Superoxide Dismutase Suppresses Human Glioma Cell Growth, Cancer Research 62(4) (2002) 1205-1212.
[140] M.W. Epperly, M. Carpenter, A. Agarwal, P. Mitra, S. Nie, J.S. Greenberger, Intraoral manganese superoxide dismutase-plasmid/liposome (MnSOD-PL) radioprotective gene therapy decreases ionizing irradiation-induced murine mucosal cell cycling and apoptosis, In vivo (Athens, Greece) 18(4) (2004) 401-10.
[141] Y. Niu, M.W. Epperly, H. Shen, T. Smith, H. Wang, J.S. Greenberger, Intraesophageal MnSOD-plasmid liposome enhances engraftment and self-renewal of bone marrow derived progenitors of esophageal squamous epithelium, Gene Ther 15(5) (2007) 347-356.
[142] A.A. Tarhini, C.P. Belani, J.D. Luketich, A. Argiris, S.S. Ramalingam, W. Gooding, A. Pennathur, D. Petro, K. Kane, D. Liggitt, T. ChampionSmith, X. Zhang, M.W. Epperly, J.S. Greenberger, A Phase I Study of Concurrent Chemotherapy (Paclitaxel and Carboplatin) and Thoracic Radiotherapy with Swallowed Manganese Superoxide Dismutase Plasmid Liposome Protection in Patients with Locally Advanced Stage III Non-Small-Cell Lung Cancer, Human Gene Therapy 22(3) (2011) 336-342.
[143] F. Campana, S. Zervoudis, B. Perdereau, E. Gez, A. Fourquet, C. Badiu, G. Tsakiris, S. Koulaloglou, Topical superoxide dismutase reduces post-irradiation breast cancer fibrosis, Journal of cellular and molecular medicine 8(1) (2004) 109-16.

[144] R. Thomas, N. Sharifi, SOD mimetics: A Novel Class of Androgen Receptor Inhibitors that Suppresses Castration-Resistant Growth of Prostate Cancer, Molecular Cancer Therapeutics 11(1) (2012) 87-97.
[145] M.H. Shah, G.-S. Liu, E.W. Thompson, G.J. Dusting, H.M. Peshavariya, Differential effects of superoxide dismutase and superoxide dismutase/catalase mimetics on human breast cancer cells, Breast Cancer Research and Treatment 150(3) (2015) 523-534.
[146] S. Yan, G. Liu, C. Pei, W. Chen, P. Li, Q. Wang, X. Jin, J. Zhu, M. Wang, X. Liu, Inhibition of NADPH oxidase protects against metastasis of human lung cancer by decreasing microRNA-21, Anti-cancer drugs 26(4) (2015) 388-98.
[147] H. Dosoki, A. Stegemann, M. Taha, H. Schnittler, T.A. Luger, K. Schroder, J.H. Distler, C. Kerkhoff, M. Bohm, Targeting of NADPH oxidase in vitro and in vivo suppresses fibroblast activation and experimental skin fibrosis, Experimental dermatology (2016).
[148] S.S. Bhandarkar, M. Jaconi, L.E. Fried, M.Y. Bonner, B. Lefkove, B. Govindarajan, B.N. Perry, R. Parhar, J. Mackelfresh, A. Sohn, M. Stouffs, U. Knaus, G. Yancopoulos, Y. Reiss, A.V. Benest, H.G. Augustin, J.L. Arbiser, Fulvene-5 potently inhibits NADPH oxidase 4 and blocks the growth of endothelial tumors in mice, The Journal of Clinical Investigation 119(8) 2359-2365.
[149] V. Jaquet, J. Marcoux, E. Forest, K.G. Leidal, S. McCormick, Y. Westermaier, R. Perozzo, O. Plastre, L. Fioraso-Cartier, B. Diebold, L. Scapozza, W.M. Nauseef, F. Fieschi, K.H. Krause, K. Bedard, NADPH oxidase (NOX) isoforms are inhibited by

celastrol with a dual mode of action, British journal of pharmacology 164(2b) (2011) 507-20.

[150] H. Zhu, X.-W. Liu, T.-Y. Cai, J. Cao, C.-X. Tu, W. Lu, Q.-J. He, B. Yang, Celastrol Acts as a Potent Antimetastatic Agent Targeting β1 Integrin and Inhibiting Cell-Extracellular Matrix Adhesion, in Part via the p38 Mitogen-Activated Protein Kinase Pathway, Journal of Pharmacology and Experimental Therapeutics 334(2) (2010) 489-499.

[151] J.X. Jiang, X. Chen, N. Serizawa, C. Szyndralewiez, P. Page, K. Schroder, R.P. Brandes, S. Devaraj, N.J. Torok, Liver fibrosis and hepatocyte apoptosis are attenuated by GKT137831, a novel NOX4/NOX1 inhibitor in vivo, Free Radic Biol Med 53(2) (2012) 289-96.

[152] E. Cifuentes-Pagano, D.N. Meijles, P.J. Pagano, The quest for selective nox inhibitors and therapeutics: challenges, triumphs and pitfalls, Antioxid Redox Signal 20(17) (2014) 2741-54.

[153] E. Crosas-Molist, E. Bertran, P. Sancho, J. López-Luque, J. Fernando, A. Sánchez, M. Fernández, E. Navarro, I. Fabregat, The NADPH oxidase NOX4 inhibits hepatocyte proliferation and liver cancer progression, Free Radical Biology and Medicine 69 (2014) 338-347.

[154] S. Wind, K. Beuerlein, T. Eucker, H. Müller, P. Scheurer, M.E. Armitage, H. Ho, H. Schmidt, K. Wingler, Comparative pharmacology of chemically distinct NADPH oxidase inhibitors, British journal of pharmacology 161(4) (2010) 885-898.

[155] K.R. Dong, S. Zheng, X. Xiao, Conservative management of neonatal hepatic hemangioma: a report from one institute, Pediatric surgery international 25(6) (2009) 493-8.

[156] S. Altenhofer, K.A. Radermacher, P.W. Kleikers, K. Wingler, H.H. Schmidt, Evolution of NADPH Oxidase Inhibitors: Selectivity and Mechanisms for Target Engagement, Antioxid Redox Signal 23(5) (2015) 406-27.

[157] J.M. Munson, L. Fried, S.A. Rowson, M.Y. Bonner, L. Karumbaiah, B. Diaz, S.A. Courtneidge, U.G. Knaus, D.J. Brat, J.L. Arbiser, R.V. Bellamkonda, Anti-Invasive Adjuvant Therapy with Imipramine Blue Enhances Chemotherapeutic Efficacy Against Glioma, Science Translational Medicine 4(127) (2012) 127ra36-127ra36.

[158] W.H. Yang, Y.H. Su, W.H. Hsu, C.C. Wang, J.L. Arbiser, M.H. Yang, Imipramine blue halts head and neck cancer invasion through promoting F-box and leucine-rich repeat protein 14-mediated Twist1 degradation, Oncogene 35(18) (2016) 2287-98.

[159] S. Garrido-Urbani, S. Jemelin, C. Deffert, S. Carnesecchi, O. Basset, C. Szyndralewiez, F. Heitz, P. Page, X. Montet, L. Michalik, J. Arbiser, C. Rüegg, K.H. Krause, B. Imhof, Targeting Vascular NADPH Oxidase 1 Blocks Tumor Angiogenesis through a PPARα Mediated Mechanism, PLoS ONE 6(2) (2011) e14665.

[160] S. Das, J.M. Dowding, K.E. Klump, J.F. McGinnis, W. Self, S. Seal, Cerium oxide nanoparticles: applications and prospects in nanomedicine, Nanomedicine (London, England) 8(9) (2013) 1483-508.

[161] S. Giri, A. Karakoti, R.P. Graham, J.L. Maguire, C.M. Reilly, S. Seal, R. Rattan, V. Shridhar, Nanoceria: A Rare-Earth Nanoparticle as a Novel Anti-Angiogenic Therapeutic Agent in Ovarian Cancer, PLoS ONE 8(1) (2013) e54578.

[162] M. Hijaz, S. Das, I. Mert, A. Gupta, Z. Al-Wahab, C. Tebbe, S. Dar, J. Chhina, S. Giri, A. Munkarah, S. Seal, R. Rattan, Folic acid tagged nanoceria as a novel therapeutic agent in ovarian cancer, BMC Cancer 16 (2016) 220.

[163] D. Oró, T. Yudina, G. Fernández-Varo, E. Casals, V. Reichenbach, G. Casals, B. González de la Presa, S. Sandalinas, S. Carvajal, V. Puntes, W. Jiménez, Cerium oxide nanoparticles reduce steatosis, portal hypertension and display anti-inflammatory properties in rats with liver fibrosis, Journal of Hepatology 64(3) 691-698.

[164] S.M. Hirst, A. Karakoti, S. Singh, W. Self, R. Tyler, S. Seal, C.M. Reilly, Bio-distribution and in vivo antioxidant effects of cerium oxide nanoparticles in mice, Environmental toxicology 28(2) (2013) 107-18.

[165] J. Grebowski, A. Krokosz, [Fullerenes in radiobiology], Postepy biochemii 56(4) (2010) 456-62.

[166] G.V. Andrievsky, V.I. Bruskov, A.A. Tykhomyrov, S.V. Gudkov, Peculiarities of the antioxidant and radioprotective effects of hydrated C60 fullerene nanostuctures in vitro and in vivo, Free Radical Biology and Medicine 47(6) (2009) 786-793.

[167] J.-Y. Xu, Y.-Y. Su, J.-S. Cheng, S.-X. Li, R. Liu, W.-X. Li, G.-T. Xu, Q.-N. Li, Protective effects of fullerenol on carbon tetrachloride-induced acute hepatotoxicity and nephrotoxicity in rats, Carbon 48(5) (2010) 1388-1396.

[168] S. Prylutska, I. Grynyuk, O. Matyshevska, Y. Prylutskyy, M. Evstigneev, P. Scharff, U. Ritter, C(60) Fullerene as Synergistic Agent in Tumor-Inhibitory Doxorubicin Treatment, Drugs in R&D 14(4) (2014) 333-340.

[169] H. Katsumi, K. Fukui, K. Sato, S. Maruyama, S. Yamashita, E. Mizumoto, K. Kusamori, M. Oyama, M. Sano, T. Sakane, A. Yamamoto, Pharmacokinetics and

preventive effects of platinum nanoparticles as reactive oxygen species scavengers on hepatic ischemia/reperfusion injury in mice, Metallomics 6(5) (2014) 1050-1056.
[170] S. Shibuya, Y. Ozawa, K. Watanabe, N. Izuo, T. Toda, K. Yokote, T. Shimizu, Palladium and Platinum Nanoparticles Attenuate Aging-Like Skin Atrophy via Antioxidant Activity in Mice, PLoS ONE 9(10) (2014) e109288.
[171] Y. Yoshihisa, A. Honda, Q.L. Zhao, T. Makino, R. Abe, K. Matsui, H. Shimizu, Y. Miyamoto, T. Kondo, T. Shimizu, Protective effects of platinum nanoparticles against UV-light-induced epidermal inflammation, Experimental dermatology 19(11) (2010) 1000-6.
[172] J. Morry, W. Ngamcherdtrakul, S. Gu, S.M. Goodyear, D.J. Castro, M.M. Reda, T. Sangvanich, W. Yantasee, Dermal delivery of HSP47 siRNA with NOX4-modulating mesoporous silica-based nanoparticles for treating fibrosis, Biomaterials 66 (2015) 41-52.
[173] D. Tarn, C.E. Ashley, M. Xue, E.C. Carnes, J.I. Zink, C.J. Brinker, Mesoporous silica nanoparticle nanocarriers: biofunctionality and biocompatibility, Accounts of chemical research 46(3) (2013) 792-801.
[174] E. Phillips, O. Penate-Medina, P.B. Zanzonico, R.D. Carvajal, P. Mohan, Y. Ye, J. Humm, M. Gönen, H. Kalaigian, H. Schöder, H.W. Strauss, S.M. Larson, U. Wiesner, M.S. Bradbury, Clinical translation of an ultrasmall inorganic optical-PET imaging nanoparticle probe, Science Translational Medicine 6(260) (2014) 260ra149.
[175] W. Ngamcherdtrakul, J. Morry, S. Gu, D.J. Castro, S.M. Goodyear, T. Sangvanich, M.M. Reda, R. Lee, S.A. Mihelic, B.L. Beckman, Z. Hu, J.W. Gray, W. Yantasee, Cationic Polymer Modified Mesoporous Silica Nanoparticles for Targeted siRNA

Delivery to HER2+ Breast Cancer, Advanced Functional Materials 25(18) (2015) 2646-2659.

[176] L. Bajenaru, D. Berger, L. Miclea, C. Matei, S. Nastase, C. Andronescu, M.G. Moisescu, T. Savopol, Correlation of the intracellular reactive oxygen species levels with textural properties of functionalized mesostructured silica, Journal of biomedical materials research. Part A 102(12) (2014) 4435-42.

[177] E.B. Ehlerding, F. Chen, W. Cai, Biodegradable and Renal Clearable Inorganic Nanoparticles, Advanced Science 3(2) (2016) 1500223-n/a.

[178] B.G. Trewyn, J.A. Nieweg, Y. Zhao, V.S.Y. Lin, Biocompatible mesoporous silica nanoparticles with different morphologies for animal cell membrane penetration, Chemical Engineering Journal 137(1) (2008) 23-29.

[179] Q. He, Z. Zhang, F. Gao, Y. Li, J. Shi, In vivo biodistribution and urinary excretion of mesoporous silica nanoparticles: effects of particle size and PEGylation, Small (Weinheim an der Bergstrasse, Germany) 7(2) (2011) 271-80.

[180] R. Kumar, I. Roy, T.Y. Ohulchanskky, L.A. Vathy, E.J. Bergey, M. Sajjad, P.N. Prasad, In Vivo Biodistribution and Clearance Studies Using Multimodal Organically Modified Silica Nanoparticles, ACS Nano 4(2) (2010) 699-708.

[181] J.-A. Lee, M.-K. Kim, H.-J. Paek, Y.-R. Kim, M.-K. Kim, J.-K. Lee, J. Jeong, S.-J. Choi, Tissue distribution and excretion kinetics of orally administered silica nanoparticles in rats, International Journal of Nanomedicine 9(Suppl 2) (2014) 251-260.

[182] K.R. Martin, The chemistry of silica and its potential health benefits, The journal of nutrition, health & aging 11(2) (2007) 94-7.

[183] P. Cheresh, S.J. Kim, S. Tulasiram, D.W. Kamp, Oxidative stress and pulmonary fibrosis, Biochimica et biophysica acta 1832(7) (2013) 1028-40.

[184] A. Gabrielli, S. Svegliati, G. Moroncini, D. Amico, New insights into the role of oxidative stress in scleroderma fibrosis, The open rheumatology journal 6 (2012) 87-95.

[185] B.M. Stramer, R. Mori, P. Martin, The inflammation-fibrosis link? A Jekyll and Hyde role for blood cells during wound repair, The Journal of investigative dermatology 127(5) (2007) 1009-17.

[186] B.D. Bringardner, C.P. Baran, T.D. Eubank, C.B. Marsh, The role of inflammation in the pathogenesis of idiopathic pulmonary fibrosis, Antioxid Redox Signal 10(2) (2008) 287-301.

[187] T.A. Wynn, Integrating mechanisms of pulmonary fibrosis, The Journal of experimental medicine 208(7) (2011) 1339-50.

[188] B.B. Borg, A. Seetharam, V. Subramanian, H.I. Basha, M. Lisker‐Melman, K. Korenblat, C.D. Anderson, S. Shenoy, W.C. Chapman, J.S. Crippin, Immune response to extracellular matrix collagen in chronic hepatitis C–induced liver fibrosis, Liver Transplantation 17(7) (2011) 814-823.

[189] A. Leask, D.J. Abraham, TGF-beta signaling and the fibrotic response, FASEB journal : official publication of the Federation of American Societies for Experimental Biology 18(7) (2004) 816-27.

[190] G. Wick, C. Grundtman, C. Mayerl, T.F. Wimpissinger, J. Feichtinger, B. Zelger, R. Sgonc, D. Wolfram, The immunology of fibrosis, Annual review of immunology 31 (2013) 107-35.

[191] R. Rafii, M.M. Juarez, T.E. Albertson, A.L. Chan, A review of current and novel therapies for idiopathic pulmonary fibrosis, Journal of thoracic disease 5(1) (2013) 48-73.
[192] A.L. Buchman, Side effects of corticosteroid therapy, Journal of clinical gastroenterology 33(4) (2001) 289-94.
[193] K.R. Flaherty, G.B. Toews, J.P. Lynch, 3rd, E.A. Kazerooni, B.H. Gross, R.L. Strawderman, K. Hariharan, A. Flint, F.J. Martinez, Steroids in idiopathic pulmonary fibrosis: a prospective assessment of adverse reactions, response to therapy, and survival, The American journal of medicine 110(4) (2001) 278-82.
[194] C.P. Denton, P.A. Merkel, D.E. Furst, D. Khanna, P. Emery, V.M. Hsu, N. Silliman, J. Streisand, J. Powell, A. Akesson, J. Coppock, F. Hoogen, A. Herrick, M.D. Mayes, D. Veale, J. Haas, S. Ledbetter, J.H. Korn, C.M. Black, J.R. Seibold, Recombinant human anti-transforming growth factor beta1 antibody therapy in systemic sclerosis: a multicenter, randomized, placebo-controlled phase I/II trial of CAT-192, Arthritis and rheumatism 56(1) (2007) 323-33.
[195] S. Prey, K. Ezzedine, A. Doussau, A.S. Grandoulier, D. Barcat, E. Chatelus, E. Diot, C. Durant, E. Hachulla, J.D. de Korwin-Krokowski, E. Kostrzewa, T. Quemeneur, C. Paul, T. Schaeverbeke, J. Seneschal, A. Solanilla, A. Sparsa, S. Bouchet, S. Lepreux, F.X. Mahon, G. Chene, A. Taieb, Imatinib mesylate in scleroderma-associated diffuse skin fibrosis: a phase II multicentre randomized double-blinded controlled trial, The British journal of dermatology 167(5) (2012) 1138-44.
[196] J.P. Saikia, S. Paul, B.K. Konwar, S.K. Samdarshi, Nickel oxide nanoparticles: a novel antioxidant, Colloids and surfaces. B, Biointerfaces 78(1) (2010) 146-8.

[197] M. Nomura, Y. Yoshimura, T. Kikuiri, T. Hasegawa, Y. Taniguchi, Y. Deyama, K. Koshiro, H. Sano, K. Suzuki, N. Inoue, Platinum nanoparticles suppress osteoclastogenesis through scavenging of reactive oxygen species produced in RAW264.7 cells, Journal of pharmacological sciences 117(4) (2011) 243-52.

[198] S. Onizawa, K. Aoshiba, M. Kajita, Y. Miyamoto, A. Nagai, Platinum nanoparticle antioxidants inhibit pulmonary inflammation in mice exposed to cigarette smoke, Pulmonary pharmacology & therapeutics 22(4) (2009) 340-9.

[199] A. Watanabe, M. Kajita, J. Kim, A. Kanayama, K. Takahashi, T. Mashino, Y. Miyamoto, In vitro free radical scavenging activity of platinum nanoparticles, Nanotechnology 20(45) (2009) 455105.

[200] E.G. Heckert, A.S. Karakoti, S. Seal, W.T. Self, The role of cerium redox state in the SOD mimetic activity of nanoceria, Biomaterials 29(18) (2008) 2705-9.

[201] D. Schubert, R. Dargusch, J. Raitano, S.W. Chan, Cerium and yttrium oxide nanoparticles are neuroprotective, Biochemical and biophysical research communications 342(1) (2006) 86-91.

[202] N. Hao, H. Yang, L. Li, L. Li, F. Tang, The shape effect of mesoporous silica nanoparticles on intracellular reactive oxygen species in A375 cells, New Journal of Chemistry (2014).

[203] M.A. Shahbazi, B. Herranz, H.A. Santos, Nanostructured porous Si-based nanoparticles for targeted drug delivery, Biomatter 2(4) (2012) 296-312.

[204] B. Godin, J. Gu, R.E. Serda, S. Ferrati, X. Liu, C. Chiappini, T. Tanaka, P. Decuzzi, M. Ferrari, Multistage Mesoporous Silicon-based Nanocarriers: Biocompatibility with

Immune Cells and Controlled Degradation in Physiological Fluids, Controlled release newsletter / Controlled Release Society 25(4) (2008) 9-11.
[205] Y. Nisimoto, B.A. Diebold, D. Cosentino-Gomes, J.D. Lambeth, Nox4: A Hydrogen Peroxide-Generating Oxygen Sensor, Biochemistry 53(31) (2014) 5111-5120.
[206] L. Hecker, R. Vittal, T. Jones, R. Jagirdar, T.R. Luckhardt, J.C. Horowitz, S. Pennathur, F.J. Martinez, V.J. Thannickal, NADPH oxidase-4 mediates myofibroblast activation and fibrogenic responses to lung injury, Nature medicine 15(9) (2009) 1077-81.
[207] S. Piera-Velazquez, S.A. Jimenez, Role of cellular senescence and NOX4-mediated oxidative stress in systemic sclerosis pathogenesis, Current rheumatology reports 17(1) (2015) 473.
[208] T. Spadoni, S. Svegliati Baroni, D. Amico, L. Albani, G. Moroncini, E.V. Avvedimento, A. Gabrielli, A reactive oxygen species-mediated loop maintains the increased expression of NOX2 and NOX4 in skin fibroblasts from patients with systemic sclerosis, Arthritis Rheumatol (2015).
[209] C. Michaeloudes, M.B. Sukkar, N.M. Khorasani, P.K. Bhavsar, K.F. Chung, TGF-β regulates Nox4, MnSOD and catalase expression, and IL-6 release in airway smooth muscle cells, American Journal of Physiology-Lung Cellular and Molecular Physiology 300(2) (2011) L295-L304.
[210] D. Lin, Q. Cheng, Q. Jiang, Y. Huang, Z. Yang, S. Han, Y. Zhao, S. Guo, Z. Liang, A. Dong, Intracellular cleavable poly(2-dimethylaminoethyl methacrylate) functionalized mesoporous silica nanoparticles for efficient siRNA delivery in vitro and in vivo, Nanoscale 5(10) (2013) 4291-301.

[211] J. Shen, H.C. Kim, H. Su, F. Wang, J. Wolfram, D. Kirui, J. Mai, C. Mu, L.N. Ji, Z.W. Mao, H. Shen, Cyclodextrin and polyethylenimine functionalized mesoporous silica nanoparticles for delivery of siRNA cancer therapeutics, Theranostics 4(5) (2014) 487-97.

[212] Y. Ishida, K. Nagata, Chapter nine - Hsp47 as a Collagen-Specific Molecular Chaperone, in: C.W. James, I.B. Phillip (Eds.), Methods in enzymology, Academic Press2011, pp. 167-182.

[213] K. Kuroda, R. Tsukifuji, H. Shinkai, Increased expression of heat-shock protein 47 is associated with overproduction of type I procollagen in systemic sclerosis skin fibroblasts, The Journal of investigative dermatology 111(6) (1998) 1023-8.

[214] M. Naitoh, N. Hosokawa, H. Kubota, T. Tanaka, H. Shirane, M. Sawada, Y. Nishimura, K. Nagata, Upregulation of HSP47 and collagen type III in the dermal fibrotic disease, keloid, Biochemical and biophysical research communications 280(5) (2001) 1316-22.

[215] M.S. Razzaque, A. Kumatori, T. Harada, T. Taguchi, Coexpression of collagens and collagen-binding heat shock protein 47 in human diabetic nephropathy and IgA nephropathy, Nephron 80(4) (1998) 434-43.

[216] M. Amenomori, H. Mukae, N. Sakamoto, T. Kakugawa, T. Hayashi, A. Hara, S. Hara, H. Fujita, H. Ishimoto, Y. Ishimatsu, T. Nagayasu, S. Kohno, HSP47 in lung fibroblasts is a predictor of survival in fibrotic nonspecific interstitial pneumonia, Respiratory medicine 104(6) (2010) 895-901.

[217] T. Kakugawa, S. Yokota, H. Mukae, H. Kubota, N. Sakamoto, S. Mizunoe, Y. Matsuoka, J. Kadota, N. Fujii, K. Nagata, S. Kohno, High serum concentrations of

autoantibodies to HSP47 in nonspecific interstitial pneumonia compared with idiopathic pulmonary fibrosis, BMC pulmonary medicine 8 (2008) 23.
[218] K.E. Brown, K.A. Broadhurst, M.M. Mathahs, E.M. Brunt, W.N. Schmidt, Expression of HSP47, a collagen-specific chaperone, in normal and diseased human liver, Laboratory investigation; a journal of technical methods and pathology 85(6) (2005) 789-97.
[219] Y. Sato, K. Murase, J. Kato, M. Kobune, T. Sato, Y. Kawano, R. Takimoto, K. Takada, K. Miyanishi, T. Matsunaga, T. Takayama, Y. Niitsu, Resolution of liver cirrhosis using vitamin A-coupled liposomes to deliver siRNA against a collagen-specific chaperone, Nature biotechnology 26(4) (2008) 431-42.
[220] H. Ishiwatari, Y. Sato, K. Murase, A. Yoneda, R. Fujita, H. Nishita, N.K. Birukawa, T. Hayashi, T. Sato, K. Miyanishi, R. Takimoto, M. Kobune, S. Ota, Y. Kimura, K. Hirata, J. Kato, Y. Niitsu, Treatment of pancreatic fibrosis with siRNA against a collagen-specific chaperone in vitamin A-coupled liposomes, Gut 62(9) (2013) 1328-39.
[221] Y. Obata, T. Nishino, T. Kushibiki, R. Tomoshige, Z. Xia, M. Miyazaki, K. Abe, T. Koji, Y. Tabata, S. Kohno, HSP47 siRNA conjugated with cationized gelatin microspheres suppresses peritoneal fibrosis in mice, Acta biomaterialia 8(7) (2012) 2688-96.
[222] S.A. Leachman, R.P. Hickerson, M.E. Schwartz, E.E. Bullough, S.L. Hutcherson, K.M. Boucher, C.D. Hansen, M.J. Eliason, G.S. Srivatsa, D.J. Kornbrust, F.J.D. Smith, W.H.I. McLean, L.M. Milstone, R.L. Kaspar, First-in-human Mutation-targeted siRNA Phase Ib Trial of an Inherited Skin Disorder, Mol Ther 18(2) (2009) 442-446.

[223] T. Yamamoto, S. Takagawa, I. Katayama, K. Yamazaki, Y. Hamazaki, H. Shinkai, K. Nishioka, Animal model of sclerotic skin. I: Local injections of bleomycin induce sclerotic skin mimicking scleroderma, The Journal of investigative dermatology 112(4) (1999) 456-62.

[224] A. Takashima, Establishment of fibroblast cultures, Curr Protoc Cell Biol2001, pp. 2.1.1 - 2.1.12.

[225] N.P. Omelyanenko, L.I. Slutsky, S.P. Mironov, Connective Tissue: Histophysiology, Biochemistry, Molecular Biology, CRC Press2013, pp. 17-77.

[226] O. Boucherat, M.L. Franco-Montoya, C. Thibault, R. Incitti, B. Chailley-Heu, C. Delacourt, J.R. Bourbon, Gene expression profiling in lung fibroblasts reveals new players in alveolarization, Physiol Genomics 32(1) (2007) 128-41.

[227] W. Brand-Williams, M.E. Cuvelier, C. Berset, Use of a free radical method to evaluate antioxidant activity, LWT - Food Science and Technology 28(1) (1995) 25-30.

[228] G.B. Jacobson, E. Gonzalez-Gonzalez, R. Spitler, R. Shinde, D. Leake, R.L. Kaspar, C.H. Contag, R.N. Zare, Biodegradable nanoparticles with sustained release of functional siRNA in skin, Journal of Pharmaceutical Sciences 99(10) (2010) 4261-4266.

[229] V. Hegde, R.P. Hickerson, S. Nainamalai, P.A. Campbell, F.J.D. Smith, W.H.I. McLean, D.M. Leslie Pedrioli, In vivo gene silencing following non-invasive siRNA delivery into the skin using a novel topical formulation, Journal of Controlled Release 196(0) (2014) 355-362.

[230] G. Loor, J. Kondapalli, J.M. Schriewer, N.S. Chandel, T.L. Vanden Hoek, P.T. Schumacker, Menadione triggers cell death through ROS-dependent mechanisms

involving PARP activation without requiring apoptosis, Free Radic Biol Med 49(12) (2010) 1925-36.

[231] M.L. Read, S. Singh, Z. Ahmed, M. Stevenson, S.S. Briggs, D. Oupicky, L.B. Barrett, R. Spice, M. Kendall, M. Berry, J.A. Preece, A. Logan, L.W. Seymour, A versatile reducible polycation-based system for efficient delivery of a broad range of nucleic acids, Nucleic acids research 33(9) (2005) e86.

[232] T. Kawakami, H. Ihn, W. Xu, E. Smith, C. LeRoy, M. Trojanowska, Increased expression of TGF-beta receptors by scleroderma fibroblasts: evidence for contribution of autocrine TGF-beta signaling to scleroderma phenotype, The Journal of investigative dermatology 110(1) (1998) 47-51.

[233] P. Sambo, S.S. Baroni, M. Luchetti, P. Paroncini, S. Dusi, G. Orlandini, A. Gabrielli, Oxidative stress in scleroderma: maintenance of scleroderma fibroblast phenotype by the constitutive up-regulation of reactive oxygen species generation through the NADPH oxidase complex pathway, Arthritis and rheumatism 44(11) (2001) 2653-64.

[234] D. Pohlers, J. Brenmoehl, I. Loffler, C.K. Muller, C. Leipner, S. Schultze-Mosgau, A. Stallmach, R.W. Kinne, G. Wolf, TGF-beta and fibrosis in different organs - molecular pathway imprints, Biochimica et biophysica acta 1792(8) (2009) 746-56.

[235] Q. Xu, J.T. Norman, S. Shrivastav, J. Lucio-Cazana, J.B. Kopp, In vitro models of TGF-beta-induced fibrosis suitable for high-throughput screening of antifibrotic agents, American journal of physiology. Renal physiology 293(2) (2007) F631-40.

[236] G. Lakos, S. Takagawa, S.-J. Chen, A.M. Ferreira, G. Han, K. Masuda, X.-J. Wang, L.A. DiPietro, J. Varga, Targeted Disruption of TGF-β/Smad3 Signaling

Modulates Skin Fibrosis in a Mouse Model of Scleroderma, The American journal of pathology 165(1) (2004) 203-217.
[237] H. Sasaki, T. Sato, N. Yamauchi, T. Okamoto, D. Kobayashi, S. Iyama, J. Kato, T. Matsunaga, R. Takimoto, T. Takayama, Induction of heat shock protein 47 synthesis by TGF-β and IL-1β via enhancement of the heat shock element binding activity of heat shock transcription factor 1, The Journal of Immunology 168(10) (2002) 5178-5183.
[238] E.C. Chan, H.M. Peshavariya, G.-S. Liu, F. Jiang, S.-Y. Lim, G.J. Dusting, Nox4 modulates collagen production stimulated by transforming growth factor β1 in vivo and in vitro, Biochemical and biophysical research communications 430(3) (2013) 918-925.
[239] F. Jiang, G.-S. Liu, G.J. Dusting, E.C. Chan, NADPH oxidase-dependent redox signaling in TGF-β-mediated fibrotic responses, Redox Biology 2(0) (2014) 267-272.
[240] J.L. Barnes, Y. Gorin, Myofibroblast differentiation during fibrosis: role of NAD(P)H oxidases, Kidney Int 79(9) (2011) 944-956.
[241] A.L. Yu, J. Moriniere, M. Birke, C. Neumann, R. Fuchshofer, A. Kampik, H. Bloemendal, U. Welge-Lussen, Reactivation of Optic Nerve Head Astrocytes by TGF-β2 and H2O2 Is Accompanied by Increased Hsp32 and Hsp47 Expression, Investigative Ophthalmology & Visual Science 50(4) (2009) 1707-1717.
[242] A. Gosslau, P. Ruoff, S. Mohsenzadeh, U. Hobohm, L. Rensing, Heat shock and oxidative stress-induced exposure of hydrophobic protein domains as common signal in the induction of hsp68, J Biol Chem 276(3) (2001) 1814-21.
[243] B.I. Sikic, Biochemical and cellular determinants of bleomycin cytotoxicity, Cancer surveys 5(1) (1986) 81-91.

[244] V.I. Sayin, M.X. Ibrahim, E. Larsson, J.A. Nilsson, P. Lindahl, M.O. Bergo, Antioxidants Accelerate Lung Cancer Progression in Mice, Science Translational Medicine 6(221) (2014) 221ra15-221ra15.
[245] K. Le Gal, M.X. Ibrahim, C. Wiel, V.I. Sayin, M.K. Akula, C. Karlsson, M.G. Dalin, L.M. Akyürek, P. Lindahl, J. Nilsson, M.O. Bergo, Antioxidants can increase melanoma metastasis in mice, Science Translational Medicine 7(308) (2015) 308re8-308re8.
[246] A. Weiss, S. Goldman, I. Ben Shlomo, V. Eyali, S. Leibovitz, E. Shalev, Mechanisms of matrix metalloproteinase-9 and matrix metalloproteinase-2 inhibition by N-acetylcysteine in the human term decidua and fetal membranes, American journal of obstetrics and gynecology 189(6) (2003) 1758-63.
[247] T. Ramaesh, K. Ramaesh, S.C. Riley, J.D. West, B. Dhillon, Effects of N-acetylcysteine on matrix metalloproteinase-9 secretion and cell migration of human corneal epithelial cells, Eye 26(8) (2012) 1138-1144.
[248] I.V. Voronkina, K.M. Kirpichnikova, L.V. Smagina, I.A. Gamaley, Activity of matrix metalloproteinases in normal and transformed mouse fibroblasts exposed to antioxidants, Cell and Tissue Biology 3(1) (2009) 56-60.
[249] A. Supabphol, V. Muangman, W. Chavasiri, R. Supabphol, W. Gritsanapan, N-acetylcysteine inhibits proliferation, adhesion, migration and invasion of human bladder cancer cells, Journal of the Medical Association of Thailand = Chotmaihet thangphaet 92(9) (2009) 1171-7.
[250] A. Albini, F. D'Agostini, D. Giunciuglio, I. Paglieri, R. Balansky, S. De Flora, Inhibition of invasion, gelatinase activity, tumor take and metastasis of malignant cells by N-acetylcysteine, International Journal of Cancer 61(1) (1995) 121-129.

[251] C. Mehner, A. Hockla, E. Miller, S. Ran, D.C. Radisky, E.S. Radisky, Tumor cell-produced matrix metalloproteinase 9 (MMP-9) drives malignant progression and metastasis of basal-like triple negative breast cancer, Oncotarget 5(9) (2014) 2736-2749.

[252] E.M. Yousef, M.R. Tahir, Y. St-Pierre, L.A. Gaboury, MMP-9 expression varies according to molecular subtypes of breast cancer, BMC Cancer 14(1) (2014) 609.

[253] K.-i. Matsumoto, F. Hyodo, A. Matsumoto, A.P. Koretsky, A.L. Sowers, J.B. Mitchell, M.C. Krishna, High-Resolution Mapping of Tumor Redox Status by Magnetic Resonance Imaging Using Nitroxides as Redox-Sensitive Contrast Agents, Clinical Cancer Research 12(8) (2006) 2455-2462.

[254] K. Cai, H.N. Xu, A. Singh, L. Moon, M. Haris, R. Reddy, L. Li, Breast Cancer Redox Heterogeneity Detectable with Chemical Exchange Satruation Transfer (CEST) MRI, Molecular imaging and biology : MIB : the official publication of the Academy of Molecular Imaging 16(5) (2014) 670-679.

[255] M.L. Turski, D.J. Thiele, New Roles for Copper Metabolism in Cell Proliferation, Signaling, and Disease, The Journal of Biological Chemistry 284(2) (2009) 717-721.

[256] D. Horn, A. Barrientos, Mitochondrial copper metabolism and delivery to cytochrome c oxidase, IUBMB life 60(7) (2008) 421-9.

[257] J.A. Tainer, E.D. Getzoff, J.S. Richardson, D.C. Richardson, Structure and mechanism of copper, zinc superoxide dismutase, Nature 306(5940) (1983) 284-287.

[258] R.B. Rucker, T. Kosonen, M.S. Clegg, A.E. Mitchell, B.R. Rucker, J.Y. Uriu-Hare, C.L. Keen, Copper, lysyl oxidase, and extracellular matrix protein cross-linking, The American journal of clinical nutrition 67(5 Suppl) (1998) 996s-1002s.

[259] M.C. Linder, Ceruloplasmin and other copper binding components of blood plasma and their functions: an update, Metallomics 8(9) (2016) 887-905.
[260] G. Khan, S. Merajver, Copper chelation in cancer therapy using tetrathiomolybdate: an evolving paradigm, Expert Opinion on Investigational Drugs 18(4) (2009) 541-548.
[261] H. Xie, Y.J. Kang, Role of copper in angiogenesis and its medicinal implications, Current medicinal chemistry 16(10) (2009) 1304-14.
[262] F. Martin, T. Linden, D.M. Katschinski, F. Oehme, I. Flamme, C.K. Mukhopadhyay, K. Eckhardt, J. Troger, S. Barth, G. Camenisch, R.H. Wenger, Copper-dependent activation of hypoxia-inducible factor (HIF)-1: implications for ceruloplasmin regulation, Blood 105(12) (2005) 4613-9.
[263] G. MacDonald, I. Nalvarte, T. Smirnova, M. Vecchi, N. Aceto, A. Dolemeyer, A. Frei, S. Lienhard, J. Wyckoff, D. Hess, J. Seebacher, J.J. Keusch, H. Gut, D. Salaun, G. Mazzarol, D. Disalvatore, M. Bentires-Alj, P.P. Di Fiore, A. Badache, N.E. Hynes, Memo is a copper-dependent redox protein with an essential role in migration and metastasis, Sci Signal 7(329) (2014) ra56.
[264] A. Gupte, R.J. Mumper, Elevated copper and oxidative stress in cancer cells as a target for cancer treatment, Cancer Treatment Reviews 35(1) (2009) 32-46.
[265] S. Jain, J. Cohen, M.M. Ward, N. Kornhauser, E. Chuang, T. Cigler, A. Moore, D. Donovan, C. Lam, M.V. Cobham, S. Schneider, S.M. Hurtado Rúa, S. Benkert, C. Mathijsen Greenwood, R. Zelkowitz, J.D. Warren, M.E. Lane, V. Mittal, S. Rafii, L.T. Vahdat, Tetrathiomolybdate-associated copper depletion decreases circulating

endothelial progenitor cells in women with breast cancer at high risk of relapse, Annals of Oncology (2013).

[266] S. Fu, A. Naing, C. Fu, M.T. Kuo, R. Kurzrock, Overcoming Platinum Resistance through the Use of a Copper-Lowering Agent, Molecular Cancer Therapeutics 11(6) (2012) 1221-1225.

[267] T.D. Perrine, W.R. Landis, Analysis of polyethylenimine by spectrophotometry of its copper chelate, Journal of Polymer Science Part A-1: Polymer Chemistry 5(8) (1967) 1993-2003.

[268] M.A. Barakat, New trends in removing heavy metals from industrial wastewater, Arabian Journal of Chemistry 4(4) (2011) 361-377.

[269] Z. Yuan, N. Cai, Y. Du, Y. He, E.S. Yeung, Sensitive and selective detection of copper ions with highly stable polyethyleneimine-protected silver nanoclusters, Analytical chemistry 86(1) (2014) 419-26.